EDSON MATEUS SIGNOR

SEMICLASSICAL THEORY FOR EXTREME EVENTS OF QUANTUM MAPS EIGENSTATES

PORTO ALEGRE, RS
2022

EDSON MATEUS SIGNOR

SEMICLASSICAL THEORY FOR EXTREME EVENTS OF QUANTUM MAPS EIGENSTATES

Dissertação de Mestrado apresentado como requisito parcial para obtenção do título de Mestre em Física pelo Instituto de Física da Universidade Federal do Rio Grande do Sul.

Orientadora: Prof^{a}. Sandra Denise Prado

PORTO ALEGRE, RS
2022

EDSON MATEUS SIGNOR

SEMICLASSICAL THEORY FOR EXTREME EVENTS OF QUANTUM MAPS EIGENSTATES

Dissertação de Mestrado apresentado como requisito parcial para obtenção do título de Mestre em Física pelo Instituto de Física da Universidade Federal do Rio Grande do Sul.

Profa. Dra. Sandra Denise Prado
Orientadora

PORTO ALEGRE, RS
2022

Signor, Edson Mateus.
Semiclassical theory for extreme events of quantum maps eigenstates / Edson Mateus Signor. -- 2022.
160 f.

Orientador: Sandra Denise Prado

Dissertação (Mestrado) - Universidade Federal do Rio Grande do Sul, Instituto de Física, Programa de Pós-Graduação em Física, Porto Alegre, BR-RS, 2022.

Caos Quântico. Eventos extremos. Distribuição de autoestados. Sistemas caóticos. Física Semiclássica. I. Prado, Sandra Denise., orient.

"I ... a universe of atoms, an atom in the universe." *(Richard P. Feynman, 1955)*

Agradecimentos

À minha orientadora Prof.ª Dra. Sandra Denise Prado pela sua orientação, atenção, ensinamentos e entusiasmo contagiante pela física.

À Gabriela Scalon pelo apoio e carinho durante a escrita desse trabalho.

À minha família que sempre me incentivaram ao longo do curso.

Aos colegas de metrado: Enrique Calderoli, Guilherme Shoiti e Antônio Carlan.

Por fim, à CAPES, ao CNPq e à UFRGS pelo suporte à pesquisa.

Resumo

Neste trabalho examinamos os eventos extremos das intensidades dos autoestados na base de posição de três mapas quânticos dependentes de parâmetros: o mapa padrão, mapa do gato perturbado e o mapa quicado de Harper. A fim de ampliar trabalhos anteriores, consideramos não apenas estados totalmente caóticos mas também autoestados nos regimes quase-integráveis e mistos. Especificamente, propusemos medir a curtose para quantificar e avaliar a cauda das distribuições das intensidades. Para todos os mapas abordados, um resultado notável são picos na curtose para valores de parâmetro específicos na região mista. Portanto, uma expressão semiclássica da curtose é alcançada através de uma média dupla pela posição e pelo espectro de energia dos autoestados, o qual nos permite a discutir possíveis explicações para o fenômeno. Por uma perspectiva semiclássica, ou seja, $\hbar \to 0$, defendemos a contribuição das ilhas estáveis para os picos na curtose, mas deixamos outras estruturas clássicas abertas para investigações futuras. Por fim, abordamos as fases quânticas e mostramos que elas também desempenham um papel importante.

Palavras-chave: Caos Quântico. Eventos extremos. Distribuição de autoestados. Sistemas caóticos. Física Semiclássica.

Abstract

In this work, we explore the extreme events of the eigenstate intensities in the position basis of three parameter-dependent quantum maps: standard map, perturbed cat map, and kicked Harper map. In order to expand previous works, we move forward considering not only fully chaotic states but eigenstates from near-integrable and mixed regimes. Namely, we propose the kurtosis measure to quantify and assess the tail of the intensities distributions. For all addressed maps, a conspicuous result is sharp peaks in the kurtosis for specific parameters in the mixed regime. Therefore, a semiclassical expression of kurtosis is achieved through a doubled average by the position and the energy spectrum of the eigenstates, which enables us to discuss possible explanations for the phenomenon. From a semiclassical perspective, i.e., $\hbar \to 0$, we advocate for the stable island contribution to the peaks in the kurtosis but let other classical structures open to forward inspections. Ultimately, we discourse the quantum phases and show that they also important play a role.

Key-words: Quantum chaos. Extreme events. Eigenstate distribution. Chaotic systems. Semiclassical physics.

Contents

1 Introduction **3**

2 Classical Mechanics **7**
2.1 Foundations of classical systems 8
2.1.1 Lagrange's mechanics 9
2.1.2 Hamilton-Jacobi's mechanics 13
2.1.3 Integrability 20
2.1.4 Periodic orbits 30
2.2 Classical Chaos 35
2.2.1 KAM theorem and Poincaré-Birkhoff fixed point theorem 37
2.2.2 Onset of chaos 39
2.3 Systems addressed 44
2.3.1 Kicked rotor 47
2.3.2 Kicked Harper Hamiltonian 50
2.3.3 Perturbed cat map 52

3 Semiclassical physics **55**
3.1 Stationary phase method 57
3.2 Semiclassical integrable systems 59
3.2.1 Trace formula for integrable systems 63
3.3 Semiclassical non-integrable systems 66
3.3.1 The propagator and the Green function 67
3.3.2 Semiclassical Green function 69
3.3.3 Gutzwiller trace formula 74
3.4 Semiclassical physics of classical maps 79

4 Extreme events in eigenstates of quantum maps **87**
4.1 Extreme statistics 88
4.2 Kurtosis 95
4.3 Inverse Participation Ratio 98

5 Semiclassical kurtosis and localization subject **101**
5.1 Bogomolny's scar formula 102
5.2 Results of the intensities kurtosis 112
5.3 Quantum phase contribution 118

6 Conclusion **123**

A The Maslov phase **127**

Bibliography **133**

Chapter 1

Introduction

Extended from east-central Africa to the Mediterranean Sea, the renowned Nile River provided adequate irrigation and fertile soil to ancient Egypt; in turn, it was essential to render them one of the world's earliest great civilizations. Such an achievement was only possible by means of the relentless awareness of the ancient civilization toward the river's conditions and primarily its depth variation. Consequently, for over five thousand years, Nile's water levels have been recorded, furnishing a whole spectrum of depth marks: from the lowest to the highest level. The precedence of the longest river in the world for the Egyptians is featured by their calendar, which was accordingly to the river floods (providing appropriate conditions for plantation) and droughts (the time when food was scarce) [1].

Namely, this specimen of humankind's history may enlighten us on how paramount the wisdom of the extreme values of the Nile's water levels, such as the period of floods (highest level marks) or droughts (lowest level marks). Moreover, the study of extreme events has been conducive to endless examples, e.g., stock market fluctuations, dynamical systems, meteorology, rogue wave predictions, and so forth [1, 2]. Our focal point in this work is to inspect the contribution of extreme event theory to quantum mechanics, especially to the eigenstates of quantum maps in the semiclassical regime, i.e., when $\hbar \to 0$, and delve into both theories in order to grasp the forthcoming outcomes.

Despite having taken time to arise, the extreme events theory has already shown a diverse richness of coverage and usefulness in quantum systems. For instance, experiments in quantum optics with light waves - which phases are initially random - have

revealed that the appearance of rogue waves (exceedingly light intensity) increased as the correlation between neighboring phases enhanced [3, 4]. In addition, the cumulative distributions of extreme variables have been shown to acknowledge a traveling front solution, perceived by a particle moving in a random potential [5] or a directed polymer on a Cayley tree [6].

Regarding quantum chaology, the prominent example is the Tracy-Widom distribution for the largest eigenvalues of an ensemble of random matrices [7, 8]. Conversely, when the subject is the eigenstates of such systems, the coverage is even more recent and less explored. In particular, the work of Lakshminaryan *et al.* [9] has addressed the distribution of the maximum intensities of the quantum standard map eigenstates when the classical counterpart of the quantum system is completely chaotic - dubbed chaotic states. Likewise, the paper of Srivastava *et al.* [10] has explored the upper records of the same eigenstates intensities. Hence, we intend to give a few more steps on this way to go.

Besides the extreme events problem being interesting per se, there is an aside subject that this study entails: the localization of the wavefunction. The eigenstates of the quantum maps are from the evolution operator in position or momentum basis, and consequently, extreme events of their respective intensities imply high probabilities in a specific state, i.e., the position or momentum of the system. In the 1990s and the beginning of the 2000s, wavefunction localization was one of the hot topics in quantum chaology. A myriad of quantum systems with their chaotic classical analogs or a mixture of stable and chaotic regions was analyzed, and many entities were discovered that could produce or enhance localization. For instance, in the semiclassical limit, unstable periodic orbits strikingly leave their traces in the quantum states, dubbed by Heller as "*scars*" [11].

In addition, other well-known classical structures give rise to localization: classical transport barriers as cantori [12], bifurcation of orbits resulting in the "twinkling" exponents [13, 14], and stable orbits [15]. On the other hand, purely quantum properties also play a significant role in the concentration of the wavefunction. For instance, the momentum eigenfunctions of the quantum kicked rotor - with an exponential localization - have been connected successfully to localized eigenstates of the Anderson

model, i.e., the electrical conductivity in systems with random scattering potentials [16]. On top of that, originating from the two-torus topology of the quantum maps and control parity and time-reversal symmetry, the quantum phases equally influence localization, as will be covered by this work. Therefore, all these underlying considerations will be reviewed when addressing the extreme events of the intensities.

Our work entails the extreme events occurring in the intensities of the eigenstates of three well-known quantum maps: the kicked rotor, the perturbed cat map, and the kicked Harper map. Handpicked by their perturbation-parameter dependence, these maps transit classically through stable and unstable structures by a simple modification in a parameter. As a consequence, their influence on the intensities is strikingly perceptible. Namely, we are interested in expanding the results of Lakshminaryan *et al.* [17] by including not only chaotic states but also mixed and near-integrable states.

Moreover, instead of using the conventional measure of localization of wavefunctions, the inverse partition ratio (IPR). We propose a simple, equivalent measure that is more familiar to statisticians, therefore, more inviting for a broad view of the problem: the kurtosis of the intensities distributions. It is the fourth standardized moment and measures the tail weight of the probability distribution - suitable to detect extremes in data. Hence, with the kurtosis and the perturbation parameter of each quantum map, we have a prompt response about what classical regimes are more favorable for extreme events.

In order to discern kurtosis' results, we bring up Keating & Prado's [14] approach. Firstly, we rely upon Bolgomony's scar formula for the semiclassical wavefunction of chaotic systems, which provides a separable expression into a mean plus a fluctuation. This arrangement yields access to the moment of the eigenstates intensities and, consequently, a semiclassical expression for the kurtosis. Since the semiclassical limit ($\hbar \to 0$) is settled, we dive into the asymptotic behavior of the kurtosis with the $\hbar$ and relate it to the quantum maps data. Along with those foundations, we can discriminate some dependencies and pinpoint prospective classical contributions to the kurtosis to comprehend extreme events' panorama. Ultimately, we include a more qualitative description of the symmetries' contribution to the tail regions of the

intensities distribution.

The work is presented according to the following: in chapter 2, all required classical topics for semiclassical physics will be addressed. Particularly, we shall go through the tenets of integrable systems and take a general overview of their chaotic counterparts. In addition, special attention will be given to the periodic orbits since, as pointed out by Poincaré, they are intelligible informants about the systems' general behavior.

In chapter 3, we shall turn to the quantum framework, but not through the Schrödinger equation. In fact, we shall rely upon semiclassical physics in order to bring classical chaotic behavior into quantum mechanics. Consequently, many concepts must be addressed: the stationary phase method, the semiclassical Green function, and the renowned Guztwiller's trace formula. Thus, all culminates in quantizing our classical maps and perceiving their semiclassical behavior.

In particular, chapter 2 and chapter 3 present a thorough, meticulous inspection of the former about classical mechanics and the latter about semiclassical physics. This measure has been adopted because the conventional literature is widely diffused and complicated to pursue, especially for new students interested in the topic. Therefore, professors and doctorates more acquainted with those concepts are invited to tunnel the dissertation to chapter 4. Any subject that seems unfamiliar can be promptly checked in the previous chapter.

Chapter 4 will introduce the main results of the dissertation when we shall set the eigenstates intensities of our quantum maps and explore their extreme values. Benefiting from the kurtosis definition, we can investigate the extreme events for different classical regimes: near-integrable, mixed, and chaotic. The exploration will unveil an inquisitive region where the kurtosis reaches sharp peaks, indicating wavefunction localization. Finally, in chapter 5, we shall implement semiclassical physics to grasp better what is occurring in these regions of the quantum maps. Thereafter, chapter 6 will finish the work by presenting our conclusions and perspectives.

Chapter 2

Classical Mechanics

Our work encompasses quantum systems whose Hamiltonian has a perturbation parameter in its non-linearity. Despite being deterministic, their classical counterparts are known to furnish natural randomness from chaos theory. When we consider the semiclassical limit, i.e., the characteristic action of the quantum system is larger than $\hbar$, classical and quantum properties start to coalesce. Therefore, the present chapter is committed to exploiting fundamental topics of classical mechanics to discriminate and evaluate when we shall bring the quantum Hamiltonian to the semiclassical approximation. We initiate examining Lagrange's and Hamilton-Jacobi's formulations in which the first has time as a parameter and the second has energy as a parameter. Those developments discriminate the different caustics that influence the semiclassical wavefunction of the system afterward.

Moreover, we have to grasp the role of the invariant surfaces and the integrability of the systems. From Arnold-Liouville's theorem, the set of invariant surfaces builds up constants of motion that allow us to define the action-angle variables. They transform positions into angles and conjugate moments into action variables, whereby both configure an invariant tori in phase space - the quintessence of integrable systems. Subsequently, we dig into prominent hallmarks included in a general Hamiltonian system, such as KAM and Poincaré-Birkhoff fixed point theorems, stable and unstable trajectories, periodic orbits, and bifurcations. In order to exemplify the aggregate of the classical chaos, we select periodic-driven systems which result in classical maps. Boasting a simple manipulation and a straightforward route to chaos, they will be tapped into to discuss the influence of non-linearity in the quantum system in the semiclassical regime later on.

2.1 Foundations of classical systems

Despite Newton's law guaranteeing to solve any classical problem, some have constraints that make pursuing a solution arduous. From this reasoning, emerging in the 18th century, the variational principle replaced Newton's approach providing an elegant and transparent treatment for classical systems. The French mathematician Pierre Louis Moreau de Maupertuis (1698-1759) in 1744 and right after the Swiss mathematician Leonard Euler (1707-1783) were the proponents of the variational principle relying on only geometric interpretations, which turns their work unique [18]. Thereafter, in 1760, Joseph Louis Lagrange (1736-1813) contributed by introducing the variational calculus, but William Rowan Hamilton (1805-1865), approximately 75 years later, presented the Lagrangian $L = T - V$ and furthered the basic notions of variational principle that we use today [19].

That said, adopting a definition of Gutzwiller [19], we split classical mechanics into two: the mechanics of Lagrange - where time is the primary parameter - and the mechanics of Hamilton-Jacobi - where energy is the primary parameter. The difference between these classifications in a classical system may not immediately make sense; however, when we shall cover the semiclassical regime, the distinction will be fundamental.

Before going any further, there is an inherent dichotomy about paths and trajectories in classical and quantum mechanics, and a distinct definition of both must be settled. Since the position coordinates $\mathbf{q} = (q_1, q_2, \ldots, q_n)$ and velocities $\dot{\mathbf{q}} = (\dot{q}_1, \dot{q}_2, \ldots, \dot{q}_n)$ describe a mechanical system in any fixed instant of time t, a path will be an arbitrary, continuous function $\mathbf{q}(\tau)$ where τ is a real variable that varies from the initial time t' to final time t''. The smoothness of $q_i(\tau)$ is imposed to avoid mathematical issues, and by definition, a myriad of paths are available for a given time interval. On the other hand, with the initial position $\mathbf{q}(t') = \mathbf{q}'$ and the final position $\mathbf{q}(t'') = \mathbf{q}''$, a trajectory is a function $\mathbf{q}(t)$ that corresponds to the variational principle and is the solution of the equations of motion.

2.1.1 Lagrange's mechanics

First, we define a function that depends on the position $\mathbf{q}(t)$ and the velocity $\dot{\mathbf{q}}(t)$ and provides us with information about how these variables evolve through time. The function is dubbed the Lagrangian $L(\mathbf{q}(t), \dot{\mathbf{q}}(t), t)$ which its most common form is $L = T - V$ (T is kinetic energy and V potential energy). In addition, the variational principle requires another variable called momentum. Its formal definition takes place when the principle is stated. However, in possession of the Lagrangian, the momentum p_i conjugated to the position q_i is

$$p_i = \frac{\partial}{\partial \dot{q}_i} L(\mathbf{q}(t), \dot{\mathbf{q}}(t), t). \tag{2.1}$$

Thus, we are equipped to state the variational principle.

Fixing the initial $\mathbf{q}(t')$ and final $\mathbf{q}(t'')$ positions, we follow a trajectory $\mathbf{q}_0(t)$ evolving through the interval $t' \leq t \leq t''$. Now, surrounding $\mathbf{q}_0(t)$, different neighboring paths take place and can be characterized by a smooth function dubbed displacement $\delta\mathbf{q}(t) = (\delta q_1, \delta q_2, \ldots, \delta q_n)$. Consequently, their position are simply $\mathbf{q}(t) = \mathbf{q}_0(t) + \delta\mathbf{q}(t)$, as it is shown in the figure 2.1. With this knowledge of the neighborhood, the variational principle is based on a functional: the integral of the Lagrangian over t in the fixed interval $[t', t'']$

$$\mathcal{R}(\mathbf{q}', t', \mathbf{q}'', t'') = \int_{t'}^{t''} L(\mathbf{q}(t), \dot{\mathbf{q}}(t), t) dt. \tag{2.2}$$

In order to evaluate the functional, we can expand it in powers of $\delta\mathbf{q}(t)$ and obtain

$$\mathcal{R}(\mathbf{q}', t', \mathbf{q}'', t'') = \mathcal{R}(\mathbf{q}_0', t', \mathbf{q}_0'', t'') + \sum_i \frac{\partial \mathcal{R}}{\partial q_i} \delta q_i + \frac{1}{2} \sum_{ij} \frac{\partial^2 \mathcal{R}}{\partial q_i \partial q_j} \delta q_i \delta q_j + \mathcal{O}(3). \tag{2.3}$$

In classical mechanics, the first third terms are notorious and have significant implications. The first is known as Hamilton's principal function or merely the action integral. Since it only depends on the trajectory $\mathbf{q}_0(t)$ along the interval $t' \leq t \leq t''$, we rewrite it as

$$\mathcal{R}(\mathbf{q}_0', t', \mathbf{q}_0'', t'') = R(\mathbf{q}', t', \mathbf{q}'', t'') = \int_{t'}^{t''} L(\mathbf{q}_0(t), \dot{\mathbf{q}}_0(t), t) dt. \tag{2.4}$$

The regular example is the free particle ($V = 0$ and $T = m\dot{q}^2/2$) which has an action integral equals to

$$R(\mathbf{q}', t', \mathbf{q}'', t'') = \frac{m(q'' - q')^2}{2(t'' - t')}. \tag{2.5}$$

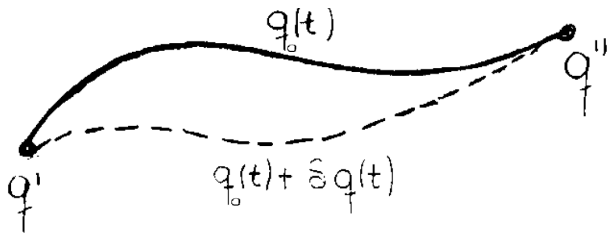

FIGURE 2.1. Illustration of a trajectory (solid line) which follows the function $\mathbf{q}_0(t)$ and a neighboring path (dashed line), which the displacement $\delta\mathbf{q}(t)$ conducts its evolution [20].

Furthermore, if we fix a trajectory $\mathbf{q}_0$ and start to vary its time t, initial position $\mathbf{q}'$, or final position $\mathbf{q}''$, we must ensure that the trajectory alters continuously. Hence, the action $R(\mathbf{q}', \mathbf{q}'', t = t'' - t')$ must satisfy the following relations[1]

$$\mathbf{p}' = \mathbf{p}(t') = -\frac{\partial R(q', q'', t)}{\partial q'}, \quad \mathbf{p}'' = \mathbf{p}(t'') = \frac{\partial R(q', q'', t)}{\partial q''}, \quad E = -\frac{\partial R(q', q'', t)}{\partial t}. \tag{2.6}$$

The second term, the first variation, is the kernel of the variational principle. We begin with Maupertuis, who claimed the minimal action principle, i.e., any change in nature follows the minimal quantity of action. Although the minimal actions had a religious justification from Maupertuis, Hamilton adopted the theory and required that the first variation of the functional $\mathcal{R}(\mathbf{q}', t', \mathbf{q}'', t'')$ vanishes for any path which starts at $\mathbf{q}'_0$ and goes to $\mathbf{q}''_0$. Similarly, $\delta\mathbf{q}(t') = \delta\mathbf{q}(t'') = 0$. Imposing these conditions and involving the neighboring paths, through a careful calculation, it is possible to recover Euler's equation [18]

$$\frac{d}{dt}\left(\frac{\partial L}{\partial \dot{q}_i}\right) - \frac{\partial L}{\partial q_i} = 0, \tag{2.7}$$

which furnishes the equation of motion in Lagrange's formulation. Moreover, to broaden in generality, through Lagrange multipliers, one can even develop a formula for constraint forces. A full description of Euler's equation and the first variation can be seen in iconic textbooks of analytical mechanics [18, 21, 22].

Finally, only in 1842 Jacobi stated the first resolutions to the character of the trajectories when the extreme condition is set. The previous reasoning about the quote, unquote, "minimal action," unravel the necessary assessment of the third term on the trajectories, called the second variation. Having asserted that the first variation vanishes, we cannot affirm instantly whether the trajectory is a minimum; however, it can

[1] A complete derivation of 2.6 can be seen in [18]

be a more general extremum, such as a maximum, minimum, or saddle-point. Thus, from equation 2.3, the matrix $\partial^2\mathcal{R}/\partial q_i \partial q_j$ must be analyzed in order to grasp the character of the extremum. Because it is a real and symmetric matrix, the matrix can be diagonalized with an orthogonal transformation; in other words, we are able to encounter its eigenvectors and eigenvalues to determine the neighborhood topology.

Nevertheless, between the 1920s and 1930s, Marston Morse discovered that the answer to the nature of the extremum was in the neighboring trajectories of $\mathbf{q}_0(t)$, i.e., the displacement is not in the paths anymore but in the trajectories - so $\mathcal{R} \to R$. He carried the identical expansion around $\mathbf{q}_0(t)$ and obtained a formula with the displacement in the Fourier series. Since the constraints conditions $\delta\mathbf{q}(t') = \delta\mathbf{q}(t'') = 0$ eliminate the cosine part, and consequently,

$$\delta\mathbf{q}(t) = \sum_{n=1}^{\infty} \mathbf{a}_n \sin\left[n\pi\left(\frac{t-t'}{t''-t'}\right)\right] \tag{2.8}$$

where $\mathbf{a}_n$ are the real coefficients. Considering sufficient short times, we can neglect the effect of potentials and work with free particles. Taking the action in 2.5 and evaluating the expansion 2.8, it is straightforward to demonstrate that the trajectory indeed corresponds to a minimum, i.e., all eigenvalues of $\partial^2 R/\partial q_i \partial q_j$ are positive. Nonetheless, when time starts to run, and the potential plays its role, the matrix will be modified and its eigenvalues accordingly.

To make it clearer, let us establish the initial conditions with a null displacement, which means that the neighboring trajectories at $t = t'$ have only different initial momenta characterized by $\mathbf{p}' = \mathbf{p}_0(t') + \delta\mathbf{p}(t')$. This produces a fan of trajectories moving away from $\mathbf{q}'$ and spreading until the time t'' - the figure 2.2 exemplifies the situation. All this settled, it is expected that each trajectory (identified by the displacement in the initial momentum $\delta\mathbf{p}'$) will have a different final position yielding a deviation $\delta\mathbf{q}''$. The ratio of this relation is

$$\frac{\delta\mathbf{p}'}{\delta\mathbf{q}''} = -\frac{\partial^2 R}{\partial\mathbf{q}''\partial\mathbf{q}'} \tag{2.9}$$

where we used the first equation in 2.6 to obtain the second variation. Morse noticed that the matrix diverges for trajectories when a small displacement in the initial momentum does not change its final position. In other words, $\delta\mathbf{p}'/\delta\mathbf{q}'' \to \infty$ when $\delta\mathbf{q}'' = 0$. The times when the divergence occurs are dubbed focus, and the straightforward example is a one-dimensional harmonic oscillator. Its solution is $x(t) = A\sin\omega t$ with

initial momentum $p(0) = Am\omega$, and if we vary A, the resulting trajectories are depicted in figure 2.3. It is evident that all return to the same point $x = 0$ after an interval π/ω; therefore, the focuses take place in times $t = k\pi/\omega$ where k are integers. On top of that, the fan of trajectories can perform an envelope similar to glancing reflection from a wall, figure 2.2, we called this envelope a caustic, which also produces divergence in the second variation.

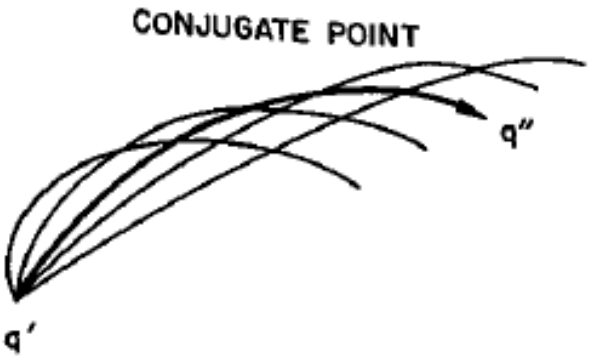

FIGURE 2.2. Fan of trajectories constructed through neighboring trajectories with only non-zero initial momentum displacement until a time t''. Moreover, the illustration exemplifies a caustic since the trajectories constitute an envelope making $\delta\mathbf{p}'/\delta\mathbf{q}'' \to \infty$ [19].

That said, Marston Morse stated the following proposition: for short times, the classic trajectories correspond to a minimum in action. Increasing the time, every instant that the trajectory crosses a point where

$$\det\left[\frac{\partial^2 R}{\partial\mathbf{q}''\partial\mathbf{q}'}\right] \to \infty, \tag{2.10}$$

the second variation of $R(\mathbf{q}', t', \mathbf{q}'', t'')$ earns a negative eigenvalue; this point is called conjugated. Consequently, the matrix will have as many negative eigenvalues as there are conjugate points along the trajectory.

Although all the caustics and conjugate points discussions seem unrelated to quantum chaos, semiclassical physics has shown their relevance when studying WKB approximation. For instance, the Gutzwiller formula predicts that the wavefunction is proportional to the square of the second variation matrix.

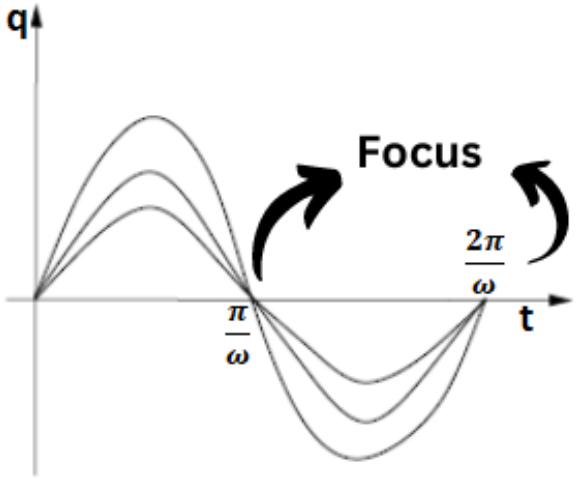

FIGURE 2.3. Solutions of the harmonic oscillator for three different amplitude values A. All the trajectories coalesce at $x = 0$ after a period of $k\pi/\omega$ [23].

2.1.2 Hamilton-Jacobi's mechanics

Now, to change the dependence on time to energy, we will introduce Hamilton-Jacobi's mechanics. Classically, some problems benefit from a time-energy modification. For example, whether we require to calculate the necessary energy for an expedition to Mars. To begin, in Lagrange's formalism, position $\mathbf{q}$ and velocity $\dot{\mathbf{q}}$ describe the system with the assistance of the Lagrangian L. In Hamilton's formalism, the first step is to alter the specificity of the system's state to position $\mathbf{q}$ and momentum $\mathbf{p}$ (equation 2.1). The easiest way is through a Legendre transformation, whereby the new function - the Hamiltonian - employs the derivatives of the previous one - the Lagrangian - as a new variable.

We, ergo, settle the relationship between the Hamiltonian and the Langrangian

$$H(\mathbf{q}, \mathbf{p}, t) = \sum_i p_i \dot{q}_i - L(\mathbf{q}, \dot{\mathbf{q}}, t) \tag{2.11}$$

and from the Legendre transformation, the differential is

$$\begin{aligned} dH &= \sum_i \frac{\partial H}{\partial q_i} dq_i + \frac{\partial H}{\partial p_i} dp_i + \frac{\partial H}{\partial t} dt, \\ &= \sum_i \dot{q}_i dp_i + p_i d\dot{q}_i - \frac{\partial L}{\partial q_i} dq_i - \frac{\partial L}{\partial p_i} dp_i - \frac{\partial L}{\partial t} dt, \\ &= \sum_i \dot{q}_i dp_i - \frac{\partial L}{\partial q_i} dq_i - \frac{\partial L}{\partial t} dt. \end{aligned} \tag{2.12}$$

Comparing the last line with the first of the differential, we obtain the equations of motion:

$$\dot{q}_i = \frac{\partial H}{\partial pi} \quad \text{and} \quad \dot{p}_i = -\frac{\partial H}{\partial qi}. \tag{2.13}$$

With a careful look at the equations of motion, we can interpret a vector field in the phase space with the gradient of H driving the flow in a peculiar manner - because of the opposite signs. Regarding this reasoning, for a system with n degrees of freedom, we define a single vector $\eta = (q_1 \dots q_n p_1 \dots p_n)^T$ and a corresponding gradient $\nabla_\eta = (\partial/\partial q_1 \dots \partial/\partial q_n \, \partial/\partial p_1 \dots \partial/\partial p_n)^T$. In order to address opposing signs, we define the symplectic matrix

$$\mathbf{J} = \begin{pmatrix} \mathbf{0} & \mathbf{1} \\ -\mathbf{1} & \mathbf{0} \end{pmatrix}, \tag{2.14}$$

as a consequence, the equations of motion are simply $\dot{\eta} = \mathbf{J}\nabla_\eta H$ [2].

Finally, we inspect that the total time derivative of H is equal to the partial time derivative

$$\begin{aligned} \frac{dH}{dt} &= \sum_i \frac{\partial H}{\partial q_i}\frac{\partial q_i}{\partial t} + \frac{\partial H}{\partial p_i}\frac{\partial p_i}{\partial t} + \frac{\partial H}{\partial t}, \\ &= \sum_i (-\dot{p}_i)\dot{q}_i + \dot{q}_i\dot{p}_i + \frac{\partial H}{\partial t}, \\ &= \frac{\partial H}{\partial t}. \end{aligned} \tag{2.15}$$

From the third line of 2.12, we get

$$\frac{dH}{dt} = \frac{\partial H}{\partial t} = -\frac{\partial L}{\partial t}. \tag{2.16}$$

Hence, if the Lagrangian does not depend on time, the Hamiltonian $H(\mathbf{q}, \mathbf{p})$ remains constant along the trajectory. Naturally, we define a constant value E that conform $H(\mathbf{q}, \mathbf{p}) = E$. The immediate parity of the Hamiltonian and the energy is not always true, even though H is conservative. Nevertheless, for the systems utilized throughout the dissertation, the equality holds, in addition to the formula $H = T + V$ with $T = \mathbf{p}^2/2m$. Therefore, the variable E is the precise candidate to replace t for a given trajectory, and their duality has innate meaning when we deal with quantum mechanics.

[2] Therefore, the classical mechanics is part of the symplectic geometry which $\mathbf{J}$ is its cornerstone.

Having defined the constant value E, we are able to interchange with t as a system's variable. The foremost transformation lies in the action where we have to replace the old action $R(\mathbf{q}', \mathbf{q}'', t)$ to a new one $S(\mathbf{q}', \mathbf{q}'', E)$. The resulting interpretation is still fixing the initial and final position of a trajectory; however, instead of considering a interval of time t, now the trajectory must follow a constant energy E. Thus, similarly to the Hamiltonian definition, we apply a Legendre transformation

$$S(\mathbf{q}', \mathbf{q}'', E) = R(\mathbf{q}', \mathbf{q}'', t) + Et, \tag{2.17}$$

and the differential is

$$\begin{aligned} dS &= \frac{\partial S}{\partial \mathbf{q}'} d\mathbf{q}' + \frac{\partial S}{\partial \mathbf{q}''} d\mathbf{q}'' + \frac{\partial S}{\partial t} dt, \\ &= Edt + tdE + \frac{\partial R}{\partial \mathbf{q}'} d\mathbf{q}' + \frac{\partial R}{\partial \mathbf{q}''} d\mathbf{q}'' + \frac{\partial R}{\partial t} dt, \\ &= Edt + tdE - \mathbf{p}' d\mathbf{q}' + \mathbf{p}'' d\mathbf{q}'' + Edt, \\ &= -\mathbf{p}' d\mathbf{q}' + \mathbf{p}'' d\mathbf{q}'' + tdE, \end{aligned} \tag{2.18}$$

where we have used the equation 2.6. Comparing the first and the last line of 2.18, we arrive at the relations with the new action

$$\mathbf{p}' = -\frac{\partial S(\mathbf{q}', \mathbf{q}'', E)}{\partial \mathbf{q}'}, \quad \mathbf{p}'' = \frac{\partial S(\mathbf{q}', \mathbf{q}'', E)}{\partial \mathbf{q}''}, \quad t = \frac{\partial S(\mathbf{q}', \mathbf{q}'', E)}{\partial E}. \tag{2.19}$$

As aforementioned in Lagrange's mechanics, in order to evaluate the extremum of the classical trajectory, we took a fan of it starting from the same position but with different initial momenta (different energy) and let them evolve in a defined time. On the other hand, we are now restricted to the energy $H = E$, which will intuitively lead to a new interpretation of 2.9 since the momenta are not arbitrary anymore, in addition to new sorts of caustics and conjugate points.

The new role of the caustics requires more meticulous deliberation because of their discrepancies from Lagrange's formulation. Previously, we fixed the initial $\mathbf{q}'$ and evolved trajectories with different initial momentum $\mathbf{p}'$, which generates a variation in energy δE, until a time t - the caustic was the ratio divergence of the deviation in the initial momentum and the deviation in the final position (see figure 2.4a). On the contrary, now the trajectories must have the same energy, so the time to roam from $\mathbf{q}'$ to $\mathbf{q}''$ will be different (see figure 2.4b). The correction for the new configuration is the

insertion of an energy variation in the initial momentum and a time variation in the final position leading to

$$\frac{\delta \mathbf{p}'/\delta E}{\delta \mathbf{q}''/\delta t} = \frac{\partial \mathbf{p}'}{\partial \mathbf{q}''}\frac{\partial t}{\partial E} = -\frac{\partial^2 R}{\partial \mathbf{q}''\partial \mathbf{q}'}\Bigg/\frac{\partial^2 R}{\partial t^2}, \tag{2.20}$$

which we used the old action with the equations 2.6. The inclusion of the energy and time variations into the ratio $\partial \mathbf{p}'/\partial \mathbf{q}''$ can be interpreted as if we perform a variation in energy δE with fixed initial and final positions, then the time elapsed must also vary to the swarm of trajectories remain constrained in the energy surface [19].

The paramount result lies in the determinant of 2.20, known as the density of trajectories on the energy of surface $D(\mathbf{q}', \mathbf{q}'', E)$

$$D(\mathbf{q}', \mathbf{q}'', E) = \det\left[-\frac{\partial^2 R}{\partial \mathbf{q}''\partial \mathbf{q}'}\right]\Bigg/\frac{\partial^2 R}{\partial t^2}. \tag{2.21}$$

This function essentially describes how the neighborhood of a trajectory spreads out, and in the next chapter, we shall see that the square root of $D(\mathbf{q}', \mathbf{q}'', E)$ will be directly proportional to the amplitude of the quantum system wavefunction for a given trajectory. However, we need to adjust 2.21 to include $S(\mathbf{q}', \mathbf{q}'', E)$.

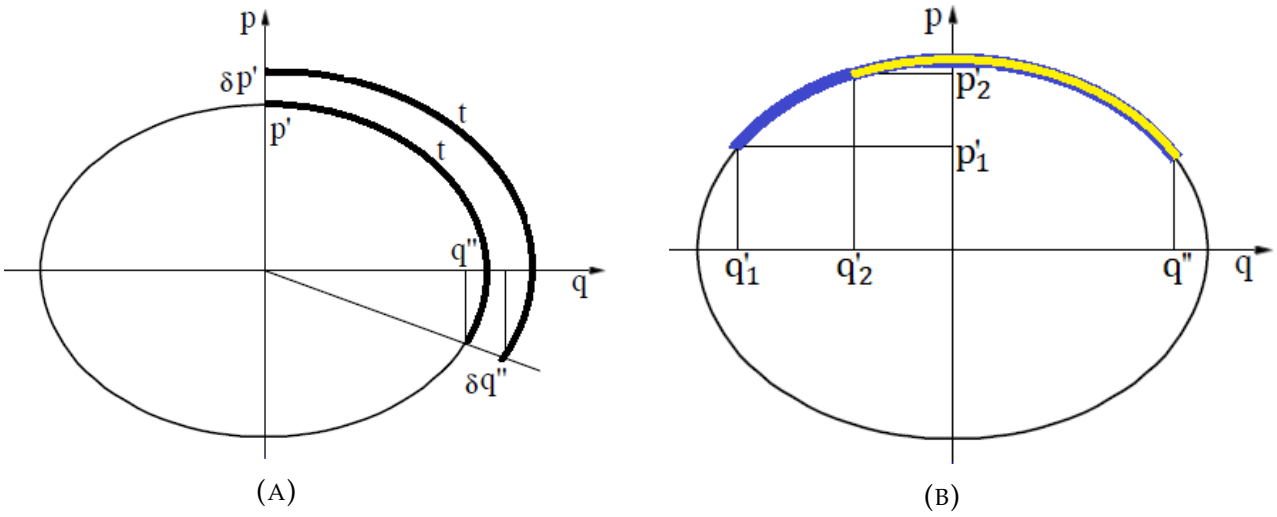

FIGURE 2.4. (A) Two trajectories with distinct initial momentum resulting in a displacement in the final position after elapsed a time t. In Lagrange's mechanics, a caustic is constituted when the ratio $\mathbf{p}'/\mathbf{q}''$ diverges. (B) Illustration of two trajectories that must remain in a constant energy surface with the identical final position, respecting Hamilton-Jacobi's formulation. Both the initial position and momentum of the second trajectory can be described as $q_2' = q_1' + \epsilon \dot{q}_1'$ and $p_2' = p_1' + \epsilon \dot{p}_1'$, respectively.

From the third equation in 2.19, the time as a function of the independent variables $t = t(\mathbf{q}', \mathbf{q}'', E)$ is obtained. So, with the third equations of 2.6 and 2.19, the denominator of D is

$$\frac{\partial^2 R}{\partial t^2} = -\frac{\partial E}{\partial t} = -\left[\frac{\partial t}{\partial E}\right]^{-1} = -\left[\frac{\partial^2 S}{\partial E^2}\right]^{-1}. \tag{2.22}$$

The determinant, otherwise, has a more elaborated calculation. Starting from the first derivative according to 2.17 and applying the third equation of 2.19

$$\frac{\partial R}{\partial \mathbf{q}''} = \frac{\partial S}{\partial \mathbf{q}''} + \frac{\partial E}{\partial \mathbf{q}''}\frac{\partial S}{\partial E} - t\frac{\partial E}{\partial \mathbf{q}''} = \frac{\partial S}{\partial \mathbf{q}''}, \tag{2.23}$$

the matrix is

$$\frac{\partial^2 R}{\partial \mathbf{q}'\partial \mathbf{q}''} = \frac{\partial^2 S}{\partial \mathbf{q}'\partial \mathbf{q}''} + \frac{\partial^2 S}{\partial E \partial \mathbf{q}''}\frac{\partial E}{\partial \mathbf{q}'}. \tag{2.24}$$

We can rewrite the derivative $\partial E/\partial \mathbf{q}'$ as

$$\begin{aligned}
\frac{\partial E}{\partial \mathbf{q}'} &= -\frac{\partial^2 R}{\partial \mathbf{q}'\partial t} = -\frac{\partial}{\partial t}\left[\frac{\partial R}{\partial \mathbf{q}}\right], \\
&= -\frac{\partial}{\partial t}\left[\frac{\partial S}{\partial \mathbf{q}}\right] = -\frac{\partial^2 S}{\partial \mathbf{q}'\partial E}\frac{\partial E}{\partial t}, \\
&= -\frac{\partial^2 S}{\partial \mathbf{q}'\partial E}\left(-\frac{\partial^2 R}{\partial t^2}\right) = \frac{\partial^2 S}{\partial \mathbf{q}'\partial E}\left[\frac{\partial^2 S}{\partial E^2}\right]^{-1},
\end{aligned} \tag{2.25}$$

and by substituting the previous equation in the matrix $\partial^2 R\partial/\mathbf{q}'\partial \mathbf{q}''$, the density culminates in

$$D(\mathbf{q}', \mathbf{q}'', E) = \frac{\partial^2 S}{\partial E^2}\det\left[\frac{\partial^2 S}{\partial \mathbf{q}'\partial \mathbf{q}''} - \frac{\partial^2 S}{\partial \mathbf{q}''\partial E}\frac{\partial^2 S}{\partial \mathbf{q}'\partial E}\left(\frac{\partial^2 S}{\partial E^2}\right)^{-1}\right]. \tag{2.26}$$

Now, if we set the ensuing definition

$$B_{ij} = \frac{\partial^2 S}{\partial q_i \partial q_j}, \quad u_i = \frac{\partial^2 S}{\partial q_i'' \partial E}, \quad v_i = \frac{\partial^2 S}{\partial q_i' \partial E} \quad q = \frac{\partial^2 S}{\partial E^2} \tag{2.27}$$

the density will have an elementary form

$$D(\mathbf{q}', \mathbf{q}'', E) = q\det\left[B_{ij} - u_i v_j/q\right] = \det\left|\begin{array}{c|c} \mathbf{B} & \mathbf{u} \\ \hline \mathbf{v} & q \end{array}\right|. \tag{2.28}$$

The demonstration of the previous outcome initiates by opening the determinant

$$\det\left|\begin{array}{c|c} \mathbf{B} & \mathbf{u} \\ \hline \mathbf{v} & q \end{array}\right| = \begin{vmatrix} B_{11} & B_{12} & \dots & B_{1n} & u_1 \\ B_{21} & B_{22} & \dots & B_{2n} & u_2 \\ \vdots & \vdots & \ddots & \vdots & \vdots \\ B_{n1} & B_{n2} & \dots & B_{nn} & u_n \\ v_1 & v_2 & \dots & v_n & q \end{vmatrix}, \tag{2.29}$$

and the first procedure is to take advantage of the invariance property of determinants by performing the substitution:

$$(k\text{th row}) \to (k\text{th row}) - \frac{u_k}{q}(\text{last row}), \qquad \text{for } k = 1, 2, \ldots, n,$$

resulting in

$$\det \left| \begin{array}{c|c} \mathbf{B} & \mathbf{u} \\ \hline \mathbf{v} & q \end{array} \right| = \begin{vmatrix} B_{11} - u_1 v_1/q & B_{12} - u_2 v_2/q & \ldots & B_{1n} - u_n v_n/q & 0 \\ B_{21} - u_2 v_1/q & B_{22} - u_2 v_2/q & \ldots & B_{2n} - u_n v_n/q & 0 \\ \vdots & \vdots & \ddots & \vdots & \vdots \\ B_{n1} - u_n v_1/q & B_{n2} - u_n v_2/q & \ldots & B_{nn} - u_n v_n/q & 0 \\ v_1 & v_2 & \ldots & v_n & q \end{vmatrix} \tag{2.30}$$

Hence, taking the cofactor expansion of the last column, the determinant is simply

$$\det \left| \begin{array}{c|c} \mathbf{B} & \mathbf{u} \\ \hline \mathbf{v} & q \end{array} \right| = q \det \left[B_{ij} - u_i v_j / q \right]. \tag{2.31}$$

Returning to the original variables, the density becomes

$$D(\mathbf{q}', \mathbf{q}'', E) = \det \begin{vmatrix} \frac{\partial^2 S}{\partial \mathbf{q}' \partial \mathbf{q}''} & \frac{\partial^2 S}{\partial \mathbf{q}'' \partial E} \\ \frac{\partial^2 S}{\partial \mathbf{q}' \partial E} & \frac{\partial^2 S}{\partial E^2} \end{vmatrix}. \tag{2.32}$$

Another simplification of the density expression can be performed if we establish distinctive coordinates of the system. Gutzwiller [19] has introduced a local coordinate system that accentuates the neighborhood of a trajectory from $\mathbf{q}'$ to $\mathbf{q}''$. The first coordinate $q_1 = x$ runs along the particular trajectory in phase space; the remaining coordinates $(q_2, \ldots, q_{n-1}) = (y_2, \ldots, y_{n-1})$ are transverse to the trajectory - they are at right angles to the motion direction along the trajectory. To begin, regardless of the coordinate system, the energy is conserved. As a consequence,

$$H\left(\mathbf{q}', -\frac{\partial S}{\partial \mathbf{q}'}\right) = E = H\left(\mathbf{q}'', +\frac{\partial S}{\partial \mathbf{q}''}\right), \tag{2.33}$$

we differentiate both sides with respect to E to obtain

$$\sum_{i=1}^{n} -\frac{\partial^2 S}{\partial E \partial q_i'} \frac{\partial H}{\partial p_i'} = 1 = \sum_{i=1}^{n} +\frac{\partial^2 S}{\partial E \partial q_i''} \frac{\partial H}{\partial p_i''}, \tag{2.34}$$

Introducing our new local coordinates, we have

$$\dot{\mathbf{q}} = \frac{\partial H}{\partial \mathbf{p}} = (|\dot{x}|, 0 \ldots, 0), \tag{2.35}$$

and the equation 2.34 is non-null solely for $i = 1$ leading to

$$\frac{\partial^2 S}{\partial E \partial x'} = -\frac{1}{|\dot{x}'|} = -\frac{1}{|\dot{\mathbf{q}}'|}, \qquad \frac{\partial^2 S}{\partial E \partial x''} = +\frac{1}{|\dot{x}''|} = +\frac{1}{|\dot{\mathbf{q}}''|}. \tag{2.36}$$

Now, with the equation 2.33, we differentiate it with respect to q_i'' for the left-handed side and with respect to q_i' for the right-handed side

$$\sum_j \frac{\partial H}{\partial p_j'} \frac{\partial^2 S}{\partial q_i'' q_j'} = 0 = \sum_j \frac{\partial H}{\partial p_j''} \frac{\partial^2 S}{\partial q_i' q_j''}, \quad \text{for } i, j = 1, 2, \ldots, n. \tag{2.37}$$

The equation 2.35 can be implemented, and we get the ensuing result

$$\frac{\partial^2 S}{\partial q_i'' \partial x'} = \frac{\partial^2 S}{\partial q_i' \partial x''} = 0, \quad \text{for all } i. \tag{2.38}$$

Therefore, opening the density once more

$$D(\mathbf{q}', \mathbf{q}'', E) = \det \begin{vmatrix} \frac{\partial^2 S}{\partial \mathbf{q}' \partial \mathbf{q}''} & \frac{\partial^2 S}{\partial \mathbf{q}'' \partial E} \\ \frac{\partial^2 S}{\partial \mathbf{q}' \partial E} & \frac{\partial^2 S}{\partial E^2} \end{vmatrix} = \begin{vmatrix} \frac{\partial^2 S}{\partial x' \partial x''} & \frac{\partial^2 S}{\partial x' \partial y_1''} & \cdots & \frac{\partial^2 S}{\partial x' \partial y_{n-1}''} & \frac{\partial^2 S}{\partial x'' \partial E} \\ \frac{\partial^2 S}{\partial y_1' \partial x''} & \frac{\partial^2 S}{\partial y_1' \partial y_1''} & \cdots & \frac{\partial^2 S}{\partial y_1' \partial y_{n-1}''} & \frac{\partial^2 S}{\partial y_1'' \partial E} \\ \frac{\partial^2 S}{\partial y_2' \partial x''} & \frac{\partial^2 S}{\partial y_2' \partial y_1''} & \cdots & \frac{\partial^2 S}{\partial y_2' \partial y_{n-1}''} & \frac{\partial^2 S}{\partial y_2'' \partial E} \\ \vdots & \vdots & \ddots & \vdots & \vdots \\ \frac{\partial^2 S}{\partial y_{n-1}' \partial x''} & \frac{\partial^2 S}{\partial y_{n-1}' \partial y_1''} & \cdots & \frac{\partial^2 S}{\partial y_{n-1}' \partial y_{n-1}''} & \frac{\partial^2 S}{\partial y_{n-1}'' \partial E} \\ -\frac{\partial^2 S}{\partial x' \partial E} & \frac{\partial^2 S}{\partial y_1' \partial E} & \cdots & \frac{\partial^2 S}{\partial y_{n-1}' \partial E} & \frac{\partial^2 S}{\partial E^2} \end{vmatrix}, \tag{2.39}$$

it can be rewritten using 2.36 and 2.38

$$D(\mathbf{q}', \mathbf{q}'', E) = \begin{vmatrix} 0 & 0 & \cdots & 0 & \frac{1}{|\dot{\mathbf{q}}''|} \\ 0 & \frac{\partial^2 S}{\partial y_1' \partial y_1''} & \cdots & \frac{\partial^2 S}{\partial y_1' \partial y_{n-1}''} & \frac{\partial^2 S}{\partial y_1'' \partial E} \\ 0 & \frac{\partial^2 S}{\partial y_2' \partial y_1''} & \cdots & \frac{\partial^2 S}{\partial y_2' \partial y_{n-1}''} & \frac{\partial^2 S}{\partial y_2'' \partial E} \\ \vdots & \vdots & \ddots & \vdots & \vdots \\ 0 & \frac{\partial^2 S}{\partial y_{n-1}' \partial y_1''} & \cdots & \frac{\partial^2 S}{\partial y_{n-1}' \partial y_{n-1}''} & \frac{\partial^2 S}{\partial y_{n-1}'' \partial E} \\ -\frac{1}{|\dot{\mathbf{q}}'|} & \frac{\partial^2 S}{\partial y_1' \partial E} & \cdots & \frac{\partial^2 S}{\partial y_{n-1}' \partial E} & \frac{\partial^2 S}{\partial E^2} \end{vmatrix} \tag{2.40}$$

and again employing first the cofactor expansion of the first row and subsequently the cofactor expansion of the first column, we earn an intelligible formula for the density of trajectories

$$D(\mathbf{q}', \mathbf{q}'', E) = \frac{1}{|\dot{\mathbf{q}}'||\dot{\mathbf{q}}''|} \det \left[\frac{\partial^2 S}{\partial \mathbf{y}' \partial \mathbf{y}''} \right]. \tag{2.41}$$

After these series of calculations with the Gutzwiller special coordinates, we can clearly perceive that, in Hamilton-Jacobi's mechanics, exist two classes of caustics, i.e.,

$D(\mathbf{q}', \mathbf{q}'', E) \to \infty$. The first is when the trajectory from $\mathbf{q}'$ to $\mathbf{q}''$ reaches a returning point ($E = V$), then $|\dot{\mathbf{q}}| = 0$. And the second kind is when the determinant diverges

$$\det\left[\frac{\partial^2 S}{\partial \mathbf{y}' \partial \mathbf{y}''}\right] \to \infty.$$

The caustics from returning points are the most effortless to comprehend. We have to take neighboring trajectories with the same energy E, and the displacement is created perpendicular to the aimed trajectories, i.e., $(\mathbf{q}', \mathbf{p}') + \epsilon(\dot{\mathbf{q}}', \dot{\mathbf{p}}')$ until it reaches the same final position $\mathbf{q}''$ - see figure 2.4b. Therefore, the caustic will take place whenever they pass through a point that is parallel to the momentum axis since $\dot{\mathbf{q}} = 0$. Similarly, the second sort of caustics emerges when the ratio $|\delta \mathbf{p}'_y / \delta \mathbf{y}''|$ diverges. This reveals to us that the caustic will occur whenever the trajectories cross a point that is parallel to the other momenta $\mathbf{p}_y$. When we shall define the Lagrangian surface in the next section, There will be a discussion about the caustics in the Lagrange and Hamilton-Jacobi mechanics to build up their comprehension even further, besides being fundamental for semiclassical theory.

2.1.3 Integrability

The concept of integrability is paramount to understanding and characterizing classical systems. Integrable systems divide classical mechanics with ergodic or non-integrable systems, and their definition relies on Arnold-Liouville's theorem, especially with regard to constants of motion. Nevertheless, before going any further in this development, we need to designate some crucial concepts that classical formalism brings with it. First, both Lagrange's and Hamilton-Jacobi's mechanics leave freedom in the coordinate systems since they obey Euler's equations and Hamilton's equations, respectively. A characteristic and convenient choice of coordinates are well-known as canonical transformations, which preserve the physics of the system but modify the coordinates into elementary Hamiltonian with trivial equations of motion. The basis of this prescription is the variational principle, the fact that the first variation vanishes, i.e.,

$$\delta R(\mathbf{q}', t', \mathbf{q}'', t'') = \delta \int_{t'}^{t''} L(\mathbf{q}(t), \dot{\mathbf{q}}(t), t) dt = \delta \int_{t'}^{t''} \left[\sum_i p_i \dot{q}_i - H(\mathbf{q}, \mathbf{p}, t)\right] dt = 0. \quad (2.42)$$

Consequently, without changing the null value of the integral, we can sum a generic function $F(\mathbf{q}, t)$ in the previous integral

$$\delta \int_{t'}^{t''} \frac{dF(\mathbf{q}(t), t)}{dt} dt = \delta \left[F(\mathbf{q}(t''), t'') - F(\mathbf{q}(t'), t') \right] = 0. \tag{2.43}$$

The freedom permits us to switch to a new Hamiltonian K that will depend on new variables $(\mathbf{Q}, \mathbf{P})$, which can provide a straightforward solution to the equations of motion. Therefore, comparing both the new and the old Hamiltonian in addition to the generic function F, we get

$$\sum_i P_i \dot{Q}_i - K(\mathbf{Q}, \mathbf{P}, t) = \sum_i p_i \dot{q}_i - H(\mathbf{q}, \mathbf{p}, t) - \frac{dF_1(\mathbf{q}, \mathbf{Q}, t)}{dt}, \tag{2.44}$$

which we conveniently already set the format of F, but it will be justified as we go on in the analysis. Extending the total derivative of $F_1(\mathbf{q}, \mathbf{Q}, t)$

$$\sum_i P_i \dot{Q}_i - K(\mathbf{Q}, \mathbf{P}, t) = \sum_i p_i \dot{q}_i - \frac{\partial F_1}{\partial q_i} \dot{q}_i - \frac{\partial F_1}{\partial Q_i} \dot{Q}_i - H(\mathbf{q}, \mathbf{p}, t) - \frac{\partial F_1}{\partial t}, \tag{2.45}$$

we may notice this holds only if

$$p_i = \frac{\partial F_1(\mathbf{q}, \mathbf{Q}, t)}{\partial q_i}, \quad P_i = -\frac{\partial F_1(\mathbf{q}, \mathbf{Q}, t)}{\partial Q_i}, \tag{2.46}$$

$$K(\mathbf{Q}, \mathbf{P}, t) = H\big(\mathbf{q}(\mathbf{Q}, \mathbf{P}, t), \mathbf{p}(\mathbf{Q}, \mathbf{P}, t), t\big) + \frac{\partial F_1\big(\mathbf{q}(\mathbf{Q}, \mathbf{P}, t), \mathbf{Q}, t\big)}{\partial t}. \tag{2.47}$$

The equations $\mathbf{q} = \mathbf{q}(\mathbf{Q}, \mathbf{P}, t)$ and $\mathbf{p} = \mathbf{p}(\mathbf{Q}, \mathbf{P}, t)$ come naturally resolving and then inverting the equations 2.46. Moreover, $F_1(\mathbf{q}, \mathbf{Q}, t)$ underlies the fundamental aspect of the canonical transformation; for this reason, it is dubbed as generating function. Any transformation in H that one considers will be suitable for the system will rely on a particular generating function F. [3].

The most natural selection of a new Hamiltonian is $K = 0$ since the equations of motion will give Q_i and P_i equal to constants. The time-dependent generating function $\sigma(\mathbf{q}, \mathbf{P}, t)$ furnishes the proper transformation equations we need in order to reach $K =$

[3] Classical mechanics textbooks are complete with examples and applications of the canonical transformations. For a broaden description of it and meaningful instances, I recommend Goldstein [18] and Landau & Lifshitz [22]

0. In accordance with what we previously established about canonical transformation, they must obey

$$H\big(\mathbf{q}, \mathbf{p}(q, \mathbf{P}, t), t\big) + \frac{\partial \sigma\big(\mathbf{q}, \mathbf{P}, t\big)}{\partial t} = 0 \tag{2.48}$$

$$p_i = \frac{\partial \sigma(\mathbf{q}, \mathbf{P}, t)}{\partial q_i}, \quad Q_i = \frac{\partial \sigma(\mathbf{q}, \mathbf{P}, t)}{\partial P_i}. \tag{2.49}$$

The first equation in 2.49 can be inserted in 2.48 to obtain

$$H\big(\mathbf{q}, \frac{\partial \sigma(\mathbf{q}, \mathbf{P}, t)}{\partial \mathbf{q}}, t\big) + \frac{\partial \sigma\big(\mathbf{q}, \mathbf{P}, t\big)}{\partial t} = 0. \tag{2.50}$$

Because $\mathbf{P}$ is constant, this partial differential equation is actually $(n+1)$ equations requiring $(n+1)$ constants of motion to be solved. It is reasonable that n of the constants of motion $\boldsymbol{\alpha} = (\alpha_1, \ldots, \alpha_n)$ are directly related to the new constant momenta $\mathbf{P} = (P_1, \ldots P_n)$, and for simplicity it is possible to set $\boldsymbol{\alpha} = \mathbf{P}$. Furthermore, from the equations of motion, the new positions $\mathbf{Q}$ are also constants, dubbed $\beta_1, \ldots, \beta_n$, and the canonical transformations 2.49 can be rewritten as

$$p_i = \frac{\partial \sigma(\mathbf{q}, \boldsymbol{\alpha}, t)}{\partial q_i}, \quad Q_i = \beta_i = \frac{\partial \sigma(\mathbf{q}, \boldsymbol{\alpha}, t)}{\partial \alpha_i}. \tag{2.51}$$

We acquire $\mathbf{q}$ and $\mathbf{p}$ through inversion of the second equation to result $\mathbf{q} = \mathbf{q}(\boldsymbol{\alpha}, \boldsymbol{\beta}, t)$ and then the first to result $\mathbf{p} = \mathbf{p}(\boldsymbol{\alpha}, \boldsymbol{\beta}, t)$. Therefore, it becomes evident that $\boldsymbol{\alpha}$ and $\boldsymbol{\beta}$ are related to the initial conditions $\mathbf{q}_0$ and $\mathbf{p}_0$, whereby $\mathbf{q}_0 = \mathbf{q}(\boldsymbol{\alpha}, \boldsymbol{\beta}, 0)$ and $\mathbf{p}_0 = \mathbf{q}(\boldsymbol{\alpha}, \boldsymbol{\beta}, 0)$ are then inverted to $\boldsymbol{\alpha} = \boldsymbol{\alpha}(\mathbf{q}_0, \mathbf{p}_0)$ and $\boldsymbol{\beta} = \boldsymbol{\beta}(\mathbf{q}_0, \mathbf{p}_0)$. Finally, we can resolve the equation of Hamilton-Jacobi through techniques of partial differential equations.

Now, whether we take the total derivative of the generating function $\sigma(\mathbf{q}, \alpha, t)$ and apply Hamilton-Jacobi's equation

$$\begin{aligned} \frac{d\sigma}{dt} &= \sum_i \frac{\partial \sigma}{\partial q_i}\dot{q}_i + \frac{\partial \sigma}{\partial t}, \\ &= \sum_i (\dot{p}_i)\dot{q}_i - H(\mathbf{q}, \mathbf{p}, t) = L(\mathbf{q}, \dot{\mathbf{q}}, t), \end{aligned} \tag{2.52}$$

we reach the definition of the system's action as in equation 2.2. Hence, the solution of the differential equation is

$$\sigma(\mathbf{q}, \boldsymbol{\alpha}, t) = R(\mathbf{q}_0, \alpha, 0) + \int L(\mathbf{q}, \dot{\mathbf{q}}, t)dt = R(\mathbf{q}_0, \alpha) + \int_{\mathbf{q}_0, 0}^{\mathbf{q}, t} \left[\sum_i \dot{p}_i \dot{q}_i - H(\mathbf{q}, \mathbf{p}, t)\right] dt \tag{2.53}$$

which $\mathbf{q}_0$ is the initial position of the system's trajectory such that it reaches $\mathbf{q}$ in the time t. In addition, the trajectory can be specified by the initial conditions $(\mathbf{q}_0, \mathbf{p}_0)$ or the dyad $(\mathbf{q}_0, \boldsymbol{\alpha})$ because of 2.51, but regardless of the option, the formal solution of the action is stated by providing $2n$ conditions.

Nevertheless, Hamilton-Jacobi's formalism seems to furnish the resolution of any Hamiltonian system through its action and a simple canonical transformation. We shall see next that Arnold-Liouville's theorem exhibits the proper conditions that the systems must hold in order to meet the solution, by which the concepts of integrable system and chaos underlie the theorem.

That said, with $\sigma(\mathbf{q}, \boldsymbol{\alpha}, t)$, we are able to construct a surface conducive to treating both integrability and caustics in the phase space, dubbed as Lagrangian surface [24]. For a fixed $\boldsymbol{\alpha}$, we define a surface of n dimensions $\Sigma_t(\boldsymbol{\alpha})$ from the first equation in 2.51. As a consequence, in $t = 0$, the momentum is given by $\mathbf{p}_0 = \mathbf{p}(\mathbf{q}_0, \boldsymbol{\alpha}, 0)$ generating the initial surface $\Sigma_0(\boldsymbol{\alpha})$. A point in the initial surface means selecting $\boldsymbol{\beta}$ since $\boldsymbol{\alpha}$ is fixed, as aforementioned in the canonical transformation delimitation. Each point in the surface will have a respectively dyad $(\mathbf{q}, \mathbf{p} = \partial\sigma(\mathbf{q}, \boldsymbol{\alpha}, t)/\partial q_i)$ which forms the Lagrangian surface $\Sigma_t(\boldsymbol{\alpha})$ depicted in the figure 2.5.

If we consider a time-independent Hamiltonian $H(\mathbf{q}, \mathbf{p})$, the action can written as

$$\sigma(\mathbf{q}, \boldsymbol{\alpha}, t) = W(\mathbf{q}, \boldsymbol{\alpha}) - \gamma(\boldsymbol{\alpha})t, \tag{2.54}$$

and we obtain a straightforward Hamilton-Jacobi equation

$$\begin{aligned} H\left(\sigma(\mathbf{q}, \frac{\partial W}{\partial \mathbf{q}})\right) &= -\frac{\partial}{\partial t}\left[W(\mathbf{q}, \boldsymbol{\alpha}) - \gamma(\boldsymbol{\alpha})t\right] \\ &= \gamma(\boldsymbol{\alpha}) \end{aligned} \tag{2.55}$$

which the momentum is simply

$$\mathbf{p} = \frac{\partial W}{\partial \mathbf{q}}. \tag{2.56}$$

This equation displays that the Lagrangian surface does not change its form through time; it is invariant under the flow of H. Consequently, we name it as an invariant surface $\Sigma(\boldsymbol{\alpha})$, which means that the initial dyad $(\mathbf{q}_0, \mathbf{p}_0)$ will be propagated

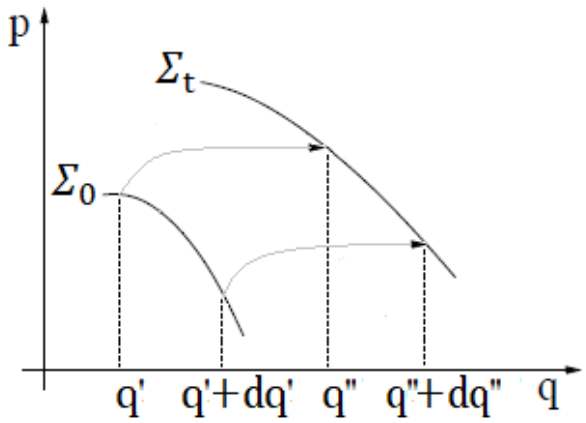

FIGURE 2.5. Illustration of Lagrangian surface evolution. The surfaces Σ_t are constructed by the momentum $\mathbf{p} = \partial\sigma(\mathbf{q}, \boldsymbol{\alpha}, t)/\partial q_i)$ and time [23].

to $(\mathbf{q}, \mathbf{p})$ after a time t and they will continue to pertain the same surface $\Sigma(\boldsymbol{\alpha})$. For $n = 1$ as an instance, Hamilton-Jacobi's equation is

$$\begin{aligned} \frac{1}{2m}\left(\frac{\partial W}{\partial q}\right)^2 + V(q) &= \gamma(\alpha) \\ \frac{\partial W}{\partial q} = p &= \sqrt{2m(\gamma(\alpha) - V(q))}. \end{aligned} \tag{2.57}$$

Thus, $\gamma(\alpha)$ is the energy, and the Lagrangian surface is the energy surface $\Sigma(\alpha) = \Sigma_E$.

Whether we enhance the degrees of freedom, the Lagrangian surface consideration becomes more intricate. The energy surface will always be invariant under the flow of H and, for n-degrees of freedom, will have a dimension equal to $\dim(\Sigma_E) = 2n - 1$. Nonetheless, the role of constraints comes into play in order to acquire invariant surfaces with lower dimensions; $n - 1$ constants of motion are required to perform the partition in 2.54. This statement is the essence of Arnold-Liouville's theorem, but before asserting it properly, let us take advantage of the Lagrangian surface formulation to obtain a different and more transparent view of the caustics in the Lagrange's and Hamilton-Jacobi's mechanics.

As we exhaustively stated and restated the concept of caustics in Lagrange's and Hamilton-Jacobi's mechanics throughout the sections 2.1.1 and 2.1.2, respectively. The Lagrangian surfaces furnish us with a clear-cut perspective about them. First, we set an initial Lagrangian surface Σ_0 and propagate through time to reach Σ_t as shown in figure 2.6. Whether the system generates such distribution, we can see that there is

a point $\bar{\mathbf{q}}$ which the surface curves and any small variation around $\bar{\mathbf{q}}$ will lead to the same final position, i.e., $\delta\mathbf{q}'' = 0$. Therefore, the ratio $\delta\mathbf{q}'/\delta\mathbf{q}''$ diverges.

On top of that, we can also examine that its sign before $\bar{\mathbf{q}}$ is positive since a small positive variation in $\mathbf{q}_1$ leads to a positive variation in the final position $\delta\mathbf{q}'' > 0$. On the other hand, for a point after $\bar{\mathbf{q}}$ the sign of the ratio is negative since a positive variation in $\mathbf{q}_2$ leads to a negative variation in the final position $\delta\mathbf{q}'' < 0$. The change of the sign is the heart of Morse's theorem and is evident in this surface composition.

Alternatively, addressing energy as a variable, the concepts of caustics must also be adjusted. The Lagrangian surface is generated by the initial positions $\mathbf{q}'$ and the relation $H(\mathbf{q}, \mathbf{p}) = E$; so we have the momentum constraint $|\mathbf{p}| = \sqrt{2m(E - V(\mathbf{q}'))}$. The remaining momenta $p_1, p_2, \ldots, p_n$ are $n - 1$ independent variables, and then the n-dimensional Lagrangian surface Σ is generated from the evolution of those $n - 1$ variables. We can notice that along a trajectory, described by the Gutzwiller coordinate x, the vector $(\dot{x}, \dot{p_x})$ is tangent to Σ_t for every instant of time. Therefore, the first sort of caustics occurs when the tangent plane to Σ_t is parallel to the momentum axis since $\dot{x} = 0$, which is a returning point. Similarly, the second sort of caustics takes place when the remaining vectors of the tangent plane to Σ_t are parallel to trajectory-transverse momenta $\mathbf{p}_y = p_{y,1}, \ldots, p_{y,n-1}$ resulting in a divergence in the $|\delta\mathbf{p}'_y|/|\delta\mathbf{y}''|$.

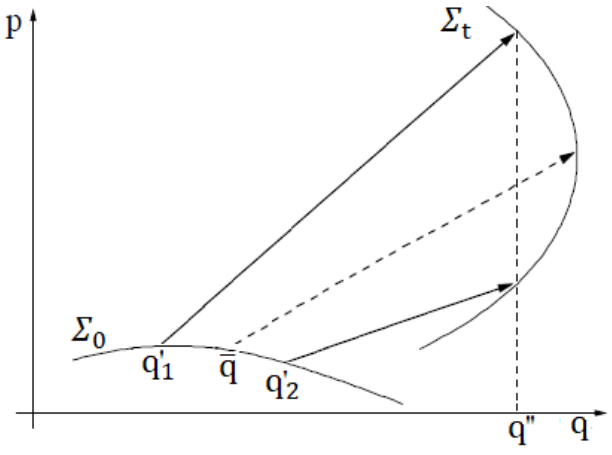

FIGURE 2.6. Illustration of Lagrangian surface evolution. However, in this case, the surface Σ_0 contains a point $\bar{\mathbf{q}}$ where small variations around it will generate the same final position in Σ_t. The point $\bar{\mathbf{q}}$ then is caustic in Lagrange's description. [25]

Returning to the integrability problem, we shall address Arnold-Liouville's theorem without stating it directly but through a discussion encompassing the main issues. In addition, in order to guarantee the dissertation's finitude, we shall not formally prove all assertions; however, I recommend Arnold's book [21] for a transparent proof of any affirmation and a formal treatment of the theorem.

That said, recalling the action in Hamilton-Jacobi's formalism, $2n$ conditions are required to obtain a formal solution of it. Nevertheless, Arnold-Liouville's theorem states that the pivotal concept is the existence of constants of motion in addition to energy. Constants of motion are functions of the position and momentum $F = F(\mathbf{q}, \mathbf{p})$. When time starts to vary, and consequently, the positions and momenta - following the equations of motion 2.13 - this proper function will stay constant. In most systems, it is difficult to encounter these functions. For instance, in Kepler's problem of attraction of two bodies - besides the straightforward energy and angular momentum conservation - there is a third constant of motion, the Laplace-Runge-Lenz vector, that requires an elaborate description. Despite underlying most systems, constants of motion become perceived since they generate invariant tori, as we shall see later on.

From this reasoning, we can acquire a crucial relation for $F(\mathbf{q}, \mathbf{p})$ because of their time independency

$$\begin{aligned} \frac{d}{dt}F(\mathbf{q},\mathbf{p}) &= 0 \\ \frac{\partial F}{\partial \mathbf{q}}\frac{\partial \mathbf{q}}{\partial t} + \frac{\partial F}{\partial \mathbf{p}}\frac{\partial \mathbf{p}}{\partial t} &= 0 \\ \frac{\partial H}{\partial \mathbf{p}}\frac{\partial F}{\partial \mathbf{q}} - \frac{\partial H}{\partial \mathbf{q}}\frac{\partial F}{\partial \mathbf{p}} = \{H, F\} &= 0 \end{aligned} \tag{2.58}$$

Therefore, for F to be a constant of motion, it must commute - null Poisson bracket - with the Hamiltonian. Geometrically speaking, both vectorfields of constant of motion $F(\mathbf{q}, \mathbf{p}) = const$ and $H(\mathbf{q}, \mathbf{p}) = E$ are perpendicular to each other surface. In other words, the vectorfield $(-\partial F/\partial \mathbf{q}, \partial F/\partial \mathbf{p})$ is transverse to the surface $H = E$ and the vectorfield $(-\partial H/\partial \mathbf{q}, \partial H/\partial \mathbf{p})$ is transverse to the surface $F = const$. As an upshot, the intersection of the surfaces is where the trajectory lies.

In general, a system has many constants of motion $F_1, F_2, \ldots$, they all are in involution with H - null Poisson bracket - and by the theorem, one function F_i cannot be expressed in terms of the other functions F_j for $i \neq j$, meaning they are independent

of one another. Moreover, a last crucial property, which will lead to the irreducible circuits, is the involution of the constants of motion F_i with each other; as a consequence, the resulting trajectory lies in the intersection of all constants and the energy surface.

With all this at hand, for a n-degrees-of-freedom system, we admit that it has n constants of motion leading to $(2n - n = n)$- dimensional manifold for the trajectory in the phase space. Arnold-Liouville's theorem affirms that whether all the previous considerations about the constants of motion are satisfied, we are able to find a new Hamiltonian through a canonical transformation $(\mathbf{q}, \mathbf{p}) \to (\boldsymbol{\varphi}, \mathbf{I})$ that only depends on the new momentum, i.e., $H = H(\mathbf{I})$. By this specification, the equations of motion are

$$\dot{\varphi}_i = \frac{\partial H(I_1, \ldots, I_n)}{\partial I_i} = \omega_i \quad \text{and} \quad \dot{I}_i = -\frac{\partial H(I_1, \ldots, I_n)}{\partial \varphi_i} = 0, \tag{2.59}$$

which solution is trivial because the new momenta are constants of motion, and the first equation leads to a function $\boldsymbol{\omega}$ that only depends on the constants $\mathbf{I}$ - simply called the frequencies. Integrating it, we stay with a linear relation for the new positions

$$\varphi_i = \omega_i t + D_i \tag{2.60}$$

where $\varphi_i(t = 0) = D_i$. Through an elegantly topological description [21], the theorem states the trajectories in this new canonical coordinates are in a n-dimensional torus $\mathbb{T}^n$. Namely, the transformation through a torus is pleasingly acknowledged when we deal with the vectorfields of the constants of motion. On the torus manifold, any vectorfield ever vanishes; on the other hand, this property does not hold for a sphere since it is impossible to specify a non-vanishing vectorfield on a sphere[4]. Therefore, from the topology of the torus, it is evident that the new position is an angle, i.e., $0 \leq \varphi_i \leq 2\pi$; and the linear relation 2.60 legitimates our naming of ω_i as frequencies. Furthermore, the curves described by the angles are known as irreducible circuits γ_i.

The generating function for the canonical transformation can be written as $\sigma = \sigma(\mathbf{q}, \mathbf{I})$. As we have seen, this is also the action of the system, which has the following relations

$$p_i = \frac{\partial \sigma(\mathbf{q}, \mathbf{I})}{\partial q_i}, \quad \varphi_i = \frac{\partial \sigma(\mathbf{q}, \mathbf{I})}{\partial I_i}. \tag{2.61}$$

The first equation can be integrated to provide us with the action

$$\sigma(\mathbf{q}, \mathbf{I}) = \int \mathbf{p}(\mathbf{q}, \mathbf{I}) \cdot d\mathbf{q}. \tag{2.62}$$

[4]This result is known by the quote, "you cannot comb a sphere" [23]

However, it is convenient to integrate it around an irreducible circuit γ_i within the torus and result in the integral

$$A_i(\mathbf{I}) = \oint_{\gamma_i} \mathbf{p}(\mathbf{q}, \mathbf{I}) \cdot d\mathbf{q}, \tag{2.63}$$

we then derive in relation to I_j

$$\begin{aligned} \frac{\partial A_i}{\partial I_j} &= \sum_k \oint_{\gamma_i} \frac{\partial p_k}{\partial I_j} dq_k = \sum_k \oint_{\gamma_i} \frac{\partial}{\partial q_k} \frac{\partial S}{\partial I_j} dq_k \\ &= \sum_k \oint_{\gamma_i} \frac{\partial \varphi_j}{\partial q_k} dq_k = \oint_{\gamma_i} d\varphi_j = 2\pi\delta_{ij}, \end{aligned} \tag{2.64}$$

so that the delta emerges since the angles φ_j will only run along the respective irreducible circuits as by their definition. Therefore, it is explicit that $A_i = 2\pi I_i$ and

$$I_i = \frac{1}{2\pi} \oint_{\gamma_i} \mathbf{p} \cdot d\mathbf{q}. \tag{2.65}$$

The format of the new momentum in 2.65 legitimates its name as the action; consequently, both new coordinates are known as action-angle. From the Arnold-Liouville theorem, whether a system has constants of motion as many as degrees of freedom all in involution, the action-angle variables provide the complete solution of the equations of motion. To summarize, the procedure to solve consists of the following: from the n constants of motion $F_i = F_i(\mathbf{q}, \mathbf{p})$, one starts by inverting them and finding the momenta $p_i = p_i(\mathbf{q}, \mathbf{F})$ (recalling that the energy is included as $F_1 = E$). Then inserting the momentum in 2.65, we obtain $\mathbf{I} = \mathbf{I}(\mathbf{F})$. After, the action is inverted $\mathbf{F} = \mathbf{F}(\mathbf{I})$ to finally get the momenta depending on the actions and substitute them in 2.62 to reach the action $\sigma(\mathbf{q}, \mathbf{I})$; the action is the generating function that provides the required relation in 2.61.

One important aspect that should be addressed is the differentiation when we can call a torus as rational or irrational depending on their respective frequencies. For instance, we take a two-dimensional integrable system in which trajectories are running along a two-dimensional torus $\mathbb{T}^2$ and with their respective frequencies ω_1 and ω_2. If the ratio ω_1/ω_2 is equal to a rational number r/s with r and s mutually prime integers, the trajectory will close after a s-period and circulates the torus r times - this trajectory is named as rational or resonant. Now, whether the ratio is an irrational number, the trajectory will never close and will densely fill the torus - the respective

trajectory is called quasi-periodic, and the torus is dubbed irrational or non-resonant. In general, for n-dimensional torus, the trajectory will be resonant if the frequencies $\omega_1, \ldots, \omega_n$ are mutually commensurable, i.e., the relation of commensurability holds

$$K_1\omega_1 + K_2\omega_2 + \cdots + K_n\omega_n = 0 \tag{2.66}$$

with K_i as being non-zero integers.

Dealing with systems of two or more dimensions, the phase space will have four or more dimensions. On the other hand, we are limited to perceiving in, at most, a three-dimensional depiction of it. Therefore, we introduce what is known as Poincaré sections, in which we roughly cut the phase space and mark every trajectory's passage through it, as in the figure 2.7a. By performing a Poincaré section in the torus as shown in figure 2.7b, we can efficiently identify rational or irrational tori through this two-dimensional map. For instance, when the trajectory is periodic, it will run through its respective torus and will punch the Poincaré section as many times as its period - see figure 2.8a. In addition, we have to acknowledge that in each rational torus, there is an infinity of possible trajectories, each punching the Poincaré section s times, however, in different points of the phase space. When the commensurability does not hold, the trajectory on the irrational torus will punch the Poincaré section indefinitely, which lead to only one trajectory completing the whole circle (figure 2.8b).

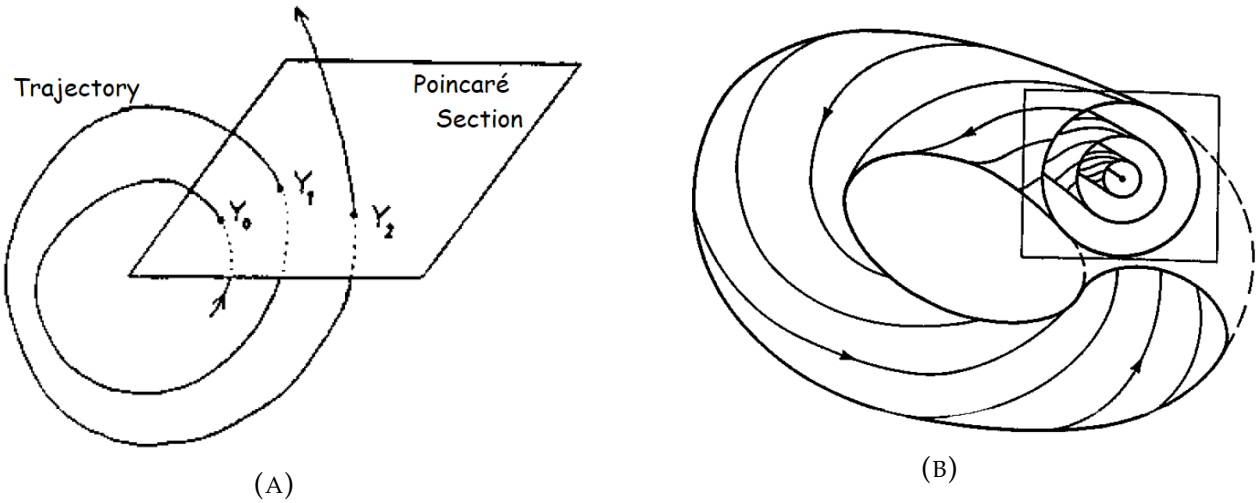

(A) (B)

FIGURE 2.7. (A) Depiction of a trajectory in which we select a Poincaré surface to mark the point $Y_0, Y_1, \ldots$ where the trajectory cuts it [20]. (B) Illustration of a natural POincaré section for a two-dimensional torus [19].

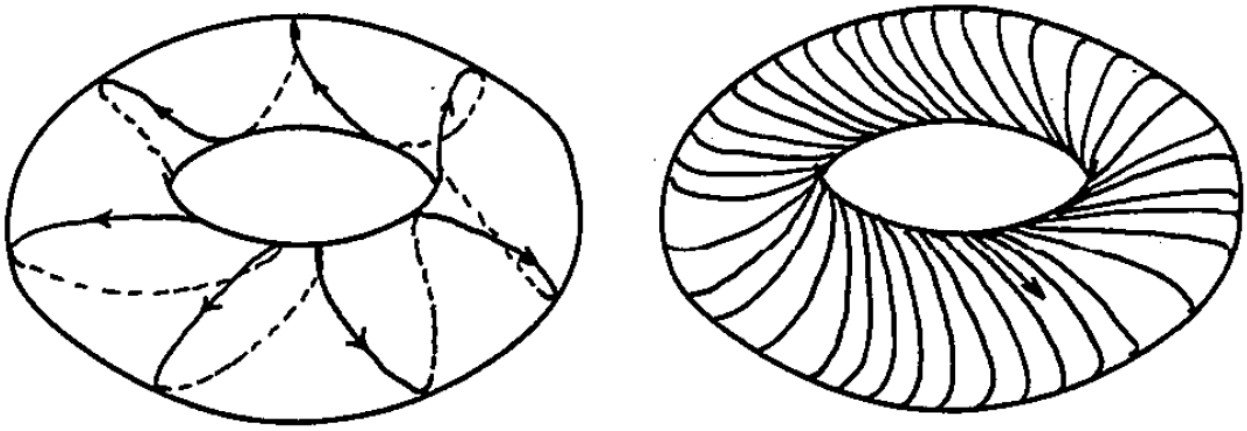

(A) (B)

FIGURE 2.8. Possible trajectories circulating the tori and characterizing a rational torus (A) when they close after a certain period, and an Irrational torus (B) when the trajectory never closes [26].

Thus, alluding Arnold-Liouville's theorem, we showed that some classical systems could be solved when there are certain conditions, such as constants of motion and symmetries. However, in nature, the systems are not integrable and neither readily solvable. In order to address these non-linear systems, we have to see both classical and quantum fundamental facets to treat them: the periodic orbits.

2.1.4 Periodic orbits

The French physicist and mathematician Poincaré have made countless contributions of major implication in both areas, and he has not disappointed us when the issue has been to shed some light on non-integrable systems. These systems are naturally intricate, and one cannot find solutions in the form of integrals or by quadratures, such as elliptic integrals. Nonetheless, Poincaré has discovered that the solutions of the equation of motions that return to their initial conditions - periodic orbits - can be used to provide us with information about the overall behavior of any classical system. What he could not predict is the significance of periodic orbits in quantum mechanics, as we will see in section 3.3. Gutzwiller's trace formula encompasses classical features, especially periodic orbits, to obtain quantum information, such as the density of states in the transition region of the classical and quantum regimes.

To begin, from definition of the periodic orbits $(\bar{\mathbf{q}}, \bar{\mathbf{p}})$ of period τ, they are the solution of 2.13 with $\bar{\boldsymbol{\eta}}(t) = \bar{\boldsymbol{\eta}}(t+\tau)$ in the symplectic notation. It is reasonable to assume that for sufficiently small neighboring trajectories that start at $(\mathbf{q}', \mathbf{p}')$, the final position $(\mathbf{q}'', \mathbf{p}'')$ will return to the neighborhood of $(\bar{\mathbf{q}}, \bar{\mathbf{p}})$. In order to obtain the stability of the orbits, we will allow initial and final positions to vary. However, we have to keep in mind that those points are connected by a whole trajectory; consequently, varying the initial and final position of all the trajectories will also modify them accordingly. In addition, to study the neighborhood of the periodic orbits, we need to address the perpendicular coordinates to the trajectory. So, the Gutzwiller's local coordinates will be used once more with $q_1 = x$ running along the trajectory and the other $n-1$ coordinates $(q_2, \ldots, q_{n-1}) = (y_1, \ldots, y_{n-1})$ are transverse to it. Therefore, a small initial displacement from the periodic orbit, identified by $(\delta\mathbf{y}', \delta\mathbf{p}'_y)$, will run in the neighborhood of the orbit and arrive at a small final displacement $(\delta\mathbf{y}'', \delta\mathbf{p}''_y)$.

After that, moving at energy E, the neighboring trajectory has an action $S(\mathbf{q}', \mathbf{q}'', E) = S(x', \mathbf{y}', x'', \mathbf{y}'', E)$ which enables us to write the perpendicular-momentum displacements as a function of the perpendicular-position displacements, i.e., $\delta\mathbf{p}'_y = \delta\mathbf{p}'_y(\delta\mathbf{y}', \delta\mathbf{y}'')$ and $\delta\mathbf{p}''_y = \delta\mathbf{p}''_y(\delta\mathbf{y}', \delta\mathbf{y}'')$. Considering a linear approximation, the resulting equations of the displacements are

$$\delta p'_{y,i} = \sum_{i=1}^{n-1} \frac{\partial p'_{y,i}}{\partial y'_j}\delta y'_j - \frac{\partial p'_{y,i}}{\partial y''_j}\delta y''_j = \sum_{i=1}^{n-1} -\frac{\partial^2 S}{\partial y'_i y'_j}\delta y'_j - \frac{\partial^2 S}{\partial y'_i y''_j}\delta y''_j \tag{2.67}$$

$$\delta p''_{y,i} = \sum_{i=1}^{n-1} \frac{\partial p''_{y,i}}{\partial y'_j}\delta y'_j - \frac{\partial p''_{y,i}}{\partial y''_j}\delta y''_j = \sum_{i=1}^{n-1} \frac{\partial^2 S}{\partial y''_i y'_j}\delta y'_j + \frac{\partial^2 S}{\partial y''_i y''_j}\delta y''_j. \tag{2.68}$$

Moreover, we can arrange these equations in an abbreviated manner

$$\delta\mathbf{p}'_y = -\boldsymbol{\mathcal{A}}\delta\mathbf{y}' - \boldsymbol{\mathcal{B}}\delta\mathbf{y}'' \tag{2.69}$$

$$\delta\mathbf{p}''_y = +\boldsymbol{\mathcal{C}}\delta\mathbf{y}' + \boldsymbol{\mathcal{D}}\delta\mathbf{y}'' \tag{2.70}$$

with the definitions of the $(n-1)$ by $(n-1)$ matrices

$$\mathcal{A}_{ij} = \frac{\partial^2 S}{\partial y'_i y'_j}, \quad \mathcal{B}_{ij} = \frac{\partial^2 S}{\partial y'_i y''_j}, \quad \mathcal{C}_{ij} = \frac{\partial^2 S}{\partial y''_i y_j} = (\mathcal{B}^T)_{ij}, \quad \mathcal{D}_{ij} = \frac{\partial^2 S}{\partial y''_i y'_j}. \tag{2.71}$$

Nonetheless, 2.69 and 2.70 have to be inverted in order to supply us with relevant information about the neighborhood of the periodic orbit. The expected format is to

distinguish how the initial displacements affect the final ones in the neighborhood; that is, we want to know $\delta\mathbf{y}''$ and $\delta\mathbf{p}_y''$ in terms of $\delta\mathbf{y}'$ and $\delta\mathbf{p}_y'$

$$\delta\mathbf{y}'' = \boldsymbol{A}\delta\mathbf{y}' + \boldsymbol{B}\delta\mathbf{p}_y' \tag{2.72}$$

$$\delta\mathbf{p}_y'' = \boldsymbol{C}\delta\mathbf{y}' + \boldsymbol{D}\delta\mathbf{p}_y'. \tag{2.73}$$

The previous equation can be written as

$$\begin{pmatrix}\delta\mathbf{y}''\\ \delta\mathbf{p}_y''\end{pmatrix} = \begin{pmatrix}\mathbf{A} & \mathbf{B}\\ \mathbf{C} & \mathbf{D}\end{pmatrix}\begin{pmatrix}\delta\mathbf{y}'\\ \delta\mathbf{p}_y'\end{pmatrix}, \tag{2.74}$$

and we identify the $2(n-1)$ by $2(n-1)$ matrix as the monodromy matrix $\mathbf{M}$

$$\mathbf{M} = \begin{pmatrix}\mathbf{A} & \mathbf{B}\\ \mathbf{C} & \mathbf{D}\end{pmatrix}, \tag{2.75}$$

which is a function of the action matrices. Now, comparing the equations 2.69 and 2.70 with 2.72 and 2.73, the result is

$$\mathbf{A} = -\boldsymbol{\mathcal{B}}^{-1}\boldsymbol{\mathcal{A}} \quad , \qquad \mathbf{B} = -\boldsymbol{\mathcal{B}}^{-1} \tag{2.76}$$

$$\mathbf{C} = \boldsymbol{\mathcal{B}}^{T} - \boldsymbol{\mathcal{D}}\boldsymbol{\mathcal{B}}^{-1}\boldsymbol{\mathcal{A}} \quad , \qquad \mathbf{D} = -\boldsymbol{\mathcal{D}}\boldsymbol{\mathcal{B}}^{-1}. \tag{2.77}$$

We substitute it in the monodromy matrix and obtain

$$\mathbf{M} = \begin{pmatrix}-\boldsymbol{\mathcal{B}}^{-1}\boldsymbol{\mathcal{A}} & -\boldsymbol{\mathcal{B}}^{-1}\\ \boldsymbol{\mathcal{B}}^{T} - \boldsymbol{\mathcal{D}}\boldsymbol{\mathcal{B}}^{-1}\boldsymbol{\mathcal{A}} & -\boldsymbol{\mathcal{D}}\boldsymbol{\mathcal{B}}^{-1}\end{pmatrix}. \tag{2.78}$$

The monodromy matrix describes the linear transformation of the trajectories around the periodic orbits. Therefore, we need to calculate its eigenvalues in order to establish the orbit stability. The characteristic polynomial of $\mathbf{M}$ is the function that gives us the stability information

$$F(\lambda) = \begin{vmatrix}\mathbf{A}-\lambda\mathbf{I} & \mathbf{B}\\ \mathbf{C} & \mathbf{D}-\lambda\mathbf{I}\end{vmatrix} = \begin{vmatrix}-\boldsymbol{\mathcal{B}}^{-1}\boldsymbol{\mathcal{A}}-\lambda\mathbf{I} & -\boldsymbol{\mathcal{B}}^{-1}\\ \boldsymbol{\mathcal{B}}^{T} - \boldsymbol{\mathcal{D}}\boldsymbol{\mathcal{B}}^{-1}\boldsymbol{\mathcal{A}} & -\boldsymbol{\mathcal{D}}\boldsymbol{\mathcal{B}}^{-1}-\lambda\mathbf{I}.\end{vmatrix} \tag{2.79}$$

We can write $F(\lambda)$ in a simpler expression if we first made the operation:

$$(\text{2nd row}) \to (\text{2nd row}) - \boldsymbol{\mathcal{D}}(\text{1st row}),$$

and have

$$F(\lambda) = \begin{vmatrix}-\boldsymbol{\mathcal{B}}^{-1}\boldsymbol{\mathcal{A}}-\lambda\mathbf{I} & -\boldsymbol{\mathcal{B}}^{-1}\\ \boldsymbol{\mathcal{B}}^{T}+\lambda\boldsymbol{\mathcal{D}} & -\lambda\mathbf{I}\end{vmatrix}. \tag{2.80}$$

Furthermore, we multiply the first row by $\boldsymbol{\mathcal{B}}$ and compensates the determinant with the term $1/|\boldsymbol{\mathcal{B}}|$, and after that we perform the substitution:

$$(\text{2nd row}) \to (\text{2nd row}) - \lambda(\text{1st row}),$$

to acquire

$$F(\lambda) = \frac{1}{|\boldsymbol{\mathcal{B}}|}\begin{vmatrix} -\boldsymbol{\mathcal{A}} - \lambda\boldsymbol{\mathcal{B}} & -\mathbf{I} \\ \boldsymbol{\mathcal{B}}^T + \lambda\boldsymbol{\mathcal{D}} & -\lambda\mathbf{I} \end{vmatrix} = \frac{1}{|\boldsymbol{\mathcal{B}}|}\begin{vmatrix} -\boldsymbol{\mathcal{A}} - \lambda\boldsymbol{\mathcal{B}} & -\mathbf{I} \\ \boldsymbol{\mathcal{B}}^T + \lambda(\boldsymbol{\mathcal{A}} + \boldsymbol{\mathcal{D}}) + \lambda^2\boldsymbol{\mathcal{B}} & \mathbf{0} \end{vmatrix} \tag{2.81}$$

Finally, we merely reduce the determinant and obtain the final function

$$F(\lambda) = \frac{|\boldsymbol{\mathcal{B}}^T + \lambda(\boldsymbol{\mathcal{A}} + \boldsymbol{\mathcal{D}}) + \lambda^2\boldsymbol{\mathcal{B}}|}{|\boldsymbol{\mathcal{B}}|}. \tag{2.82}$$

The eigenvalues come from the λ that are solution of $F(\lambda) = 0$. From our definitions in 2.71, the matrices are real, which implies that the roots of the characteristic polynomial are also real or are pairs of complex conjugates. In addition, since $\boldsymbol{\mathcal{A}}$ and $\boldsymbol{\mathcal{C}}$ are symmetric, and the determinant is invariant under a transposition, the $1/\lambda$ is also a solution of $F(\lambda) = 0$. With all this settled, there are only four forms of the eigenvalues λ, whereby each of them describes a different neighborhood around the periodic orbits:

1. $\lambda = 1$ is called direct parabolic orbit, or $\lambda = -1$ inverse parabolic orbit (see figure 2.9a);
2. $\lambda = \exp(i\chi), \exp(-i\chi)$ with χ real is known as elliptic orbit (see figure 2.9b);
3. $\lambda = \exp(\chi), \exp(-\chi)$ is called direct hyperbolic orbit, or $\lambda = -\exp(\chi), -\exp(-\chi)$ inverse hyperbolic orbit (see figure 2.9c);
4. $\lambda = \exp(u + iv), \exp(-u - iv)$ is called loxodromic orbit for u and v real.

Furthermore, the determinant $F(1) = |\mathbf{M} - \mathbf{I}|$ will be extremely crucial when we shall address Gutzwiller's trace formula. $F(1)$ also has a well-known designation made by Greene[27] called residue that characterizes the neighborhood of the periodic orbit. First, we can note that

$$\begin{aligned} F(1) = |\mathbf{M} - \mathbf{I}| &= \begin{vmatrix} \mathbf{A} - \mathbf{I} & \mathbf{B} \\ \mathbf{C} & \mathbf{D} - \mathbf{I} \end{vmatrix} = |\mathbf{AD} - \mathbf{BC} - \mathbf{A} - \mathbf{D} + \mathbf{I}| \\ &= ||\mathbf{M}| - \mathbf{A} - \mathbf{D} + \mathbf{I}| = |(2 - \mathrm{Tr}(\mathbf{M}))\mathbf{I}| = 2 - \lambda - \lambda^{-1}, \end{aligned} \tag{2.83}$$

which we have used that $|\mathbf{M}| = 1$. Consequently, for each sort of orbit

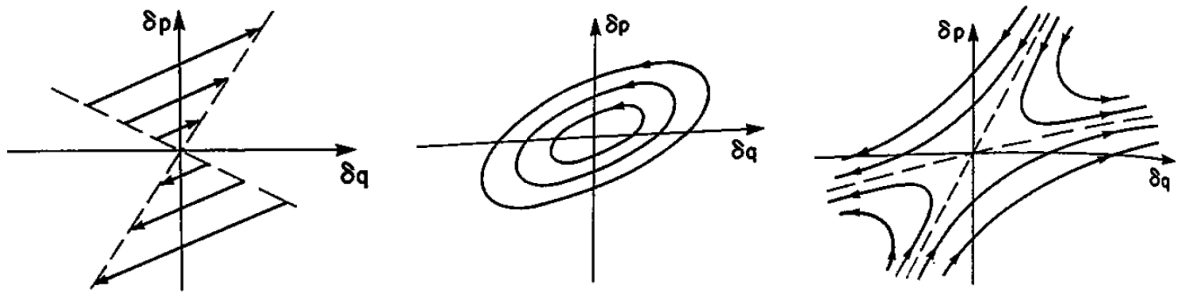

(A) (B) (C)

FIGURE 2.9. Three illustrations of the neighborhood of periodic orbits, each depicting a possible solution of Monodromy matrix's eigenvalues: (A) parabolic orbit; (B) elliptic orbit; and (C) hyperbolic orbit [19].

1. $F(1) = 2 - 1 - 1 = 0$ for direct parabolic, or 4 for inverse parabolic;
2. $F(1) = 2 - e^{i\chi} - e^{-i\chi} = 2 - 2\cos(\chi) = 4\sin^2(\chi/2)$ for elliptic;
3. $F(1) = 2 - e^{\chi} - e^{\chi} = 2 - 2\cosh(\chi) = 4\sinh^2(\chi/2)$ for direct hyperbolic, or $4\cosh^2(\chi/2)$ for inverse hyperbolic;
4. $F(1) = 2 - e^{u+iv} - e^{-u-iv}$ for loxodromic.

For integrable systems, we recall the Arnold-Liouville theorem and the trivial position and momentum formulas 2.59. The straight lines are compatible with the parabolic orbits, and consequently, the eigenvalues for integrable systems are ± 1. It becomes evident that integrable systems are far from being general - they are solely a convenient exception. Generic, non-linear Hamiltonian systems will emphasize the presence of elliptic and hyperbolic periodic orbits. As a consequence, a single and simple overall pattern is impracticable in such systems as has happened in integrable ones with the existence of rational and irrational tori in phase space.

We shall see that the systems will actually have mixed phase-space or soft chaos, in which the phase-space is divided between elliptic and hyperbolic orbits. On the other hand, when only hyperbolic orbits take place, the system will set in hard chaos. Furthermore, it became clear that elliptic and hyperbolic orbits play a fundamental role in the system's behavior. Firstly, the elliptic orbits are also called stable orbits since a neighboring trajectory is enclosed in their ellipse, and consequently, this trajectory will endure close to the orbit in linear approximation - see figure 2.9b. Secondly,

for hyperbolic or unstable orbits, we can detect two special directions - dashed lines in 2.9c. From the solutions of the monodromy matrix, the trajectories in those directions approach exponentially to the periodic orbit in one direction and move way exponentially in the other direction. Hence, the neighboring trajectories are hyperboles and tend to move away from the orbit in linear approximation.

The didactic, standard example of those classical structures is the pendulum phase space as in figure 2.10. This one-dimensional system has fixed points instead of periodic orbits, but the conclusions remain the same. The takeaway is the points in the special directions, whose trajectories will always tend asymptotically to the unstable fixed point. We dub this region as separatrix such that these directions - eigenvectors - are tangent to it. By this reasoning, the eigenvectors of the monodromy matrix determine the separatrix and present a more formal configuration for systems with n degrees of freedom. Particularly, the formulation is the following:

- The invariant set of point $(\mathbf{q}, \mathbf{p})$ is called *Stable Manifold* W_s if they tend asymptotically to an unstable orbit;
- The invariant set of point $(\mathbf{q}, \mathbf{p})$ is called *Unstable Manifold* W_u if they tend asymptotically to an unstable orbit when run backward in time.

Each unstable orbit normally has two manifolds: stable and unstable. In classical systems such as the pendulum, typically W_s and W_u are along the same line. However, when we shall consider more general non-integrable systems, those curves are typically distinct, and their crossings and distortions are the keys to the onset of chaos.

2.2 Classical Chaos

As aforementioned, integrable systems are rare in nature. They are in a particular group of systems in which Arnold-Liouville's theorem guarantees a solution through action-angle variables. Nevertheless, the majority of problems are non-integrable. Throughout history, many mathematicians, physicists, and meteorologists could take away information or even universalities from these systems that previously

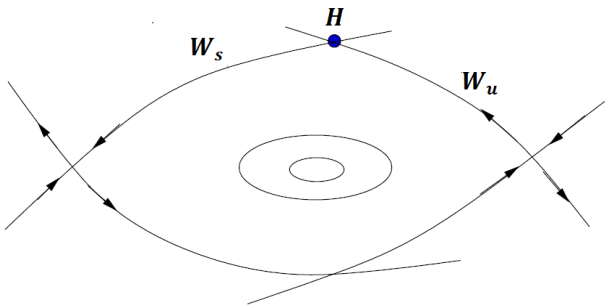

FIGURE 2.10. Phase space of a pendulum which highlights the elliptic (at the center) and hyperbolic orbits. The hyperbolic orbits have two principal lines called unstable W_u and stable W_s manifolds that surround the elliptic orbits. When a stable manifold crosses an unstable one, we have a homoclinic point h.

would seem only in turmoil. Names like Poincaré bringing the impossibility of solution of the three-body problem; Lorenz notifying the intrinsic randomness in deterministic systems in a simple thermal convection model; Ruelle and Takens introducing the strange attractors - structures locally unstable but globally stable - of dissipated systems; or even Kolmogorov, Arnold, and Moser formulating the behavior of perturbative systems formally known as the KAM theorem and providing one of the essential roles in the chaos theory.

The broader coverage should be considered dissipative systems; however, in our circumstance, we are restricted to Hamiltonian systems such that this stipulation does not wane systems' complexities. As we did with Arnold-Liouville's theorem, we shall cover the main issues about classical chaos without restricting ourselves to extensive and painstaking proofs. The clarity and finitude of the work is the principal objective, in addition to furnishing further references when needed to supplement any knowledge or subject brought here.

We start our journey to chaos through small perturbations of integrable systems and introduce the KAM theorem that regards the irrational tori. Then we investigate the Poincaré-Birkhoff fixed point theorem that addresses rational orbits in deterministic chaos, and consequently, we will be able to understand the general structures and behaviors of chaotic classical systems.

2.2.1 KAM theorem and Poincaré-Birkhoff fixed point theorem

The plausible beginning to generality is to introduce a small perturbation in integrable systems. We shall assess what occurs with the previously established structures and see if they prevail or if new arrangements emerge. The convergence of this perturbative theory was the concern of Andrey Kolmogorov (1903-1987) in 1954, in which the commensurability 2.66 was a watershed to his description. Afterward, his Ukrainian pupil Vladimir Arnold (1937 - 2010) extended it to Hamiltonian systems and turned it into a more formal proof. Finally, Jurgen Moser (1928-1999) amplified those arguments for maps. A complete demonstration can be encountered in Arnold and Alvez's book[28]; and for a less formal but digestible presentation, I highly recommend Berry's and Aguiar's articles [26, 23] in which we shall bring conclusions from those references.

Without further ado, we commence by including a small perturbation ϵ for a non-degenerate, two-dimensional integrable system $H = H_0(I_{10}, I_{20}) + \epsilon H_1$. The H_0 describes the system fulfilled with tori (I_1, I_2) and their respective frequencies $(\omega_{10}, \omega_{20})$. Each torus is described by the ratio $\alpha_0 = \omega_{10}/\omega_{20}$, called winding number, and it is irrational or rational depending on α_0 outcome. If we consider the perturbative Hamiltonian depending solely on the prior actions $H_1 = H_1(I_{10}, I_{20})$, the resulting system is proved to be also integrable [23]. Therefore, there will be new action-angles variables (I_{11}, φ_{11}) and (I_{21}, φ_{21}) with their respective frequencies ω_{11} and ω_{21} to provide the solution of the system.

Since H_0 is not degenerate, at least locally, the winding number will determine what will happen with each torus after the introduction of the perturbation [26]. Increasing ϵ smoothly, the surface of the torus distorts, and if emerge a new torus with the same winding number in the distorted phase space, we say that the torus survived the perturbation. Nevertheless, when the perturbative system is also integrable means that all tori survived the disturbance, then what leads us to achieve novel developments to considerate a general perturbation of the form $H_1 = H_1(I_{11}, I_{21}, \varphi_{11}, \varphi_{21})$. The resulting system is not integrable anymore, and consequently, we cannot know in advance which irrational tori survive the perturbation. However, the KAM theorem states that the convergence of the perturbative theory for irrational tori is only valid if the winding number is "sufficiently irrational" which means to satisfy the next relation

$$\left|\frac{\omega_1}{\omega_2} - \frac{r}{s}\right| > \frac{K(\epsilon)}{s^{\mu}} \tag{2.84}$$

with r and s integers, $\mu > 2$, and $K(\epsilon)$ is a function that tend to zero when ϵ goes to zero and is independent of r and s [28]. Through this reasoning, any frequency that admits rapid convergence to a rational number will be the first to be destroyed by the perturbation. Therefore, in order to investigate what number is the most irrational corresponding to an enduring torus, number theory subjects such as continued fractions take place immediately into consideration.

The KAM theorem points out what happens with the surrounding of a rational torus but says nothing about proper torus. In addition, the theorem does not affirm anything when the system does not have any rational and irrational tori. Hence, we shall see the Poincaré-Birkhoff fixed point theorem to examine the rational tori explicitly and how the non-integrable systems subsequently conduct the implementation of both theorems.

For Hamiltonian systems, when we introduce a small perturbation in an integrable system, the Poincaré-Birkhoff theorem fixed point addresses the rational tori. Michel Berry [26] provides a ough explanation by using twist maps - which consist of a Poincaré section of a rational torus as figure 2.8a amidst two neighboring irrational tori as in figure 2.8b resulting in figure 2.11a. The perturbation will distort the invariant circles (sections of tori) as in figure 2.11b, and we can notice the formation of fixed points in the twist map (crossings between the green and red lines). Thereafter, analyzing the tori directions, it becomes explicit the development of elliptic and hyperbolic orbits - figure 2.11c. Thus, the conclusion of the theorem can be summarized as

- The rational tori covered with periodic orbits are substituted to an even number of periodic orbits, half stable and half unstable.

Both theorems unequivocally exhibit how complex the systems start to be when the perturbation is active. The systems get rid of only parabolic orbits and begin to display sequences of elliptic and hyperbolic orbits. In the next section, when we shall define the classical map operated in the work, both theorems will be illustrated mainly with the standard map, and we will understand them more effectively. Before that,

there are two more considerations to address in order to comprehend what occurs with the system when the perturbation is active.

Firstly, as we can detect in figure 2.11c, there will be some gaps close to the hyperbolic fixed points, and this region will be fundamental for capturing the general structure of perturbed systems. The second is the fractal structure of the elliptic fixed points in which they replicate their structure in small scales *ad infinitum*.

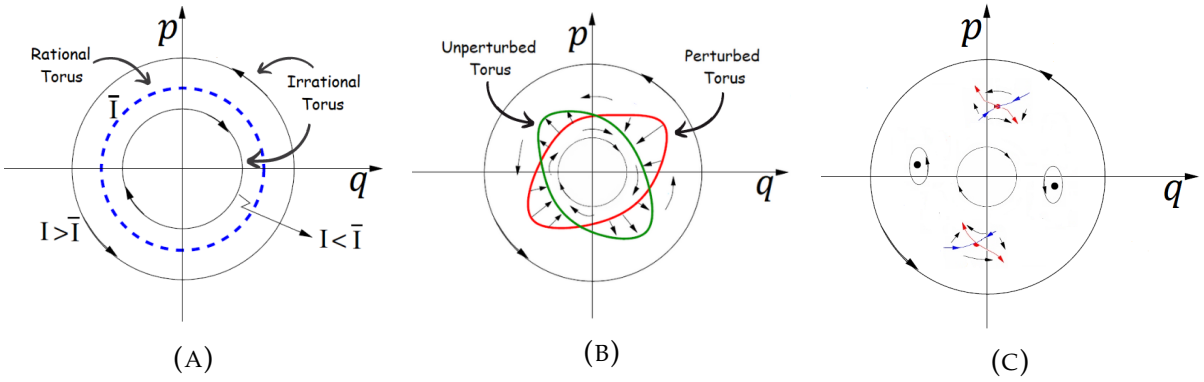

FIGURE 2.11. (A) Twist map with a blue dashed line depicting a Poincaré section of a rational torus, and the solid lines are Poincaré sections of irrational tori. The arrows correspond to the winding number α dependence on the momentum p: if $d\alpha/dp < 0$ is clockwise and if $d\alpha/dp > 0$ is counterclockwise. (B) The emergence of fixed points after a perturbation in a rational torus. (C) Two elliptic and two hyperbolic fixed points are created by the perturbation of a rational torus.

2.2.2 Onset of chaos

Through the Poincaré-Birkhoff fixed point theorem, elliptic and hyperbolic orbits assume an imperative role in the system's phase space. Meanwhile, the increase of perturbation will turn more rational tori into elliptic and hyperbolic orbits and, consequently, will destroy surrounding irrational tori. Then, we have to understand those orbits since they are not inert to the perturbation. For this, we must recall the concept of stable and unstable manifolds of hyperbolic orbits.

As aforementioned, generally, the curves W_u and W_s are distinct as in figure 2.10. That said, in order to track the demeanor of the manifolds, we take the example of an already-broken rational torus of periodicity 5 amidst two preserved irrational

tori (see figure 2.12). We must note that the five hyperbolic fixed points correspond to the same periodic orbit, whereby the same occurs to the five elliptic fixed points. Therefore, the manifolds of each fixed point being elliptic or hyperbolic are, in fact, the same manifold. The perturbation disturbs the form of that invariant curves [5] in such a way that they start to squeeze and stretch and inevitably cross each other as depicted in figure 2.13, but they cannot self-intercept. Those crosses between manifolds of the same fixed point are called homoclinic points.

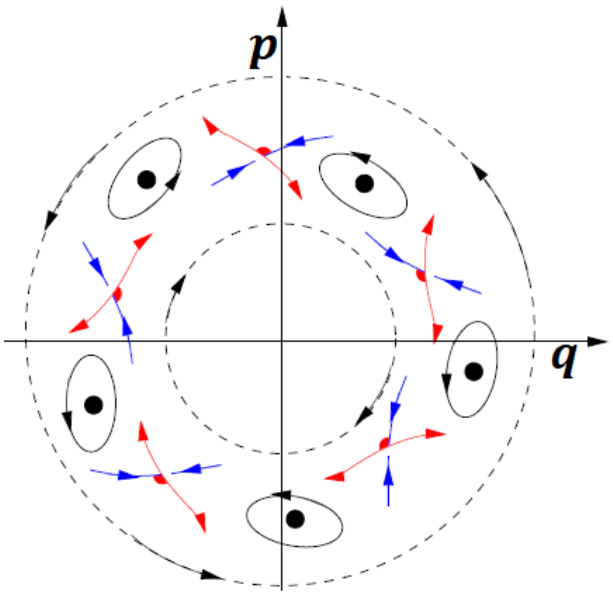

FIGURE 2.12. Twist map with two surrounding irrational tori and between a structure of sequential of five stable and unstable fixed points alluding to the previous rational torus.[23]

By the reasoning that the curves will intersect infinite times and the map has to obey the area preservation of Liouville's theorem, the manifolds squeeze and stretch even more near the unstable fixed points to compensate for the area conservation and resulting in a tangled structure as in the figure 2.14. In the schematic figure, we can take the path (ABC) in an early time as an example, and when it passes near the hyperbolic fixed point, the same piece of trajectory assumes the form $(A'B'C')$. This instance demonstrates the complexity that is presented in perturbed systems; it marks the entry of a new natural stochastic element into the discussion: the sensibility of initial conditions. In addition, owing to the indefinitely many intersections, the invariant

[5] We have to keep in mind that the adjective invariant here is regarding the time evolution, in which any point within this curves never leaves them, and not the action of the perturbation.

curves will fill the area - the empty space between the irrational tori in figure 2.11c - and consequently, there will not exist a tori in this phase space region. Therefore, going back to the five-fixed point system, the perturbation effect can be summarized as the following depiction 2.15 and the onset of chaotic trajectory starts at the surrounding of the hyperbolic fixed points where initial conditions will be scattered exponentially through the system.

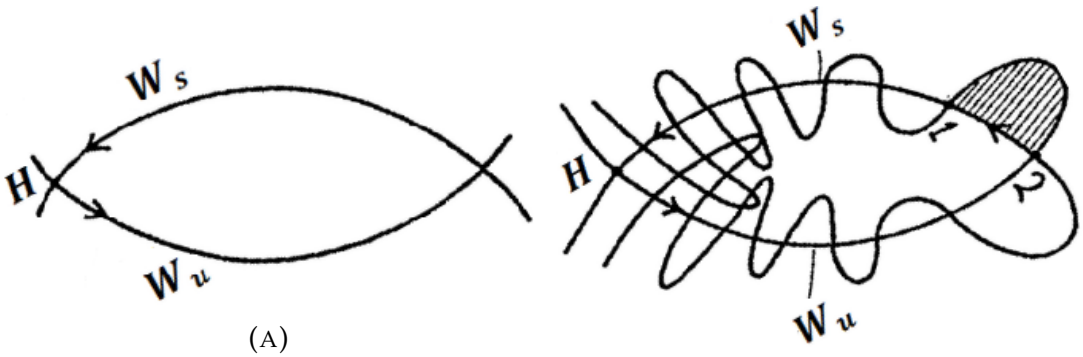

FIGURE 2.13. (A) Stable and unstable manifold before the perturbation. (B) Perturbative manifolds, which are stretched and squeezed, create a crossing point dubbed homoclinic [26].

The second consideration is about the elliptic fixed points. In every neighborhood of elliptic fixed points, there are closed invariant irrational curves. The former rational curves (or tori) turn into stable and unstable fixed points with irrational curves around them. If we amplify between these invariant irrational curves, there will be more former rational tori replaced by elliptic and hyperbolic fixed points - as represented in figure 2.16. The whole structure of the elliptic fixed points and the invariant curves around them are called islands. Any curve in an island is represented by a winding number; when it becomes close to rational, or the disturbance is sufficiently large, the curve may break and split into a second-order elliptic fixed point. Whether the second-order curves break, they will turn into third-order islands. This infinite sequence of islands orders generates the fractal structure in the perturbative systems. Furthermore, as it is expected, the breadth of the island diminishes rapidly with the period, such that numerical investigations [20] exhibit that random initial conditions will effortlessly detect islands with small periods - and our exploration with the classical maps will explicitly exemplify this characteristic.

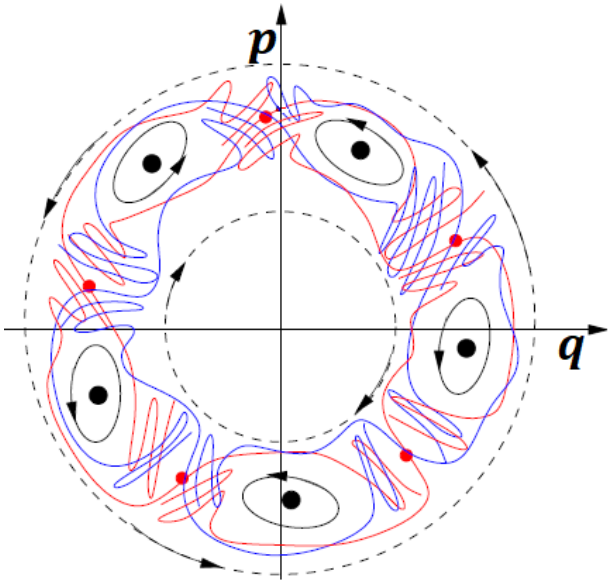

FIGURE 2.14. Schematic phase space of a non-integrable system with some perturbation-surviving irrational tori, and a region where previously settled a 5-period rational torus. The disturbance replaced the rational torus with elliptic and hyperbolic fixed points. Moreover, due to Liouville's theorem, the stable and unstable manifolds of the hyperbolic fixed points entangle throughout the whole region delimited to the irrational tori [23].

Another important scrutiny is the fact that fixed points do not last perpetually. When the perturbation or a stochastic parameter varies, the monodromy matrix will obviously change. Hence, prior elliptic or hyperbolic orbits may not exist in the system after an increase or decrease in the perturbation. The creation or destruction of orbits in dynamical systems by a parameter variation is known as bifurcation. Namely, this offshoot would deserve a thorough work per se; however, despite being actively important in semiclassical theory (section 5.1), we shall only state its elemental influence and methodology[6]. As we saw in section 2.1.4, the matrix's eigenvalues 2.75 dictate the stability of the fixed points, and in a more general description, for orbits of period n, the monodromy matrix is $\mathbf{M}^n$. The bifurcation is the point where the orbits essentially coalesce, leading to a vanishing residue $|\mathbf{M}^n - \mathbf{I}|$. The important behavior is what occurs to the elliptic orbits in conservative systems, which is known as period doubling. The perturbation coalesces a previous elliptic orbit and a new elliptic orbit with a doubled period emerges in the system, but hyperbolic orbits must also arise; and through the aforementioned discussion about unstable fixed point neighborhood,

[6]We mention Meyer [29] since it provides all bifurcations for area-preserving maps (systems that will be focused on our work). Ozorio de Almeida [24] also brings a complete and formal discussion about the topic and its implications.

the bifurcation ends up being a rote to chaos, as Edward Ott stated [30].

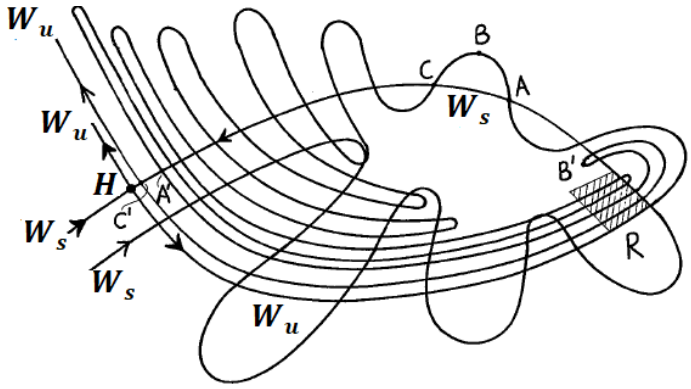

FIGURE 2.15. Trajectory of a perturbative system around unstable and stable manifolds. The perturbation influences the system in such a way that a segment of trajectory ABC in an interval of time can spread out to $A'B'C'$ when evolved near the hyperbolic fixed points [26].

Finally, we track a savvy depiction from Berry [26] to observe the demeanor in the actual torus phase space after all the conclusions we made with Poincaré sections and twist maps. First, the islands can be represented as thin wires that we start to wind into a primary loop, and the tori cover them like a concentric casing of PVCs (see figure 2.17). Thereafter, around the primary loop, there will be another casing and secondary wires that wind around the primary loop. In the secondary winding will be tertiary, then quaternary, and so forth. In addition, there will be empty spaces between the wires and casings - as we had in the Poincaré section in 2.11c. Then We have to fill with tangled, infinite long wire - a natural stochastic trajectory that onset in the neighborhood of the hyperbolic manifolds. Those irregular orbits are a single connected region and cover all the empty places (see figure 2.18); hence, the irrational tori are the sole structure that restricts the diffusion of unstable orbits - figure 2.19.

To sum up, after all the discussion of generic Hamiltonian systems through perturbation, we are able to understand a lack of general solutions for those cases. The presence of irregular orbits that cover the invariant curves without repeating themselves and, simultaneously, islands that have an underlying fractal structure are instances of the non-integrable systems' complexity. Regardless of this impediment, we are not curbed to comprehend and work with its complexities.

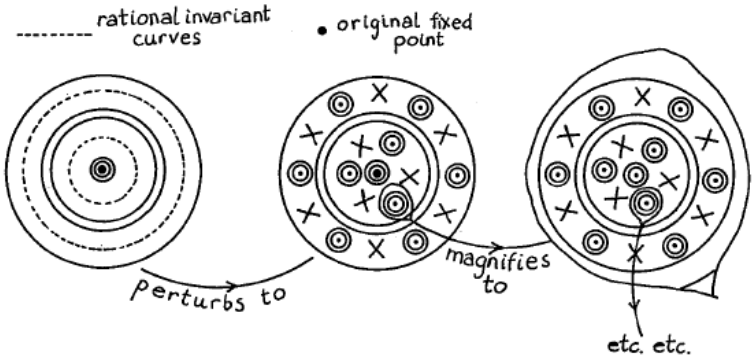

FIGURE 2.16. Illustration of the infinite sequence of stable orbits - elliptic fixed points - within invariant irrational curves. It aptly demonstrates the fractal structure present in non-integrable systems [26].

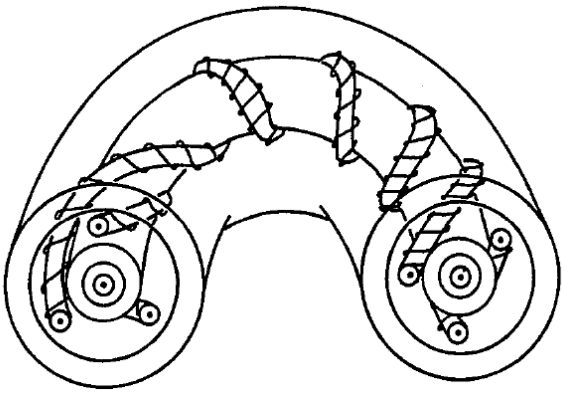

FIGURE 2.17. Phase space of a perturbative system with remaining irrational tori at the center and in the most external region. Moreover, stable islands are smaller tori wrapping the main tori and tertiary islands wrapping the secondary ones, and so forth [26].

2.3 Systems addressed

In order to study natural systems, we introduced a perturbation ϵH_1 in a well-known integrable system H_0. H_1 must have non-linear elements to disturb the phase space effectively and break irrational and rational tori through the KAM and Poincaré-Birkhoff fixed point theorems, respectively. Otherwise, if H_1 depends on the previous action-angle variables from H_0, the system will persist linear and integrable. Nevertheless, Chirikov [31] proposed another category of a system to investigate the onset of chaos. They are well-known today as periodic-driven systems, and the most renowned example is the kicked rotor. Owing to their simplicity in dealing with and broad coverage both in classical and quantum chaology, physicists and mathematicians turned

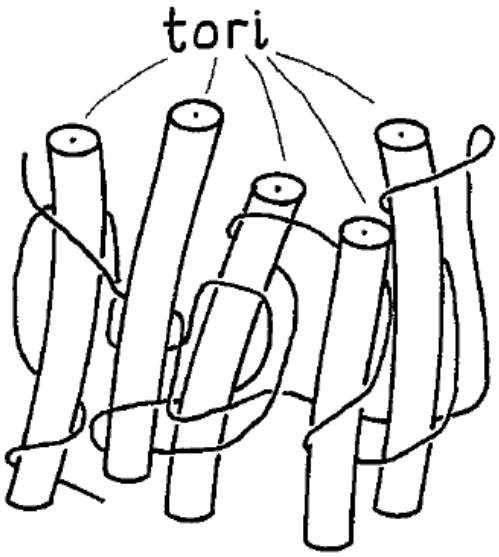

FIGURE 2.18. Schematic representation of a tangled, chaotic orbit intertwining stable tori [26].

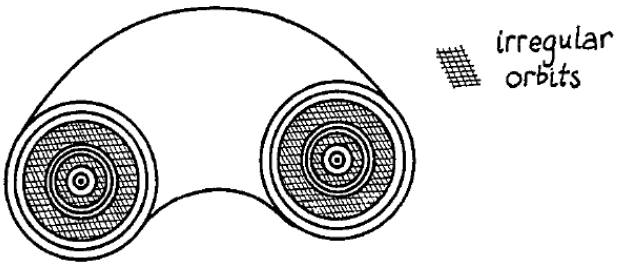

FIGURE 2.19. Phase space of a perturbative system with remaining irrational tori at the center and in the most external region. Moreover, stable islands are smaller tori wrapping the main tori and tertiary islands wrapping the secondary ones, and so forth [26].

them into one of the most exploited systems.

The general structure of their Hamiltonian is

$$H(p,q) = f(p) + V(q) \sum_{n=-\infty}^{\infty} \delta(t/\tau - n) \tag{2.85}$$

with $f(p)$ depending exclusively to the momentum, and $V(q)$ to the position and encompassing the perturbation. The Poincaré section to analyze their phase space is not an actual cut in a specific region; we indeed take advantage of the periodic configuration to establish a stroboscopic section. This means that we take pictures of the position and momentum after each period τ. Thus, they are commonly represented as

the following map

$$\begin{pmatrix} q_{n+1} \\ p_{n+1} \end{pmatrix} = \mathbf{M} \begin{pmatrix} q_n \\ p_n \end{pmatrix}. \tag{2.86}$$

which (q_n, p_n) are the position and momentum after $n\tau$ period and n is an integer. Moreover, since we are treating with conservative systems, the dyadic (q, p) generates an area-preserving map $\mathbf{M}$. In order to obtain 2.86 from 2.85, we have to start with Hamilton's equations 2.13 and get

$$\begin{aligned} \frac{dq}{dt} &= \frac{\partial H}{\partial p} = \frac{df(p)}{dp}, \\ \frac{dp}{dt} &= -\frac{\partial H}{\partial q} = -\sum_{n=-\infty}^{\infty} \delta(t/\tau - n)\frac{dV(q)}{dq}. \end{aligned} \tag{2.87}$$

In order to perform the stroboscopic section, we have just to integrate it over one period τ. First, we set the initial time as $t_0 = 0^+$, in which the superscript $+$ signifies right after the kick, and as a consequence, the superscript $-$ will denote right before the kick. Then we free the position and momentum to evolve until the nth kick. Between the interval $n^+ < t/\tau < (n+1)^-$, there is no force acting on the system, resulting in

$$\begin{aligned} q_{n+1}^- &= q_n^+ + \tau \frac{df(p)}{dp}\bigg|_{p=p_n^+} \\ p_{n+1}^- &= p_n^+. \end{aligned} \tag{2.88}$$

To complete the period, we have just to include the interval that passes through the kick $(n+1)^- < t/\tau < (n+1)^+$. Performing the integration, we have to assume that $f(p)$ is smooth - without any delta dependency - so that the position remains the same in this small interval. The momentum integration is trivial, giving the impulse contribution of the kick

$$\begin{aligned} q_{n+1}^+ &= q_{n+1}^- \\ p_{n+1}^+ &= p_{n+1}^- + \tau V(q_{q_{n+1}^+}). \end{aligned} \tag{2.89}$$

Lastly, we just sum up the two equations to culminate in the stroboscopic map

$$\begin{aligned} q_{n+1} &= q_n + \tau \frac{df(p)}{dp}\bigg|_{p=p_n}, \\ p_{n+1} &= p_n - \tau \frac{dV(q)}{dq}\bigg|_{q=q_{n+1}}, \end{aligned} \tag{2.90}$$

with the $+,-$ index dropped because (q,p) for those maps will be defined as just after the respective kicks.

The periodic-drive systems addressed in this dissertation are the kicked rotor and the kicked Harper Hamiltonian; both end up respectively in the standard map and the Harper map. In addition, we also include a prominent map to extend even more our results in section 4.2, the perturbed cat map. Now, we shall introduce the three systems separately and discuss their peculiarities. Each will provide an instance for all the concepts that we have discussed in the previous sections, such as KAM and Poincaré-Birkhoff fixed point theorems, rational and irrational tori, elliptic and hyperbolic fixed points, chaotic orbits, stable islands, and bifurcations. Those classical structures will reappear when we shall manage the quantum counterparts in the semiclassical regime, leaving characteristic signatures in the wavefunction.

2.3.1 Kicked rotor

Our scrutiny through the selected systems starts with the kicked rotor since it is invariably a suitable prospect for studying classical structures and the effects of perturbation on integrable systems. The system is simply a rotor with a constant radius that is tapped periodically. Therefore, between the kicks, the rotor is free to rotate; having completed a turn, it feels a periodic potential in the angle variable which performs the kick. Placing the words into formulas, the Hamiltonian is

$$H(p,q) = \frac{p^2}{2} - \frac{g}{(2\pi)^2}\cos(2\pi q)\sum_{n=-\infty}^{\infty}\delta(t/\tau - n) \tag{2.91}$$

with g as the kick-controlling parameter and the angle q varying in $[0,1]$. In addition, we have assumed that the rotor moment of inertia is unitary for simplicity. Comparing 2.91 with 2.85, we have

$$f(p) = \frac{p^2}{2}, \quad V(q) = \frac{g}{(2\pi)^2}\cos(2\pi q); \tag{2.92}$$

and consequently, the resulting stroboscopic map of the kicked rotor - known as the standard map - is

$$\begin{aligned} q_{n+1} &= q_n + p_n \qquad \mod 1, \\ p_{n+1} &= p_n - \frac{K}{2\pi}\sin(2\pi q_{n+1}), \end{aligned} \tag{2.93}$$

which we just rescaled $Tp \to p$ and defined a new parameter to include the perturbation $K = T^2 g$. Allowing the momentum free to vary, the topology of the phase space is confined into a cylinder, but since p has a symmetry regarding translational boost by $n \in \mathbb{Z}$, we can restrict all the momentum into the interval $[0, 1]$. The map then becomes

$$\begin{pmatrix} q_{n+1} \\ p_{n+1} \end{pmatrix} = \begin{pmatrix} 1 & 1 \\ 0 & 1 \end{pmatrix} \begin{pmatrix} q_n \\ p_n \end{pmatrix} - \frac{K}{2\pi} \sin\left(2\pi q_{n+1}\right) \begin{pmatrix} 0 \\ 1 \end{pmatrix} \mod 1. \tag{2.94}$$

To begin our analyses of the system, we start considering it without perturbation, i.e., $K = 0$. The kicked rotor is free to whirl and then is integrable. Conveniently, (p, q) is already the action-angle coordinates, and the stroboscopic map is

$$\begin{pmatrix} q_{n+1} \\ p_{n+1} \end{pmatrix} = \begin{pmatrix} 1 & 1 \\ 0 & 1 \end{pmatrix} \begin{pmatrix} q_n \\ p_n \end{pmatrix} \mod 1. \tag{2.95}$$

The momentum is naturally constant $p_n = p_0$; in addition, it will determine whether the structure of the tori is rational or irrational since $(q_{n+1} - q_n) = p_0 = \omega_0$. In figure 2.20a, we can see the phase space for different initial conditions. First, the rational tori are evident when $p_0 = r/s$ with s being the period and r the rotation times. In the map, they are represented by $(s + 1)$ points (since the modulus makes $q = 0$ and $q = 1$ the same) in a constant p value. On the other hand, if the frequency is an irrational number, we end up with KAM or irrational tori: solid lines in the map depicting trajectories that never close.

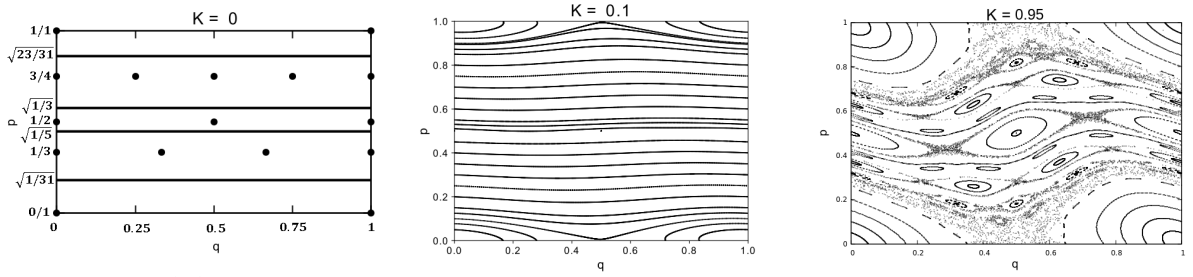

(A) (B) (C)

FIGURE 2.20. Standard map generated with the following parameters (A) $K = 0$, (B) $K = 0.1$, and (C) $K = 0.95$.

Now, with the perturbation $K \neq 0$, we shall increase gradually in order to examine all the considerations made in section 2.2. Owing to the non-null perturbation, p_0 is not the frequency anymore - ω_1 becomes more intricate to predict - but the map

will provide a reliable source of information about what will happen to each torus. We start with $K = 0.1$ in figure 2.20b; it is directly detectable that the two aforementioned theorems play their role in the non-integrable system. The Poincaré-Birkhoff fixed point theorem has already acted on the $0/1$ and $1/2$ rational tori by emerging the elliptic orbits with their invariant curves and the hyperbolic orbits with their stable and unstable manifolds, as discussed in figure 2.11c. Consequently, the KAM theorem also is present since there are some irrational tori yet preserved, such as in the region $q \approx 0.6$ or $q \approx 0.8$; in contrast to some KAM tori such as $\sqrt{1/3}$ or $\sqrt{1/7}$ that have already broken.

Increasing even more to $K = 0.95$ (figure 2.20c), the action of the perturbation into the neighborhood of hyperbolic fixed points becomes evident. Stochastic trajectories around the invariant curves take place by exploring all the free regions - they are only limited vertically by the last KAM torus depicted around the elliptic fixed point $1/2$. Now, Comparing $K = 1.2$ (figure 2.21a) and $K = 2.05$ (figure 2.21b), we can notice the trajectories predominantly submerged in the chaotic sea but dividing the phase space with substantial stable islands. Moreover, there is a clear exemplification of fractal structure within the $0/1$-island and a period-doubling bifurcation occurring in the $1/2$-island, which enhances the amount of hyperbolic fixed points, favoring chaos. Finally, to $K = 10$, there is no apparent stable structure, and the map is essentially fully chaotic - see figure 2.21c.

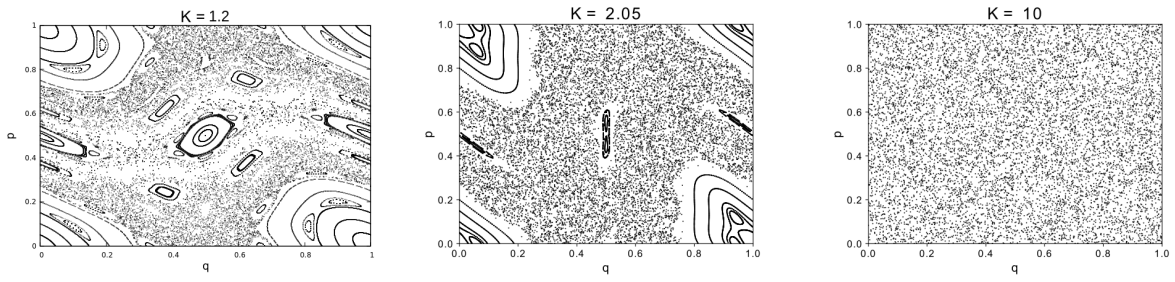

(A) (B) (C)

FIGURE 2.21. Standard map generated with the following parameters (A) $K = 0.95$, (B) $K = 2.05$, and (C) $K = 10$.

To conclude, we include the formula of the generating function $S(q_n, q_{n+1}; l_n, m_n)$ of the system. It provides an alternative method to obtain the map and will be funda-

mental when we shall address kicked rotor's semiclassical regime. Thus, from 2.19, we have

$$p_n = -\frac{\partial S}{\partial q_n}, \quad p_{n+1} = \frac{\partial S}{\partial q_{n+1}}; \tag{2.96}$$

and by integrating the previous equations and relating them, we can readily check that

$$S_{(std)}(q_n, q_{n+1}; l_n, m_n) = \frac{1}{2}(q_{n+1} - q_n + l_n)^2 + \frac{K}{4\pi^2}\cos(2\pi q_{n+1}) - m_n q_{n+1}, \tag{2.97}$$

with l_n and m_n being integers that restrict q_n and p_n respectively to the unitary modulus.

2.3.2 Kicked Harper Hamiltonian

The second covered system is the kicked Haper model introduced by Lebouef et al. [32]. Now, the periodic perturbation is present both in momentum and position coordinates, increasing generality. In order to describe the structure of the electronic energy band when submitted to an external magnetic field, Harper proposed the effective Hamiltonian of a cubic lattice considering only the nearest-neighbor [33]

$$H(q,p) = \cos p + \lambda \sin q, \quad \lambda = 1. \tag{2.98}$$

Inspired by Harper, Lebouef presented the kicked Harper Hamiltonian

$$H(p,q) = \frac{L}{(2\pi)^2}\cos(2\pi p) - \frac{A}{(2\pi)^2}\cos(2\pi q)\sum_{n=-\infty}^{\infty}\delta(t/\tau - n) \tag{2.99}$$

with A and L as parameters.

Analogous to the kicked rotor, the angle form of q and the clear symmetry in p restrict themselves to the period 2π. Similarly, we compare 2.99 with 2.85 to acquire

$$f(p) = \frac{L}{(2\pi)^2}\cos(2\pi p), \quad V(q) = \frac{A}{(2\pi)^2}\cos(2\pi q) \tag{2.100}$$

and result in the stroboscopic map of the kicked Harper Hamiltonian - known as the kicked Harper map

$$\begin{aligned} q_{n+1} &= q_n - \frac{L}{2\pi}\sin(2\pi p_n) \qquad \mod 1 \\ p_{n+1} &= p_n + \frac{A}{2\pi}\sin(2\pi q_{n+1}), \end{aligned} \tag{2.101}$$

which we have to rescale the momentum again and combine the periods τ with the parameters A and L. Introducing the periodicity in momentum, we have the following map

$$\begin{pmatrix} q_{n+1} \\ p_{n+1} \end{pmatrix} = \begin{pmatrix} 1 & 0 \\ 0 & 1 \end{pmatrix} \begin{pmatrix} q_n \\ p_n \end{pmatrix} + \frac{1}{2\pi} \begin{pmatrix} -L \sin(2\pi p_n) \\ A \sin(2\pi q_{n+1}) \end{pmatrix} \mod 1. \tag{2.102}$$

The perturbation analyses for the kicked Harper map are proximate to those for the standard map due to their similarities in the formulation. In addition, we settle $A = L$ in order to work with a single parameter whereby does not affect any measure performed throughout this dissertation.

When A is small, we can notice that some KAM tori are yet preserved; for instance, $A = 0.1$ in figure 2.22a. The irrational tori take rhombus structures reflecting the integrable system. Moreover, with the advent of another non-integrable term in the Hamiltonian, the formation of the island is premature, and they occupy a considerable volume in phase space already.

For the approximate interval $1 \lessapprox A \lessapprox 4$, all the KAM tori have already been broken. On top of that, owing to the strong non-linearity, the stochastic demeanor in the hyperbolic fixed points spreads rapidly, and the system is divided between stable islands and the chaotic sea (dubbed the mixed regime). An example of this case is the figure 2.22b with $A = 3.56$ - small islands are submerged in chaos. Finally, for $A \gtrapprox 5$, practically all of the system is chaotic with undetectable stable fixed points - see figure 2.22c with $A = 8{,}56$.

Therefore, we also need the generating function, which is also obtained from 2.96 by integrating and comparing the resulting map. Thus, the action becomes

$$\begin{aligned} S_{(hrp)}(q_n, q_{n+1}; l_n, m_n) &= \frac{L}{4\pi^2}\left[1 - \frac{4\pi^2}{L^2}(q_n - q_{n+1} - l_n)^2\right]^{1/2} - \frac{A}{4\pi^2}\cos(2\pi q_{n+1}) \\ &- \frac{1}{2\pi}(q_n - q_{n+1} - l_n)\arcsin\left(\frac{2\pi}{L}(q_n - q_{n+1} - l_n)\right) \\ &- -m_n q_{n+1}. \end{aligned} \tag{2.103}$$

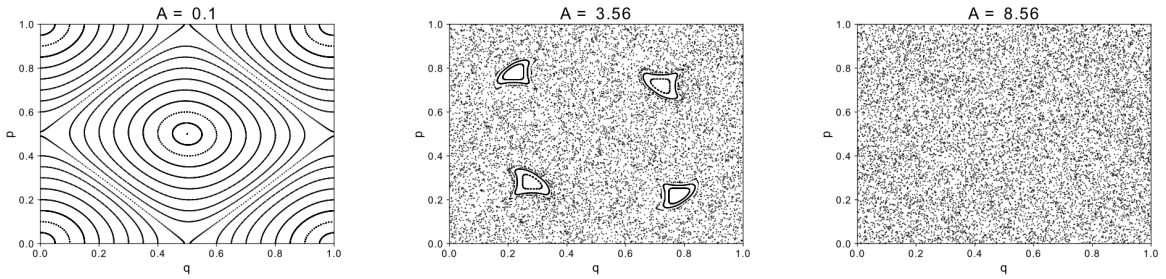

(A) (B) (C)

FIGURE 2.22. Surface of section of the kicked Harper map for different values of the perturbation parameter (A) $A = 0.1$, (B) $A = 3.56$, and (C) $A = 8.56$.

2.3.3 Perturbed cat map

For the last system considered, we deviate from the periodic-driven Hamiltonians and aim towards a well-established map in the chaos theory, a family of perturbed cat maps. They originated from the globally hyperbolic Anosov linear area-preserving map and just added a perturbation term [34, 35]. The map is defined as follows

$$\begin{pmatrix} q_{n+1} \\ p_{n+1} \end{pmatrix} = \begin{pmatrix} 2 & 1 \\ 3 & 2 \end{pmatrix} \begin{pmatrix} q_n \\ p_n \end{pmatrix} - \frac{\kappa}{2\pi} \cos(2\pi q_n) \begin{pmatrix} 1 \\ 2 \end{pmatrix} \mod 1. \tag{2.104}$$

with κ as parameter.

For $\kappa \leq (\sqrt{3}-1)/\sqrt{5} \approx 0.33$, the map is an Anosov system, which is proven to have only hyperbolic fixed points. In other words, the topology of the orbits of the perturbed system is conjugate to those of $\kappa = 0$ - figure 2.23a showcases this scenario for $\kappa = 0.2$. Increasing κ above this threshold, hyperbolic orbits can bifurcate to form elliptic orbits, consequently, stable islands. An instance is $\kappa = 6.67$ with two islands immersed in the chaotic sea (figure 2.23b).

Lastly, the generating function for the perturbed cat map is

$$\begin{aligned} S_{(cat)}(q_n, q_{n+1}; l_n, m_n) &= q_{n+1}^2 + q_n^2 - q_{n+1}q_n - \frac{\kappa}{4\pi^2}(4\pi\cos(2\pi q_n) - \sin(2\pi q_n)) \\ &- l_n q_n (1 - 2q_{n+1}) - m_n q_{n+1}. \end{aligned} \tag{2.105}$$

The classical properties of non-linear systems are interesting per se. However, we advance in content and investigate what occurs to non-linear systems when their Hamiltonians are brought to Schrodinger's equation. In other words, what are the demeanor of the energy levels and eigenstates of the classic chaotic Hamiltonians? The

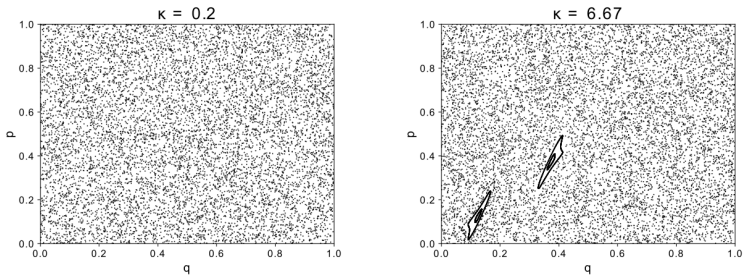

(A) (B)

FIGURE 2.23. Surface of section of the perturbed cat map for different values of the perturbation parameter (A) $\kappa = 0.2$ and (B) $\kappa = 6.67$.

effect of the classical systems on their quantum counterpart is exposed in the semi-classical regime, i.e., the action variables are much larger than the Planck constant (or summarized with the limit $\hbar \to 0$). Consequently, the influence of the stable and unstable trajectories will become meaningful, allowing parallels between the classical and quantum worlds.

In the following chapter, we shall discuss this position giving rise to the Gutzwiller trace formula - which provides the density of states in the function with only classical entities. Thereafter, in possession of the density, almost any information can be obtained from the system with a certain precision, including the eigenstates intensities for different classical regimes - fundamental for our analysis in chapter 5.

Chapter 3

Semiclassical physics

The previous chapter aptly demonstrates how exquisite and grounded the classical mechanics' properties are and how they fit our intuition. So it is reasonable that the so-called "old quantum theory" has been based on concepts that alluded to classical wisdom about the considered systems. The earliest examples have initiated with Planck dividing the classical energies into strata and Bohr postulating that the classical angular momentum has been quantized for confined potentials, which has set the allowed orbits at the rudimentary atom model.

On top of that, a generalization could be made to bring the concept of classical action. It has culminated in the Bohr-Sommerfeld quantization rule - the action has become the quantized entity. The last and most remarkable classical-based quantization in the period was constructed first by Einstein and complemented by Brillouin and Keller [36, 37, 38], the so-called EBK-quantization. Their rule has been the most full-fledged since it has generalized the Bohr-Sommerfeld formula for integrable systems. They have relied upon the action of the irreducible circuits γ_i to demonstrate that the quantum levels must follow the systems' tori in addition to counting their caustics.

However, although Einstein's appeal for a well-founded formulation, in 1926, Schrödinger presented to science community the formal quantum mechanics as we know today - totally based on probabilistic theory. Consequently, physicists have leaned their heads down to the new foundation and have started to explore all the new outcomes and oddities that have come up with it. Years later, at the end of the 60s, Physicists were searching for alternatives to grasp the quantum peculiarities and solve hard problems that, despite being well-defined in mathematical terms by quan-

tum mechanics, culminated in endless and foggy computation. For this reason, they ended up coming back to firmly grounded classical mechanics.

In order to bring classical wisdom to quantum systems, the correspondence principle has to be put into play. As stated by Niels Bohr, the principle claims that the quantum theory must lead to the classical theory under limiting conditions. This frontier has been dubbed the semiclassical limit in which the system's action variables are larger than the Planck constant ($S = \int pdq \gg \hbar$), or simply considering $\hbar \to 0$ for the quantum systems.

Semiclassical physics was intended to provide physical insights into various quantum systems that Schrodinger's wave mechanics had masked. It becomes evident from the fact that, in classical mechanics, the evolution of trajectories is promptly specified in phase space. Nevertheless, the uncertainty principle frustrates its definite characterization since we cannot perceive momentum and position with arbitrarily high precision. So the semiclassical limit has revealed that a description bringing classical knowledge was available somewhere between the worlds. It could provide information about unforeseen quantum concepts with established classical foundations.

Therefore, it had been into these considerations that classical chaotic systems started to be questioned about their quantum counterparts. Due to some of their KAM tori being destroyed, the EBK quantization rule could not be applied to those situations, and just solving Schrödinger's equation was also impractical. Consequently, in 1977, Casati and Ford [39] first brought into the discussion how would be the connection between these two seemingly disjointed strands. It was expected that quantum levels of non-integrable systems were obtained solely from classical information. With his ingenious works [40, 41, 42, 43], Gutzwiller provided answers to those investigations culminating in the trace formula. The field began to develop and became dubbed quantum chaos: the exploration of the chaotic influences in quantum properties.

That said, in this chapter, we shall inspect the semiclassical theory in all its essence by starting with a coverage of the most employed tenet of semiclassical physics: the stationary phase method. Thus, we shall be able to address the principles of the integrable systems when the limit $\hbar \to 0$ is taken. Afterward, non-integrable systems will be approached, culminating in Gutzwiller's trace formula. Finally, with

all this background, we shall see the semiclassical theory applied to classical maps.

3.1 Stationary phase method

As Gutzwiller has stated [19], there are two guideposts in the considerations of the semiclassical regime, first is the semiclassical propagator proposed by Van Vleck in 1928 [44], and the second is the employment of the stationary phase method whenever an integral comes up. We shall address the basic concepts to obtain a semiclassical expression for the intensities of our quantum maps' eigenstates. The first step is to investigate the most utilized procedure in semiclassical physics, dubbed the stationary phase method.

As we shall see later in this chapter, there will be entities with an imaginary exponential of the form $\exp\left((i/\hbar)\Omega(x)\right)$, such that Ω is a function of another variable x. Since we claim to be in the semiclassical regime, the Planck constant tends to zero $\hbar \to 0$, i.e., the imaginary exponential oscillates rapidly between -1 and 1. Therefore, any integral of a function along with $\exp\left((i/\hbar)\Omega(x)\right)$ in the integrand will be null unless there is a point in the phase where Ω is stationary.

Generally, we will be faced with the integral

$$\int_{x_1}^{x_2} e^{\left(\frac{i}{\hbar}\Omega(x)\right)} dx. \tag{3.1}$$

Having known that the function $\Omega(x)$ has a stationary point at $x = x_s$ within the interval $x_1 < x_s < x_2$, we expand the function until second order

$$\begin{aligned} \Omega(x) &= \Omega(x_s) + \left.\frac{\partial\Omega}{\partial x}\right|_{x=x_s} (x - x_s) + \frac{1}{2}\left.\frac{\partial^2\Omega}{\partial x^2}\right|_{x=x_s} (x - x_s)^2 + \mathcal{O}^3 && (3.2) \\ &\simeq \Omega(x_s) + \frac{1}{2}\left.\frac{\partial^2\Omega}{\partial x^2}\right|_{x=x_s} (x - x_s)^2 && (3.3) \end{aligned}$$

and substitute it into the integral 3.1

$$\int_{x_1}^{x_2} e^{\left(\frac{i}{\hbar}\Omega(x)\right)} dx \simeq e^{\frac{i}{\hbar}\Omega(x_s)} \int_{x_1}^{x_2} e^{\frac{i}{2\hbar}\Omega''(x_s)(x-x_s)^2} dx. \tag{3.4}$$

Owing to the integral being zero for x away from x_s, it is no difference whether we extend the integral to the entire real axis instead of only the interval $[x_1, x_2]$.

Hence, we are left with an integration of a complex Gaussian

$$e^{\frac{i}{\hbar}\Omega(x_s)}\int_{-\infty}^{\infty} e^{\frac{i}{2\hbar}\Omega''(x_s)(x-x_s)^2}dx = e^{\frac{i}{\hbar}\Omega(x_s)}\sqrt{\frac{2\pi i\hbar}{\Omega''(x_s)}} \tag{3.5}$$

$$= e^{\frac{i}{\hbar}\Omega(x_s)}\sqrt{\frac{2\pi\hbar}{|\Omega''(x_s)|}}\sqrt{\text{sgn}(\Omega''(x_s))i} \tag{3.6}$$

$$= \sqrt{\frac{2\pi\hbar}{|\Omega''(x_s)|}}e^{\frac{i}{\hbar}\Omega(x_s)+\text{sgn}(\Omega''(x_s))i\pi/4} \tag{3.7}$$

where $\sqrt{\text{sgn}(\Omega''(x_s))i}$ was rewritten following

$$\sqrt{\text{sgn}(\Omega''(x_s))i} = \sqrt{\pm i} = \sqrt{e^{\pm i\pi/2}} = e^{\pm i\pi/4} = e^{\text{sgn}(\Omega''(x_s))i\pi/4}. \tag{3.8}$$

Nevertheless, the integral 3.1 is a simple case of a one-dimensional variable x. In general, systems will revolve around multidimensional variables $\mathbf{x} = (x_1, \ldots, x_N)$ like position and momentum. Thus, the integral becomes

$$\int_{\mathbf{x_1}}^{\mathbf{x_2}} e^{\left(\frac{i}{\hbar}\Omega(\mathbf{x})\right)}d\mathbf{x}. \tag{3.9}$$

with the stationary points $\mathbf{x}_s$. Once more, we expand $\Omega(\mathbf{x})$ until the second order

$$\Omega(\mathbf{x}) \simeq \Omega(\mathbf{x}_s) + \frac{1}{2}\sum_{i,j=1}^{N}(\mathbf{x}-\mathbf{x}_s)_i^T\frac{\partial^2\Omega(\mathbf{x}_s)}{\partial x_i\partial x_j}(\mathbf{x}-\mathbf{x}_s)_j \tag{3.10}$$

and perform an orthogonal transformation due to the symmetry of the Hessian matrix $\partial^2\Omega(\mathbf{x}_s)/\partial x_i\partial x_j$. So, by defining L to be real and orthogonal, which diagonalizes the Hessian matrix, we have the transformation of $\mathbf{x}$ and the Hessian matrix [45]

$$L\mathbf{x} = \mathbf{y}, \quad \sum_{i,j=1}^{N}(\mathbf{x}-\mathbf{x}_s)_i^T\frac{\partial^2\Omega(\mathbf{x}_s)}{\partial x_i\partial x_j}(\mathbf{x}-\mathbf{x}_s)_j = \sum_{j=1}^{N}\lambda_j y_j^2 \tag{3.11}$$

respectively, with $\mathbf{y}$ being the eigenvectors and λ the eigenvalues.

The 3.9 integral can be written as

$$\int\cdots\int\prod_{i=1}^{N}dx_i e^{\left(\frac{i}{\hbar}\Omega(\mathbf{x})\right)} \simeq e^{\left(\frac{i}{\hbar}\Omega(\mathbf{x}_s)\right)}\int\cdots\int\prod_{i=1}^{N}dx_i\exp\left[\frac{i}{2\hbar}\sum_{j=1}^{N}\lambda_j y_j^2\right], \tag{3.12}$$

which is N one-dimensional integrals analog to 3.5. Therefore, we extend the interval to the real axis, and the N integrals 3.12 will culminate in

$$\sqrt{\frac{(2\pi\hbar)^N}{|\lambda_1|\dots|\lambda_N|}}e^{\left(\frac{i}{\hbar}\Omega(\mathbf{x}_s)\right)}\exp\left[\frac{i\pi}{4}\Big(\mathrm{sgn}(\lambda_1)+\cdots+\mathrm{sgn}(\lambda_N)\Big)\right] \tag{3.13}$$

$$=\sqrt{\frac{(2\pi\hbar)^N}{|\det(\Omega'')|}}e^{\left(\frac{i}{\hbar}\Omega(\mathbf{x}_s)+i\frac{\pi}{4}\gamma\right)}, \tag{3.14}$$

where γ is the number of positive eigenvalues minus negative eigenvalues, and Ω'' is the Hessian matrix.

3.2 Semiclassical integrable systems

In order to start dealing with semiclassical physics, we shall derive the expression for integrable systems leading to the EBK quantization rule. Moreover, it will enable us to identify the periodic orbits' influence following the Berry-Tabor description of quantum integrable systems.

The time-dependent WKB approximation is appropriate to evaluate the integrable systems [24]. First of all, we invoke Schrodinger's equation

$$i\hbar\frac{\partial\psi}{\partial t}=H\psi \tag{3.15}$$

and apply the WKB approximation by considering the ansatz

$$\psi(\mathbf{q},t)=A(\mathbf{q},t)e^{i\sigma(\mathbf{q},t)/\hbar}. \tag{3.16}$$

Substituting it into the Schrodinger equation, we are left with

$$i\hbar\frac{\partial A}{\partial t}-A\frac{\partial\sigma}{\partial t} = e^{-i\sigma/\hbar}H(\hat{\mathbf{q}},\hat{\mathbf{p}})e^{i\sigma/\hbar}A \tag{3.17}$$

$$= H(\hat{\mathbf{q}},\hat{\mathbf{p}}+\frac{\partial\sigma}{\partial\mathbf{q}})A. \tag{3.18}$$

As a first semiclassical approximation $\hbar\to 0$, the zero-order of $\hbar$ is simply

$$\frac{\partial\sigma}{\partial t}=H(\hat{\mathbf{q}},\hat{\mathbf{p}}+\frac{\partial\sigma}{\partial\mathbf{q}})=H(\hat{\mathbf{q}},\frac{\partial\sigma}{\partial\mathbf{q}}), \tag{3.19}$$

where the momentum is neglected from its own definition $\hat{\mathbf{p}}=-i\hbar\partial/\partial\mathbf{q}$.

Whether we compare equation 3.19 with 2.50, it is unequivocal that 3.19 is essentially the Hamilton-Jacobi equation. Consequently, the previously mentioned considerations about 2.50 may be applied here. For instance, along with an initial condition $\sigma(\mathbf{q}, t = 0) = R(\mathbf{q}_0, 0)$, we obtain the solution of the action 2.53.

Furthermore, 3.19 displays that the semiclassical wavefunction is associated with the evolution of the Lagrangian surface Σ_t - defined by $\mathbf{p}(\mathbf{q}, t) = \partial\sigma/\partial\mathbf{q}$ and depicted in figure 2.5.

From the ordinary approach of seeking solutions similar to plane waves, we request solutions where $\mathbf{p}$ is independent of time t. In other words, as in section 2.1.3, we pursue actions of the form

$$\sigma(\mathbf{q}, t) = W(\mathbf{q}) - Et. \tag{3.20}$$

In fact, they are invariant Lagrangian surfaces leading to a conserved Hamiltonian

$$H(\mathbf{q}, \mathbf{p}) = -\frac{\partial\sigma}{\partial t} = E \tag{3.21}$$

as in 2.55. Therefore, we are dealing with the time-independent Hamilton-Jacobi equation in which the solutions only exist for integrable systems, as extensively discussed in section 2.1.3.

Recalling from the integrable system, those invariant surfaces are actually the classical tori with momentum given by

$$\mathbf{p} = \mathbf{p}(\mathbf{q}, \mathbf{I}). \tag{3.22}$$

Additionally, the action $W(\mathbf{q}, \mathbf{I})$ is the generating function that has to hold the equation 2.62. The new variables $\boldsymbol{\phi}$ and $\mathbf{I}$ correspond to operators in the semiclassical limit that follow the commutation relations

$$[\hat{I}_i, \hat{I}_j] = [\hat{\phi}_i, \hat{\phi}_j] = 0 \quad [\hat{I}_i, \hat{\phi}_j] = i\hbar. \tag{3.23}$$

As a consequence of the integrable systems' description is based on the fact that $H = H(\hat{\mathbf{I}})$, H and $\hat{\mathbf{I}}$ must commute, generating good quantum numbers. This means that the wavefunction $\psi_{\mathbf{I}}(\boldsymbol{\phi})$ must have a constant amplitude

$$|\langle\phi|\psi_{\mathbf{I}}\rangle|^2 = |\psi_{\mathbf{I}}(\boldsymbol{\phi})|^2 = constant = c^2. \tag{3.24}$$

Moreover, the probability must conserve regardless of the representation, so

$$|\psi_{\mathbf{I}}(\boldsymbol{\phi})|^2 d\boldsymbol{\phi} = |\psi_{\mathbf{I}}(\mathbf{q})|^2 d\mathbf{q}. \tag{3.25}$$

From 3.16, the amplitude gives

$$A^2 = |\psi_{\mathbf{I}}(\mathbf{q})|^2 \propto \left|\det\left(\frac{\partial \boldsymbol{\phi}}{\partial \mathbf{q}}\right)\right| = \left|\det\left(\frac{\partial^2 \sigma}{\partial \mathbf{q} \partial \mathbf{I}}\right)\right|, \tag{3.26}$$

resulting in the wavefunction for the tori $\mathbf{I}$

$$\psi_{\mathbf{I}}(\mathbf{q}, t) = c\left|\det\left(\frac{\partial^2 \sigma}{\partial \mathbf{q} \partial \mathbf{I}}\right)\right|^{1/2} e^{i\sigma(\mathbf{q},\mathbf{I},t)/\hbar}, \tag{3.27}$$

or we separate the action with 3.20 and get the plane waves format

$$\psi_{\mathbf{I}}(\mathbf{q}, t) = c\left|\det\left(\frac{\partial^2 W}{\partial \mathbf{q} \partial \mathbf{I}}\right)\right|^{1/2} e^{iW(\mathbf{q},\mathbf{I})/\hbar} e^{iEt/\hbar}. \tag{3.28}$$

Furthermore, we have to consider that the Lagrangian surface, defined by $\mathbf{p}_{\mathbf{I}}(\mathbf{q})$, intercepts the L-dimensional plane $\mathbf{q} = const$ multiple times. For this reason, the action W is multivalued, and the proper solution has to be a superposition of the actions $W_j(\mathbf{q}, \mathbf{I})$. Another imperative deliberation is when a divergence takes place in the amplitude of 3.28.

The determinant can be opened with 2.61 leading to

$$\det\left(\frac{\partial^2 W}{\partial \mathbf{q} \partial \mathbf{I}}\right) = \det\left(\frac{\partial \boldsymbol{\phi}}{\partial \mathbf{q}}\right) = \det\left(\frac{\partial \boldsymbol{\phi}}{\partial \mathbf{p}}\right) \det\left(\frac{\partial \mathbf{p}}{\partial \mathbf{q}}\right). \tag{3.29}$$

The second term in equation 3.29 showcases that it diverges at the boundaries of the torus layers, i.e., the caustics of the torus. To solve this hurdle, we may follow Maslov's method and introduce a constant phase α in the wavefunction 3.28

$$\psi_{\mathbf{I}}(\mathbf{q}, t) = c\sum_j \left|\det\left(\frac{\partial^2 W_j}{\partial \mathbf{q} \partial \mathbf{I}}\right)\right|^{1/2} e^{iW(\mathbf{q},\mathbf{I})/\hbar - i\alpha_j \pi/4} e^{iEt/\hbar}, \tag{3.30}$$

which is known as the semiclassical wavefunction for integrable systems.

The insertion of the phase α_j is more transparent with a particular example. So we set aside in the appendix A a discussion about the phase presence. Additionally, in the addendum, it is revealed that the energy spectrum for integrable systems comes from stratification of the actions $\mathbf{I} = \hbar(\mathbf{n} + \boldsymbol{\mu}/4)$, resulting in

$$E_{\mathbf{n}} = H\left[\mathbf{I} = \hbar\left(\mathbf{n} + \frac{\boldsymbol{\mu}}{4}\right)\right]. \tag{3.31}$$

$\boldsymbol{\mu}$ is dubbed the Maslov index and reckons the number of times that $\partial\mathbf{q}/\partial\mathbf{p}$ becomes positive minus the number of times that $\partial\mathbf{q}/\partial\mathbf{p}$ becomes negative when run along the irreducible circuit γ_i for each degree of freedom $i = 1, \ldots, L$.

According to 3.31, the eigenenergies are the Hamiltonian surface that touches the action lattice at some point. For instance, for the two-dimensional harmonic oscillator, with the straightforward Hamiltonian

$$H = \omega_1 I_1 + \omega_2 I_2 = E \tag{3.32}$$

$$I_2 = -\frac{\omega_1}{\omega_2} I_1 + \frac{E}{\omega_2}, \tag{3.33}$$

provides an intelligible visualization of the panorama. The energy E is varied continuously in 3.33 and imprints every time a curve touches the lattice $(I_1 = \hbar(n_1 + 1/2), I_2 = \hbar(n_2 + 1/2))$ - figure 3.1 displays two curves regarding two eigenenergies.

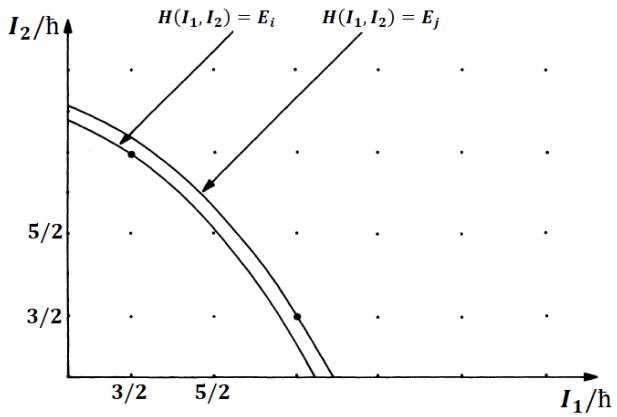

FIGURE 3.1. Illustration of two surfaces of energy for the two-dimensional harmonic oscillator. It depicts clearly how the eigenenergies are obtained from the quantized tori for integrable systems [24].

Therefore, if we bring the system to the semiclassical limit, which conveys large values of $\mathbf{n}$ and a dense lattice, and construct the energy smoothly dependent on a parameter, degeneracies will emerge, and integrable systems will boast a Poisson energy level statistic. This property is a hallmark since it differs from non-integrable systems that require more than one parameter to produce a degeneracy, indicating a strong level of rigidity.

3.2.1 Trace formula for integrable systems

We have seen through the semiclassical description that the eigenenergies are intrinsically related to the classical tori for integrable systems. Nevertheless, for non-integrable systems, Gutzwiller has discovered a dependence of classical periodic orbits on the density of states. Therefore, following Berry and Tabor's argument [46], the density of states, viz. energy levels, for integrable systems is also connected to the periodic orbits of their classical counterpart.

To begin, considering an integrable system with f degrees of freedom, the density of states' definition is

$$\rho(E) = \sum_{\mathbf{n}} \delta(E - E_{\mathbf{n}}) \tag{3.34}$$

where the vector $\mathbf{n}$ is the quantum numbers $(n_1, n_2, \ldots, n_f)$ attached to the classical actions $\mathbf{I} = (I_1, I_2, \ldots, I_f)$ by the EBK quantization 3.31. Hence, the density becomes

$$\rho(E) = \sum_{\mathbf{n}} \delta\left[E - H\left(\mathbf{I} = \hbar\left(\mathbf{n} + \frac{\boldsymbol{\mu}}{4}\right)\right)\right]. \tag{3.35}$$

The equation 3.35 per se instigates us to describe the density of states as a Fourier sum over a reciprocal lattice of integers vectors $\mathbf{M}$. As a consequence, the delta function will be a by-product of a superposition of plane waves with wave vector $\mathbf{M}$.

Instead of applying the Fourier transform directly, we shall utilize Poisson's formula to get the expression of the reciprocal lattice. So, given a function $f(x)$ and its Fourier transform $g(y)$, one can reach the relation

$$\sum_{\nu=-\infty}^{\infty} f(\nu) = \sum_{\mu=-\infty}^{\infty} g(\mu). \tag{3.36}$$

Defining f as the delta function and substituting it into Poisson's formula, we have that the density of states is given by

$$\sum_{\mathbf{n}} \delta\left[E - H\left(\hbar\left(\mathbf{n} + \frac{\boldsymbol{\mu}}{4}\right)\right)\right] = \sum_{\mathbf{M}} \int d\mathbf{n}\, \delta\left[E - H\left(\hbar\left(\mathbf{n} + \frac{\boldsymbol{\mu}}{4}\right)\right)\right] e^{2\pi i \mathbf{M}\cdot\mathbf{n}} \tag{3.37}$$

$$= \frac{1}{\hbar^f} \sum_{\mathbf{M}} e^{-\pi i \mathbf{M}\cdot\boldsymbol{\mu}/4} \int d^f I\, \delta\left[E - H\left(\mathbf{I}\right)\right] e^{2\pi i \mathbf{M}\cdot\mathbf{I}}, \tag{3.38}$$

where we have used the discrete tori $\mathbf{I}_{\mathbf{n}} = \hbar(\mathbf{n} + \boldsymbol{\mu}/4)$, and the integral in the actions is only at the first quadrant since the quantum numbers are positive integers.

In particular, we can split the density into contributions of $\mathbf{M} = 0$ and $\mathbf{M} \neq 0$. The former is the notorious Thomas-Fermi density, which addresses the lowest approximation of many interacting particles,

$$\begin{aligned} \bar{\rho}(E) &= \frac{1}{\hbar^f} \int d^f I \delta \left[E - H\left(\mathbf{I}\right)\right] && (3.39) \\ &= \frac{1}{(2\pi\hbar)^f} \int d^f I d^f \theta \delta \left[E - H\left(\mathbf{I}\right)\right] && (3.40) \\ &= \frac{1}{\hbar^f} \int d^f q d^f p \delta \left[E - H\left(\mathbf{q}, \mathbf{p}\right)\right]. && (3.41) \end{aligned}$$

In addition, its interpretation unequivocally pops up from 3.41. On average, each state occupies a volume of $\hbar^f$ in the phase space, from this fact is also called the Weyl term. The latter is the kernel of the semiclassical foundation: the fluctuation of the density of states. It showcases the deviations from the average and provides the non-trivial aspects embedded into the semiclassical system. As a result, the fluctuation reads

$$\tilde{\rho}(E) = \frac{1}{\hbar^f} \sum_{\mathbf{M} \neq 0} e^{-\pi i \mathbf{M} \cdot \boldsymbol{\mu}/4} \int d^f I \delta \left[E - H\left(\mathbf{I}\right)\right] e^{2\pi i \mathbf{M} \cdot \mathbf{I}}, \tag{3.42}$$

Arising from the Poisson formula, which requires many terms of integers $\mathbf{M}$ to produce a delta function, the integral in 3.42 is brought to the stationary phase method by the reason that the exponential varies rapidly compared to the remaining integrated.

In order to find the stationary points of $\mathbf{M} \cdot \mathbf{I}$, we take advantage of the Lagrange multipliers since the delta gives us a constraint. Thus, we define the Lagrangian function

$$\mathcal{L}(\mathbf{I}, \lambda) = \mathbf{M} \cdot \mathbf{I} - \lambda(H(\mathbf{I}) - E) \tag{3.43}$$

where

$$\nabla_{\mathbf{I},\lambda} \mathcal{L} = 0. \tag{3.44}$$

The derivative at $\mathbf{I}$ provides us the value of the Lagrange multiplier λ

$$0 = \nabla_{\mathbf{I}} \mathcal{L} = \mathbf{M} - \lambda \sum_i \frac{\partial H}{\partial I_i}. \tag{3.45}$$

Recalling the frequencies' equation for integrable systems in 2.59, we are left with

$$\begin{aligned} \mathbf{M} &= \lambda \boldsymbol{\omega} && (3.46) \\ & && (3.47) \end{aligned}$$

If we dub $\lambda = 1/\omega_0$, it becomes evident that the stationary points are the periodic orbits since their frequencies follow the result

$$\omega_i = M_i \omega_0, \quad M_i \text{ as an integer}, \tag{3.48}$$

and, consequently, hold the commensurability relation 2.66. Moreover, to perform the integral 3.42 using the stationary points, we take benefit of Gutzwiller's local coordinates, however, in the action space. The reason lies in managing to separate the delta for one integral and be left with the $f-1$ complex integrals.

To address the delta, the first new action ξ_0 points along the normal to the surface of constant energy. The remaining new actions $(\xi_1, \ldots, \xi_{f-1})$ are tangential on the surface, where figure 3.2 illustrates this scenario for an integrable system with $f = 3$.

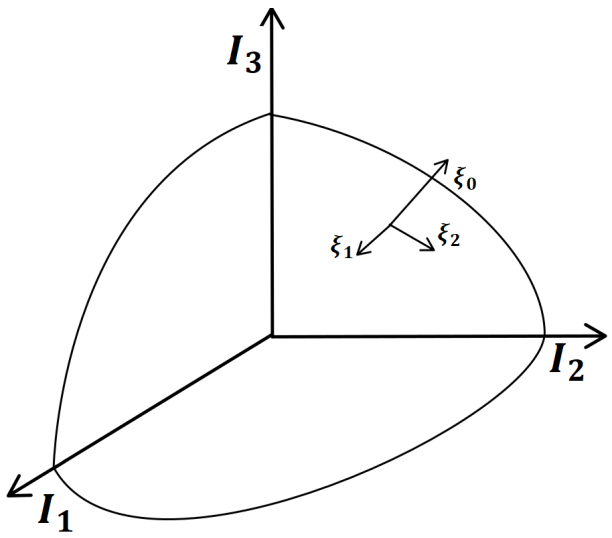

FIGURE 3.2. Energy surface depiction in the 3-dimensional action space. The vector ξ_0 is defined normal to the surface, and the other two xi_2 and ξ_3 are perpendicular to the energy shell. [23]

Along with the coordinate transformation, the integral turns into

$$\tilde{\rho}(E) = \frac{1}{\hbar^f} \sum_{\mathbf{M}\neq 0} e^{-\pi i \mathbf{M}\cdot\boldsymbol{\mu}/4} \int d^{f-1}\xi \int d\xi_0 \delta\left[E - H\left(\epsilon_0\right)\right] e^{2\pi i \mathbf{M}\cdot\mathbf{I}} \tag{3.49}$$

$$= \frac{1}{\hbar^f} \sum_{\mathbf{M}\neq 0} e^{-\pi i \mathbf{M}\cdot\boldsymbol{\mu}/4} \int d^{f-1}\xi \int d\xi_0 \delta\left(\xi_0\right) e^{2\pi i \mathbf{M}\cdot\mathbf{I}} \left|\frac{\partial \xi_0}{\partial H}\right|, \tag{3.50}$$

where we note that

$$\frac{\partial H}{\partial \xi_0} = \frac{\partial H}{\partial \mathbf{I}} \frac{\partial \mathbf{I}}{\partial \xi_0} = \boldsymbol{\omega}(\mathbf{I}) \frac{\partial \mathbf{I}}{\partial \xi_0}. \tag{3.51}$$

Taking the modulus of 3.51 and assuming a unitary Jacobian for the local transformation

$$\left|\frac{\partial \xi_0}{\partial H}\right| = \left|\frac{1}{\boldsymbol{\omega}(\mathbf{I})}\right|. \tag{3.52}$$

Finally, the $f-1$ integrals are solved by the stationary phase method, and, as aforementioned, the stationary points lie in the periodic orbits. Thus, we expand the exponential until the second order and deal with Gaussian integrals. The result is the equation 3.14 where

$$\Omega = 2\pi \sum_i M_i I_i \tag{3.53}$$

and the determinant becomes

$$|\det(\Omega'')| = (2\pi)^{f-1} \left|\det\left(\mathbf{M}\cdot\frac{\partial^2 \mathbf{I}}{\partial I_i \partial I_j}\right)\right| \tag{3.54}$$

and $\gamma_{\boldsymbol{M}}$ are the number of positive eigenvalues minus the negative eigenvalues from the matrix Ω''.

After the Gaussian integrals, the density fluctuation becomes

$$\tilde{\rho}(E) = \frac{1}{\hbar^f} \sum_{\mathbf{M}\neq 0} e^{-\pi i \mathbf{M}\cdot\boldsymbol{\mu}/4} \left|\frac{1}{\boldsymbol{\omega}(\mathbf{I})}\right| \left(\frac{\hbar}{|\mathbf{M}|}\right)^{\frac{f-1}{2}} \frac{1}{\sqrt{K(\mathbf{I})|_{\mathbf{I}_0}}} e^{2\pi i \mathbf{M}\cdot\mathbf{I}_0/\hbar + i\pi\gamma_{\boldsymbol{M}}/4}. \tag{3.55}$$

where $\mathbf{I}_0$ represents the action for the periodic orbits and $K(\mathbf{I})$ is the matrix that measures the curvature of the constant-energy surface in the action space. Rearranging the terms of 3.55

$$\tilde{\rho}(E) = \frac{1}{\hbar^{\frac{f-1}{2}}} \sum_{\mathbf{M}\neq 0} \frac{1}{|\boldsymbol{\omega}(\mathbf{I})||\mathbf{M}|^{\frac{f-1}{2}}} \frac{1}{\sqrt{K(\mathbf{I})|_{\mathbf{I}_0}}} \exp\left[\frac{2\pi i}{\hbar}\mathbf{M}\cdot\mathbf{I}_0 - \frac{\pi i}{4}\mathbf{M}\cdot\boldsymbol{\mu} + \frac{i\pi}{4}\gamma_{\boldsymbol{M}}\right] \tag{3.56}$$

and adding the mean density from the Thomas-Fermi 3.41, we get the Berry-Tabor equation in terms of periodic orbits. As we shall see in the next section 3.3, the density fluctuations 3.56 make a parallel with the prominent Gutzwiller trace formula for non-integrable systems.

3.3 Semiclassical non-integrable systems

Despite being important for promoting an acquaintance with semiclassical physics, integrable systems are far from our natural, real phenomena. So, a devel-

opment in the direction of non-integrable systems is required. However, their quantization, from semiclassical perspectives, had provided a hard time for physicists, as stated by Einstein [36], where he could not perceive a quantization when classical tori started to break in systems.

This Einstein quandary is aptly identified when we face solving the Schrodinger equation 3.15 with non-linear terms into the Hamiltonian. The previous natural solution of stationary wavefunctions led us to invariant Lagrangian surfaces. Nevertheless, those structures are actual tori that are not globally present in non-integrable systems - as thoroughly discussed in chapter 2. Therefore, their solutions are not of the form 3.30 and demand a distinct resolution.

3.3.1 The propagator and the Green function

From the lack of complete invariant surfaces, the maneuver with the wavefunction of non-linear systems will not furnish information about the energy spectrum as 3.31. The section 3.2.1, however, has enlightened us about the possibility of an additionally accessible path to the energy levels: the definition of the density of states 3.34. Namely, in quantum mechanics, when the density of states is stated, naturally emerges the Green function $G(\mathbf{q}'', \mathbf{q}', E)$ - and underlying the propagator $K(\mathbf{q}'', \mathbf{q}', t)$. Therefore, we shall investigate the non-integrable systems through both functions.

First of all, information about the physics of a quantum system can be properly obtained from the propagator $K(\mathbf{q}'', \mathbf{q}', t)$, which corresponds to the spread of the wavefunction at the position $\mathbf{q}''$ after a time t when it was previously concentrated at the position $\mathbf{q}'$. Consequently, putting it into mathematical formulae

$$K(\mathbf{q}'', \mathbf{q}', 0) = \delta(\mathbf{q}'' - \mathbf{q}') \tag{3.57}$$

$$i\hbar\frac{\partial}{\partial t}K - \hat{H}K = 0, \tag{3.58}$$

we note that K is simply a wavefunction with a delta as an initial condition. Also, we have to establish that $K(\mathbf{q}'', \mathbf{q}', t) = 0$ for $t < 0$.

Thus, from the completeness property of the wavefunctions

$$\delta(\mathbf{q}'' - \mathbf{q}') = \sum_{i=0}^{\infty} \psi_i(\mathbf{q}'')\psi_i^*(\mathbf{q}'), \tag{3.59}$$

the propagator can be written as

$$K(\mathbf{q}'', \mathbf{q}', t) = \sum_{i=0}^{\infty} \psi_i(\mathbf{q}'')\psi_i^*(\mathbf{q}')e^{-E_i t/\hbar}, \tag{3.60}$$

or in expectation value format

$$K(\mathbf{q}'', \mathbf{q}', t) = \langle \mathbf{q}'' | \, e^{i\hat{H}t/\hbar} \, | \mathbf{q}' \rangle \, . \tag{3.61}$$

The propagator 3.60 invites us to examine it like a Fourier expansion with respect to time t. From this perspective, the Green function $G(\mathbf{q}'', \mathbf{q}', E)$ rises and is defined as follows

$$G(\mathbf{q}'', \mathbf{q}', E) = \frac{1}{i\hbar} \int_0^{\infty} dt K(\mathbf{q}'', \mathbf{q}', t)e^{iEt/\hbar}, \tag{3.62}$$

which is a Laplace integral because t is positive. On top of that, in order to ensure convergence of the integral, a small positive imaginary value $i\epsilon$ can be appended to the energy $E \to E + i\epsilon$, whereby defines the Green function in the upper half of the complex plane.

We can evaluate the integral substituting the propagator's expression 3.60

$$G(\mathbf{q}'', \mathbf{q}', E + i\epsilon) = \frac{1}{i\hbar} \int_0^{\infty} dt \sum_{i=0}^{\infty} \psi_i(\mathbf{q}'')\psi_i^*(\mathbf{q}')e^{(E+i\epsilon-E_i)t/\hbar}, \tag{3.63}$$

and performing the trivial integral, we obtain an explicit form of the Green function

$$\begin{aligned} G(\mathbf{q}'', \mathbf{q}', E + i\epsilon) &= \frac{1}{i\hbar} \sum_{i=0}^{\infty} \psi_i(\mathbf{q}'')\psi_i^*(\mathbf{q}') \frac{e^{(E+i\epsilon-E_i)t/\hbar}}{(E + i\epsilon - E_i)i/\hbar} \Bigg|_0^{\infty} & (3.64) \\ &= \sum_{i=0}^{\infty} \frac{\psi_i(\mathbf{q}'')\psi_i^*(\mathbf{q}')}{(E + i\epsilon - E_i)}. & (3.65) \end{aligned}$$

The equation showcases that the Green function encompasses important physical information about the system. For instance, its poles provide energy levels, and its residues furnish wavefunctions.

Moreover, we can separate the denominator into its real and imaginary part

$$\frac{1}{E+i\epsilon-E_i}=\frac{E-E_i}{(E-E_i)^2+\epsilon^2}-\frac{i\epsilon}{(E-E_i)^2+\epsilon^2}, \tag{3.66}$$

By taking the limit of $\epsilon\to 0$, the first term becomes just $1/(E-E_i)$, and the second term advantageously cancels out. So, the real part of 3.66 is dubbed principal $P(1/(E-E_i))$ - without the pole. However, when $E=E_i$, the principal part cancels, and the imaginary part turns into a delta $\delta(E-E_i)$. To sum up, the denominator can be expressed as

$$\frac{1}{E+i\epsilon-E_i}=P\left(\frac{1}{E-E_i}\right)-i\pi\delta(E-E_i), \tag{3.67}$$

and the Green function takes on the form

$$G(\mathbf{q}'',\mathbf{q}',E+i\epsilon)=P\left[\sum_{i=0}^{\infty}\frac{\psi_i(\mathbf{q}'')\psi_i^*(\mathbf{q}')}{(E+i\epsilon-E_i)}\right]-i\pi\sum_{i=0}^{\infty}\psi_i(\mathbf{q}'')\psi_i^*(\mathbf{q}')\delta(E+i\epsilon-E_i). \tag{3.68}$$

If we take the trace of the Green function - $\mathbf{q}''=\mathbf{q}'=\mathbf{q}$, the integral in wave-functions summation will be unitary from 3.59 and we are left with

$$G(E+i\epsilon)=\mathrm{Tr}[G(\mathbf{q}'',\mathbf{q}',E+i\epsilon)]=\int d\mathbf{q}G(\mathbf{q},\mathbf{q},E+i\epsilon)=P\left[\frac{1}{(E+i\epsilon-E_i)}\right]-i\pi\delta(E+i\epsilon-E_i). \tag{3.69}$$

Therefore, from the definition of the density of states 3.34, we get

$$\rho(E)=-\frac{1}{\pi}\mathrm{Im}(G(E))=\sum_i\delta(E-E_i), \tag{3.70}$$

where the energy E is set to be complex ($E+i\epsilon$), and we shall maintain this convection to avoid always writing $i\epsilon$. It will endure until the necessity of a separation in chapter 5. The result 3.70 is paramount since it justifies our approach with the propagator and the Green function.

3.3.2 Semiclassical Green function

Now, we shall find a formula for the propagator in the semiclassical limit that will lead us to an approximation for the Green function via Fourier transforms. Thereafter, we shall have a function to obtain information about the eigenstates and eigenenergies of non-integrable systems.

First of all, in order to find the propagator, we rely upon the equation 3.60 because WKB approximation 3.16 still provides an appropriate wavefunction $\psi(\mathbf{q}, t)$. In a similar fashion to the calculation in section 3.2, we pursue an expression for the amplitude and the phase, but the action variables $\mathbf{I}$ do not provide good quantum numbers anymore.

Once more, the fundamental factor is that probability density $|\psi(\mathbf{q}, t)|^2$ is conserved. It establishes that the initial and final conditions of the wavefunction must hold

$$|\psi(\mathbf{q}', t)|^2 d\mathbf{q}' = |\psi(\mathbf{q}'', t)|^2 d\mathbf{q}'' \tag{3.71}$$

or

$$|A(\mathbf{q}'', t)| = |A(\mathbf{q}', 0)| \left| \det \frac{d\mathbf{q}'}{d\mathbf{q}''} \right|^{1/2}. \tag{3.72}$$

Thus, we have a blueprint of the wavefunction for $t > 0$

$$\psi(\mathbf{q}'', t) = A(\mathbf{q}', 0) \left| \det \frac{d\mathbf{q}'}{d\mathbf{q}''} \right|^{1/2} e^{\frac{i}{\hbar}[\sigma_0(\mathbf{q}', 0) + \sigma(\mathbf{q}', \mathbf{q}'', t)]} \tag{3.73}$$

On top of that, two considerations have to be encompassed. The first is that the generating function is multivalued, which introduces a summation in 3.73 similar to 3.30. The second is that the system can pass through points where the determinant may diverge when running along the trajectories, as in figure 2.6. Therefore, these caustics are remedied with $i\pi/2$ into the phase. The final expression is

$$\psi(\mathbf{q}'', t) = \sum_j A(\mathbf{q}'_j, 0) \left| \det \frac{\partial \mathbf{q}'_j}{\partial \mathbf{q}''_j} \right|^{1/2} e^{\frac{i}{\hbar}[R_0(\mathbf{q}'_j, 0) + R(\mathbf{q}'_j, \mathbf{q}''_j, t)] + i\pi\alpha_j/2}, \tag{3.74}$$

with α_j being the number of all sorts of position caustics of the j-th trajectory between $\mathbf{q}'$ and $\mathbf{q}''$, and we have conveniently changed to the action $R(\mathbf{q}', \mathbf{q}'', t)$ since it is the generating function itself as in 2.53.

Before inserting 3.74 into 3.60, we must consider that the Lagrangian surfaces are not invariant for non-integrable systems. In specific, the propagator uniformly assembles all the positions into the momenta at $t = 0$, defining the Lagrangian surface Σ_0, and spreads them to the appropriate Lagrangian surface Σ_t, as shown in figure 3.3. Nonetheless, there is no generation function $\sigma(\mathbf{q}, \partial\sigma/\partial\mathbf{q}, t)$ that can construct Σ_0. This

fact is effortlessly solved by shifting to the momentum representation, where the wavefunction $\psi(\mathbf{p},t)$ also conserves the probability density, and an equivalent wavefunction 3.74 can be attained

$$\psi(\mathbf{p}'',t)=\sum_j A(\mathbf{p}'_j,0)\left|\det\frac{\partial\mathbf{p}'_j}{\partial\mathbf{p}''_j}\right|^{1/2} e^{\frac{i}{\hbar}[R_0(\mathbf{p}'_j,0)+R(\mathbf{p}'_j,\mathbf{p}''_j,t)+i\pi\tilde{\alpha}_j/2]}. \tag{3.75}$$

with $\tilde{\alpha}_j$ being the number of all sorts of momentum caustics of the j-th trajectory between $\mathbf{p}'$ and $\mathbf{p}''$. The $R(\mathbf{p}'_j,\mathbf{p}''_j,t)$ is the doubled Fourier transform given by

$$R(\mathbf{p}',\mathbf{p}'',t)=R(\mathbf{q}',\mathbf{q}'',t)-\mathbf{q}''\mathbf{p}''+\mathbf{q}'\mathbf{p}'. \tag{3.76}$$

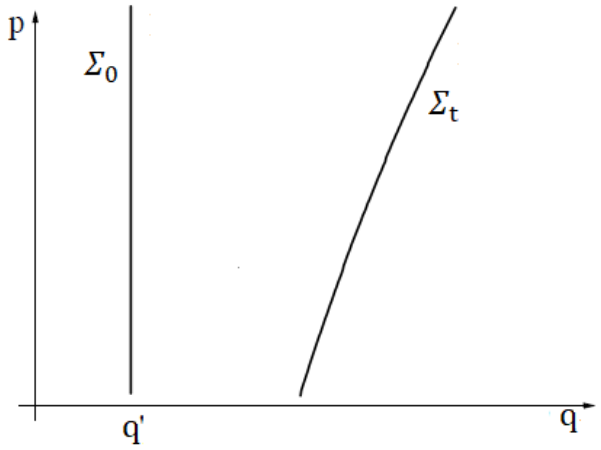

FIGURE 3.3. Lagrangian surface for the propagator $K(\mathbf{q}',\mathbf{q}'',t)$, where initially is distributed uniformly in the momentum with a fixed position and transmitted to a general Lagrangian surface as time runs.[23]

From the initial condition of the propagator 3.57, the Fourier transform is

$$\psi(\mathbf{p}',0) = \frac{1}{(2\pi\hbar)^{f/2}}\int d\mathbf{q}\delta(\mathbf{q}-\mathbf{q}')e^{-\mathbf{p}'\mathbf{q}/\hbar} \tag{3.77}$$

$$= \frac{1}{(2\pi\hbar)^{f/2}}e^{-\mathbf{p}'\mathbf{q}'/\hbar} \tag{3.78}$$

where f is the degrees of freedom. In momentum space, the initial Lagrange surface Σ_0 is well-defined providing

$$A(\mathbf{p}',0)=\frac{1}{(2\pi\hbar)^{f/2}},\quad R_0(\mathbf{p}')=-\mathbf{p}'\mathbf{q}', \tag{3.79}$$

and the wavefunction becomes

$$\psi(\mathbf{p}'',t)=\sum_j\frac{1}{(2\pi\hbar)^{f/2}}\left|\det\frac{\partial\mathbf{p}'_j}{\partial\mathbf{p}''_j}\right|^{1/2} e^{\frac{i}{\hbar}[-\mathbf{p}'_j\mathbf{q}'_j+R(\mathbf{p}'_j,\mathbf{p}''_j,t)+i\pi\tilde{\alpha}_j/2]}. \tag{3.80}$$

Consequently, the inverse Fourier transformation of 3.80 furnishes us the propagator

$$K(\mathbf{q}'', \mathbf{q}', t) = \frac{1}{(2\pi\hbar)^{f/2}} \int d\mathbf{p}'' \psi(\mathbf{p}'', t) e^{i\mathbf{q}''\mathbf{p}''/\hbar}. \tag{3.81}$$

In order to solve this integral, the stationary phase method has to be applied, which embodies the stationary condition

$$\frac{\partial}{\partial \mathbf{p}''}[R(\mathbf{p}', \mathbf{p}'', t) + \mathbf{q}''\mathbf{p}''] = 0 \tag{3.82}$$

$$\mathbf{q}'' + \frac{\partial R(\mathbf{p}', \mathbf{p}'', t)}{\partial \mathbf{p}''} = 0 \tag{3.83}$$

corresponding to the canonical transformation. Thus, the resulting phase is

$$R(\mathbf{p}', \mathbf{p}'', t) + \mathbf{q}''\mathbf{p}'' - \mathbf{q}'\mathbf{p}' = R(\mathbf{q}', \mathbf{q}'', t), \tag{3.84}$$

and for the amplitude, we expand the phase until second-order in $\mathbf{p}''$

$$R(\mathbf{q}', \mathbf{q}'', t) + \frac{\partial^2 R(\mathbf{p}', \mathbf{p}'', t)}{\partial \mathbf{p}''^2} \partial \mathbf{p}''^2 \tag{3.85}$$

and, from 3.14, the propagator reads

$$\begin{aligned} K(\mathbf{q}'', \mathbf{q}', t) &= \frac{1}{(2\pi\hbar)^{f/2}} \sum_j \left| \det \frac{\partial \mathbf{p}'_j}{\partial \mathbf{p}''} \right|^{1/2} \left| \det \frac{\partial^2 R_j(\mathbf{p}', \mathbf{p}'', t)}{\partial \mathbf{p}''^2} \right|^{-1/2} \\ &\times \exp\left[\frac{i}{\hbar} R_j(\mathbf{q}', \mathbf{q}'', t) - i\tilde{\alpha}_j \pi/2 + i\gamma_{\mathbf{q}''}\pi/4 \right] \end{aligned} \tag{3.86}$$

with $\gamma_{\mathbf{q}''}$ is the net value of the eigenvalues' signs of the matrix $\partial^2 R/\partial \mathbf{p}''^2$.

Nevertheless, we can work out with $\partial^2 R/\partial \mathbf{p}''^2$ to reach a more familiar expression for the propagator. First, we recall that equations of motion for short times can be approximated by

$$\mathbf{q}'' - \mathbf{q}' \simeq \mathbf{p}' \frac{t}{m} \quad \mathbf{p}'' - \mathbf{p}' \simeq F(\mathbf{q}', 0)t, \tag{3.87}$$

$F(\mathbf{q}', 0)$ being the force at $\mathbf{q}'$. The matrix assumes a diagonal format

$$\frac{\partial^2 R(\mathbf{p}', \mathbf{p}'', t)}{\partial \mathbf{p}''^2} = -\frac{\partial \mathbf{q}''}{\partial \mathbf{p}''} \simeq -t/m \tag{3.88}$$

with all its eigenvalues being negatives, then $\gamma = -f$ and $e^{i\pi\gamma/4} = i^{-f/2}$. Therefore, to arrive at the final expression, we may note that the determinant can be rewritten as

$$\left| \det \frac{\partial \mathbf{p}'}{\partial \mathbf{p}''} \right|^{1/2} \left| \det \frac{\partial^2 R(\mathbf{p}', \mathbf{p}'', t)}{\partial \mathbf{p}''^2} \right|^{-1/2} = \left| \det \frac{\partial \mathbf{p}'}{\partial \mathbf{p}''} \right|^{1/2} \left| \det \frac{\partial \mathbf{q}''}{\partial \mathbf{p}''} \right|^{-1/2} = \left| \det \frac{\partial \mathbf{p}'}{\partial \mathbf{q}''} \right|^{1/2}, \tag{3.89}$$

and the semiclassical propagator is

$$K(\mathbf{q}'',\mathbf{q}',t)=\frac{1}{(2\pi i\hbar)^{f/2}}\sum_j\left|\det-\frac{\partial^2 R_j(\mathbf{q}',\mathbf{q}'',t)}{\partial\mathbf{q}'\partial\mathbf{q}''}\right|^{1/2}e^{\frac{i}{\hbar}R_j(\mathbf{q}',\mathbf{q}'',t)-i\alpha\pi/2}. \tag{3.90}$$

We substituted $\tilde{\alpha}$ by α owing to the number of caustic being independent of the representation.

The equation 3.90 is well-known as Van Vleck's formula, which is our starting point to connect quantum features as the propagator $K(\mathbf{q}'',\mathbf{q}',t)$ and classical aspects as the action and caustics. For instance, the value $d\mathbf{q}''d\mathbf{q}'|K|=d\mathbf{q}''d\mathbf{q}'|R''|/(2\pi\hbar)^f$ can be interpreted as the probability to find the system at the volume element $d\mathbf{q}''$ when it was initially in the volume $d\mathbf{q}'$. In addition, as discussed in section 2.1.1, the second derivative of the action gives us information on the neighboring trajectories for classical systems. Through the propagator derivation, we can identify that the neighborhood directly influences the quantum counterpart system as well.

Nonetheless, the energy levels assessment is possible via the Green function. Therefore, with the propagator 3.90 at hand, we initiate with 3.62, which is another integral to be considered in the semiclassical limit. As usual, the stationary phase method comes into play with the stationary points given by

$$\frac{\partial}{\partial t}[R(\mathbf{q}',\mathbf{q}'',t)+Et]=0\rightarrow\frac{\partial R(\mathbf{q}',\mathbf{q}'',t)}{\partial t}+E=0. \tag{3.91}$$

The previous equation explicitly defines Hamilton-Jacobi's mechanics as in 2.1.2, where we changed the dependence of time to energy. The phase is the Hamilton-Jacobi action 2.17, and then the expansion until the second order is simply

$$S(\mathbf{q}',\mathbf{q}'',E)+\frac{\partial^2 R}{\partial t^2}\partial^2 t. \tag{3.92}$$

The result of the Green function from equation 3.7 becomes

$$G(\mathbf{q}',\mathbf{q}'',E) = \frac{1}{i\hbar}\frac{1}{(2\pi i\hbar)^{f/2}}\sum_j\left|\det-\frac{\partial^2 R_j(\mathbf{q}',\mathbf{q}'',t)}{\partial\mathbf{q}'\partial\mathbf{q}''}\right|^{1/2}\left|\det\frac{\partial^2 R_j(\mathbf{q}',\mathbf{q}'',t)}{\partial t^2}\right|^{-1/2} \tag{3.93}$$

$$\times\sqrt{2\pi\hbar}\exp\left[\frac{i}{\hbar}S_j(\mathbf{q}',\mathbf{q}'',E)-i\alpha\pi/2+i\pi\mathrm{sgn}(\ddot{R})/4\right] \tag{3.94}$$

For very short times, we can regard the system as a free particle, and then the action is 2.5 that its second derivative is always positive leading to $e^{i\pi\mathrm{sgn}(\ddot{R})/4}=\sqrt{i}$ and

a Green function

$$G(\mathbf{q}',\mathbf{q}'',E) = \frac{2\pi}{(2\pi i\hbar)^{(f+1)/2}}\sum_j \left|\det -\frac{\partial^2 R_j(\mathbf{q}',\mathbf{q}'',t)}{\partial\mathbf{q}'\partial\mathbf{q}''}\right|^{1/2}\left|\det\frac{\partial^2 R_j(\mathbf{q}',\mathbf{q}'',t)}{\partial t^2}\right|^{-1/2} \times\exp\left[\frac{i}{\hbar}S_j(\mathbf{q}',\mathbf{q}'',E)-i\alpha\pi/2\right]. \tag{3.95}$$

The determinants are precisely those discussed at the end of section 2.1.2, which defines the density of trajectories 2.21. We have aptly demonstrated that using the special Gutzwiller coordinates, the density is given by 2.41, which showcases the two sorts of caustics: returning points and tangential coordinates action divergence. Once more, the remedy for these caustics is the Maslov phase μ. Subsequently, the semiclassical Green function is

$$G(\mathbf{q}',\mathbf{q}'',E) = \frac{2\pi}{(2\pi i\hbar)^{(f+1)/2}}\sum_j \frac{1}{\sqrt{|\dot{\mathbf{q}}'||\dot{\mathbf{q}}''|}}\left|\det -\frac{\partial^2 S_j}{\partial\mathbf{y}'\partial\mathbf{y}''}\right|^{1/2} \times\exp\left[\frac{i}{\hbar}S_j(\mathbf{q}',\mathbf{q}'',E)-i\mu_j\pi/2\right], \tag{3.96}$$

providing quantum information about the systems' energy levels via its poles and wavefunctions via its residues only regarding classical elements.

3.3.3 Gutzwiller trace formula

In order to find the density of states 3.34, we have just to take the trace of the Green function as 3.69. The endpoints $\mathbf{q}''$ and the initial points $\mathbf{q}'$ must coincide; however, it does not say anything about their momenta. The last integral is

$$G(E)=\int d\mathbf{q}G(\mathbf{q},\mathbf{q},E), \tag{3.97}$$

which the stationary point with respect to $\mathbf{q}$ is given by

$$\frac{\partial S(\mathbf{q},\mathbf{q},E)}{\partial\mathbf{q}}=\left\{\frac{\partial S(\mathbf{q}',\mathbf{q}'',E)}{\partial\mathbf{q}'}+\frac{\partial S(\mathbf{q}',\mathbf{q}'',E)}{\partial\mathbf{q}''}\right\}_{\mathbf{q}'=\mathbf{q}''=\mathbf{q}}=0 \tag{3.98}$$

$$\mathbf{p}'=\mathbf{p}'' \tag{3.99}$$

where we used the relations 2.19.

The previous outcome indicates that the integral ends up interfering destructively with those trajectories that do not close smoothly. In other words, the trace of the Green function is solely a sum of all periodic orbits. From the stationary phase method, we still have to expand the action until second-order, now with respect to a periodic orbit

$$\begin{aligned} S(\mathbf{q}',\mathbf{q}'',E) &\simeq S(\mathbf{q},\mathbf{q},E)+\frac{1}{2}\delta q\Bigg\{\frac{\partial^2 S(\mathbf{q}',\mathbf{q}'',E)}{\partial \mathbf{q}'^2}+2\frac{\partial^2 S(\mathbf{q}',\mathbf{q}'',E)}{\partial \mathbf{q}'\partial \mathbf{q}''} \\ &\quad +\frac{\partial^2 S(\mathbf{q}',\mathbf{q}'',E)}{\partial \mathbf{q}''^2}\Bigg\}_{\mathbf{q}'=\mathbf{q}''=\mathbf{q}}\delta q. \end{aligned} \tag{3.100}$$

By the fact that the integration is along the periodic orbit, it is convenient to employ Gutzwiller special coordinates, which the integration with respect to the tangential coordinates provides the amplitude from 3.14

$$\frac{(2\pi\hbar)^{(f-1)/2}}{\left|\det\left(\frac{\partial^2 S(\mathbf{q}',\mathbf{q}'',E)}{\partial \mathbf{y}'^2}+2\frac{\partial^2 S(\mathbf{q}',\mathbf{q}'',E)}{\partial \mathbf{y}'\partial \mathbf{y}''}+\frac{\partial^2 S(\mathbf{q}',\mathbf{q}'',E)}{\partial \mathbf{y}''^2}\right)\right|^{1/2}}=\frac{(2\pi\hbar)^{(f-1)/2}}{\left|\det\left(W\right)\right|^{1/2}}. \tag{3.101}$$

where

$$W_{ij}=\frac{\partial^2 S(\mathbf{q}',\mathbf{q}'',E)}{\partial y_i'\partial y_j'}+\frac{\partial^2 S(\mathbf{q}',\mathbf{q}'',E)}{\partial y_i'\partial y_j''}+\frac{\partial^2 S(\mathbf{q}',\mathbf{q}'',E)}{\partial y_i''\partial y_j'}+\frac{\partial^2 S(\mathbf{q}',\mathbf{q}'',E)}{\partial y_i''\partial y_j''}. \tag{3.102}$$

Thereafter, we are let with two determinants

$$\frac{\left|\det-\frac{\partial^2 S_j}{\partial \mathbf{y}'\partial \mathbf{y}''}\right|^{1/2}}{\left|\det\left(W\right)\right|^{1/2}}. \tag{3.103}$$

The ratio 3.103 seems nothing familiar with anything else we have discussed so far. Nevertheless, if we go back to section 2.1.4 and see the definition of the monodromy matrix 2.75 and 2.71, the ratio is

$$\frac{\left|\det-\frac{\partial^2 S_j}{\partial \mathbf{y}'\partial \mathbf{y}''}\right|}{\left|\det\left(W\right)\right|}=\frac{\left|\det\boldsymbol{\mathcal{B}}\right|^{-1}}{\left|\det\left(\boldsymbol{\mathcal{A}}+\boldsymbol{\mathcal{B}}+\boldsymbol{\mathcal{B}}^{\boldsymbol{T}}+\boldsymbol{\mathcal{D}}\right)\right|}. \tag{3.104}$$

Moreover, from the expression 2.82 with $\lambda = 1$, the determinants' fraction matches perfectly with the inverse of the characteristic polynomial of the monodromy matrix $\mathbf{M}$. Therefore,

$$\frac{\left|\det-\frac{\partial^2 S_j}{\partial \mathbf{y}'\partial \mathbf{y}''}\right|^{1/2}}{\left|\det\left(W\right)\right|^{1/2}}=\frac{1}{\left|\det\left(\mathbf{M}-\mathbf{I}\right)\right|^{1/2}}=\frac{1}{\left|F(1)\right|^{1/2}} \tag{3.105}$$

which $F(1)$ are the Greene residues, as explained in section 2.1.4. It conveys that every sort of periodic orbit contributes differently to the sum in the semiclassical Green function. Substituting 3.100, 3.101, and 3.105, the trace of the semiclassical Green function 3.96 becomes

$$G(E) = \frac{2\pi(2\pi\hbar)^{(f-1)/2}}{(2\pi i\hbar)^{(f+1)/2}} \sum_j \frac{\exp\left[\frac{i}{\hbar}S_j(E) - i(2\mu_j - \nu_j)\pi/4\right]}{|\det(\mathbf{M}-\mathbf{I})|^{1/2}} \int dx \frac{1}{|\dot{x}|}, \quad (3.106)$$

with ν being the net number of eigenvalue sign from the matrix $\mathbf{W}$.

The first thing to consider is that we can readjust the Maslov index. If ν is broken up on $\nu_+ - \nu_-$ in which $\nu_\pm$ are the number of positive or negative eigenvalues, we can rewrite them as

$$\nu = (\nu_+ + \nu_-) - 2\nu_- = (f-1) - 2\nu_-, \quad (3.107)$$

and the exponent becomes

$$e^{-i(2\mu-\nu)\pi/4} = e^{i(L-1)\pi/4} e^{-i(\mu+\nu_-)\pi/2} = i^{(f-1)/2} e^{-i\sigma\pi/2} \quad (3.108)$$

where σ is defined as the Maslov index of the periodic orbit. Furthermore, the last integral over the periodic orbit is acquainted since it is essentially the primitive period of the orbit T_0. Finally, the semiclassical Green function is

$$G(E) = \frac{1}{i\hbar} \sum_j \frac{T_{0,j}}{|\det(\mathbf{M}-\mathbf{I})|^{1/2}} \exp\left[\frac{i}{\hbar}S_j(E) - i\sigma_j\pi/2\right]. \quad (3.109)$$

Nevertheless, the result 3.109 is not the complete semiclassical Green function. Actually, it is just its fluctuations. Through this sort of trace formula's derivation, we ended up leaving out the contributions of trajectories that have a null period, called zero-length trajectories. They start from a point $\mathbf{q}'$ and arrive at $\mathbf{q}_1$ at the time t_1 but $(\mathbf{q}' - \mathbf{q}_1) \to 0$. These orbits contribute to a mean value for the Green function $G_0(E)$, and especially, their energy density value is

$$\rho_0(E) = -\frac{1}{\pi}\mathrm{Im}(G_0) = \frac{1}{h^f} \int d\mathbf{q} d\mathbf{p} \delta(E - H(\mathbf{q},\mathbf{p})). \quad (3.110)$$

Comparing it with 3.41, we instantly note that it is the Thomas-Fermi density. Therefore, the Gutzwiller trace formula is

$$G(E) = G_0(E) + \frac{1}{i\hbar} \sum_j \frac{T_{0,j}}{|\det(\mathbf{M}-\mathbf{I})|^{1/2}} \exp\left[\frac{i}{\hbar}S_j(E) - i\sigma_j\pi/2\right] \quad (3.111)$$

or in terms of the density

$$\rho(E) = \rho_0(E) + \frac{1}{\pi\hbar}\sum_p \frac{T_{0,p}}{|\det(\mathbf{M}-\mathbf{I})|^{1/2}}\cos\left[\frac{1}{\hbar}S_p(E) - \sigma_p\pi/2\right]. \tag{3.112}$$

Namely, for a two-dimensional system, we can get a more intelligible expression for the trace formula following the results of the Greene residues and substitute them at the determinant of the monodromy matrix

$$|\det(\mathbf{M}-\mathbf{I})|^{1/2} = \begin{cases} 2\cosh(\chi/2) & \text{for inverse hyperbolic orbit,} \\ 2\sinh(\chi/2) & \text{for direct hyperbolic orbit,} \\ 2\sin(\theta/2) & \text{for elliptic orbit,} \end{cases} \tag{3.113}$$

where θ is the stability angles for stable orbits and χ divided by the period of the unstable orbit τ is the well-known Lyapounoff exponent, which measures the separation rate of neighboring orbits. As a consequence, the fluctuation of the density for two-dimensional systems is written as

$$\tilde{\rho}(E) = \frac{1}{\pi\hbar}\sum_k\sum_{n=1}^{\infty}\frac{T_0}{2\left|\cosh\frac{n\chi_{0k}}{2}, \sinh\frac{n\chi_{0k}}{2}, \sin\frac{n\theta_{0k}}{2}\right|}\cos\left[\frac{in}{\hbar}S_{0k}(E) - i\sigma_{0k}\pi/2\right], \tag{3.114}$$

which the first sum is of the distinct primitive orbits, and the second sum counts the repetition of each primitive orbit. In addition, the denominator takes over different responses of the monodromy matrix for each sort of periodic orbit.

As discussed in section 2.2.1, the systems, in general, have both contributions from unstable and stable periodic orbits leading to non-trivial sums. Thus, to have a knowledge of their contribution, we shall select a particular sort of orbit. First, for elliptic orbits, we have the sine input, and it can be written as

$$\frac{1}{2i\sin\frac{n\theta}{2}} = \frac{1}{e^{in\frac{\theta}{2}} - e^{-in\frac{\theta}{2}}} = \frac{e^{-in\frac{\theta}{2}}}{1-e^{in\theta}} \tag{3.115}$$

$$= e^{in\frac{\theta}{2}}\sum_{l=0}^{\infty}e^{-inl\theta} = \sum_{l=0}^{\infty}e^{-in(l+1/2)\theta} \tag{3.116}$$

just applying the geometric sum. So, the fluctuation part of the Green function for a specific primitive stable periodic orbit becomes

$$\tilde{G}(E) = \frac{T_0}{i\hbar}\sum_n\sum_l \exp\left[in\left(\frac{S}{\hbar}\right) - in(l+1/2)\theta\right], \tag{3.117}$$

and performing the geometric progression in n, we have

$$\tilde{G}(E) = \frac{T_0}{i\hbar} \sum_l \frac{\exp\left[i(\frac{S}{\hbar}) - i(l+1/2)\theta\right]}{1 - \exp\left[i(\frac{S}{\hbar}) - i(l+1/2)\theta\right]}. \tag{3.118}$$

Recalling the definition 3.65, the pole of the Green function gives us energy levels. In this case, it is evident that they occur when the action is

$$\frac{S}{\hbar} - i(l+1/2)\theta = 2\pi m \tag{3.119}$$

$$S(E) = 2\pi\hbar \left[m + \left(l + \frac{1}{2} \right) \frac{\theta}{2\pi} \right] \tag{3.120}$$

which becomes the quantization rule for this particular case. However, when considered within other periodic orbits, the relation 3.120 would give rise to many energy levels. On top of that, this quantization says that long-period orbits should not contribute to the density but collectively interfere with other primitive orbits.

In the diametrically opposed case, the direct hyperbolic periodic orbits have their contribution as

$$\frac{1}{2|\sinh\frac{n\chi}{2}|} = \frac{1}{e^{n\chi/2} + e^{n\chi/2}} = \frac{e^{-n\chi/2}}{1 + e^{n\chi}} \tag{3.121}$$

$$= e^{n\frac{\chi}{2}} \sum_{l=0}^{\infty} (-1)^l e^{-nl\chi} = \sum_{l=0}^{\infty} (-1)^l e^{-n(l+1/2)\chi}. \tag{3.122}$$

Once more, the geometric progression in n takes place and gives us the Green function fluctuation

$$\tilde{G}(E) = \frac{T_0}{i\hbar} \sum_l (-1)^l \frac{\exp\left\{-\chi\left(l+\frac{1}{2}\right) + i\left[\frac{S}{\hbar} - \frac{\pi\sigma}{2}\right]\right\}}{1 - \exp\left\{-\chi\left(l+\frac{1}{2}\right) + i\left[\frac{S}{\hbar} - \frac{\pi\sigma}{2}\right]\right\}} \tag{3.123}$$

where there are no poles since the exponent is complex. Then in order to obtain information about the hyperbolic energies, we can resort to the density and see states along the real energy axis [42]. What we find are broadened peaks with their maxima located at

$$S(E) = 2\pi\hbar[m + \sigma/4] \tag{3.124}$$

and width $2\chi\hbar$. Gutzwiller [42] has shown that the fluctuation densities are actually a series of Lorentzian. On top of that, whether we want to identify the peaks, the mean energy displacement should be smaller than their width; however, from Thomas-Fermi density 3.110, the mean displacement is proportional to $\hbar^f$, which goes to zero

extremely faster than the width ($\sim \hbar$). From this fact, it is impossible to see individual contributions of unstable orbits in the semiclassical limit. To work around this issue, we usually take averages over states smoothing with the imaginary part of the energy ϵ.

To conclude, whereas elliptic orbits give rise to δ functions in the density of states, hyperbolic orbits show broadened peaks composed by a summation of Lorentzians. This feature conveys that in dealing with general systems that have both periodic orbits, there will invariably be a continuous background that cannot be neglected owing to the idiosyncrasy of the unstable periodic orbits themselves.

3.4 Semiclassical physics of classical maps

This dissertation revolves around classical maps and their quantum counterparts: quantum maps. Therefore, a semiclassical approximation for them is required, and we shall see how their classical behavior is reflected in the quantum realm.

For the classical maps, we take advantage of their topology to perform the quantization. We can adopt a suitable Hilbert space that incorporates a two-torus $\mathbb{T}^2$ if the wavefunctions' amplitude is imposed to be periodic both in the position representation $\Psi(q)$ and in the momentum representation $\Psi(p)$

$$|\Psi(q+j)| = |\Psi(q)|; \quad j \in \mathbb{N} \tag{3.125}$$

$$|\Psi(p+l)| = |\Psi(p)|; \quad l \in \mathbb{N} \tag{3.126}$$

where j and l are the revolution repetitions. When we take out the modulus of previous equations

$$\Psi(q+j) = e^{\frac{i}{\hbar}j\beta}\Psi(q) \tag{3.127}$$

$$\Psi(p+l) = e^{\frac{i}{\hbar}l\alpha}\Psi(p), \tag{3.128}$$

we earn phases α and β, which are known as quantum phase since there is no classical analogous. Moreover, α and β respectively control parity and time-reversal symmetry and are both in the interval $[0, 1]$. So, remarkable values are: $\beta = 0$ leading to a periodic

boundary condition, $\beta = 1/2$ giving an anti-periodic condition, otherwise the time-reversal symmetry is broken. The parity symmetry works similarly where $\alpha \neq 0, 1/2$ breaks the symmetry.

Aside from the quantum phases, the periodicity of the wavefunction implies finite quantum mechanics; in other words, a finite Hilbert space. If we recall that each state occupies a volume of $2\pi\hbar$ and state that the dimensionality of the Hilbert space is N, we have N states per unit of phase space, then the following relation holds

$$2\pi\hbar = \frac{\text{Total area of phase space}}{\text{Total number of states}} = \frac{1}{N}. \tag{3.129}$$

Therefore, for these systems, the semiclassical limit $\hbar \to 0$ corresponds to $N \to \infty$.

The evolution of the wavefunctions can rely on a unitary operator $\hat{U}$, dubbed as the propagator or Floquet operator. In the position representation, $U_{Q_1 Q_2}$ is represented by an $N \times N$ unitary matrix which maps the values of a given wavefunction at the sites $q = Q/N$ (where Q take integers values between 0 and $N-1$) to give the corresponding values at the next observation time

$$\Psi(Q_2; t = (k+1)) = \sum_{Q_1=0}^{N-1} U_{Q_1 Q_2} \Psi(Q_1; t = k). \tag{3.130}$$

So, the wavefunctions are described by complex vectors of size N.

On top of that, if we give an initial state $|\psi(0)\rangle$, the propagator can be applied multiple times

$$|\Psi(k)\rangle = \hat{\mathbf{U}}^k |\Psi(0)\rangle \tag{3.131}$$

leading to a state after multiple repetitions. However, in order to deal with the powers of the operator $\hat{\mathbf{U}}$, we can essentially determine its eigenvalues and eigenvectors

$$\hat{\mathbf{U}} |\psi_n\rangle = e^{iE_n} |\psi_n\rangle \tag{3.132}$$

resulting in an eigenvalue problem.

$\hat{\mathbf{U}}$ eigenvalues E_n are called eigenangles or quasi-energies. The former regards their configuration in the complex plane (unitary circle format), whereas the latter points out that E_n are not eigenenergies in the ordinary quantum mechanics sense.

Indeed, the systems have a time-dependent Hamiltonian $H(t)$, which results in non-conserved energy. Yet $H(t)$ is periodic in time $H(t) = H(t+\tau)$ leading to conservation in a stroboscopic manner. The eigenvectors $|\psi_n\rangle$ - the objects of our study - following the same condition of the eigenvalues are called Floquet stationary eigenstates.

Through this reasoning, we just need the form of the evolution operator to obtain information about the quantum system and make $N \to \infty$ reaching the semiclassical regime afterward. First, it would be convenient if $\hat{\mathbf{U}}$ was similar to the classical map 2.86. The map was constructed through Hamilton's equations 2.87, and the quantum counterpart of the mapping is 3.130, which must come from Schrodinger's equation. However, applying classical reasoning, we can construct the operator $\hat{\mathbf{U}}$.

From the classical perspective, the kicked systems have purely kinetic energy $f(p)$ between the kicks and the potential $V(q)$ action at the precise moment of the kicks. Therefore, quantumly, this is translated for the operator by splitting it into contributions of the form

$$\hat{\mathbf{U}} = \exp\left(\frac{-iV(\hat{q})\tau}{\hbar}\right)\exp\left(\frac{-i\hat{p}^2\tau}{2\hbar}\right). \tag{3.133}$$

Because we have been considering $\tau = 1$, the potential becomes

$$\hat{\mathbf{U}} = \exp\left(-2\pi i N V(\hat{q})\right)\exp\left(\frac{-2\pi i N\hat{p}^2}{2}\right), \tag{3.134}$$

where we implemented the $\hbar$-N relation 3.129

Now we shall restrict the quantum map in position representation. Hence, we are looking for

$$U_{Q_1,Q_2} = \langle q_1|\,\hat{\mathbf{U}}\,|q_2\rangle\,, \quad q_{1,2} = Q_{1,2}/N. \tag{3.135}$$

To begin, we have to settle the momentum and position eigenvalues. If there were no phase α and β, their eigenvalues would be simply Q/N and m/N, with Q and m being integers values between 0 and $N-1$. However, the quantum phases are present and have to be considered. They simply modify the position and momentum eigenvalues to $(Q+\alpha)/N$ and $(m+\beta)/N$, respectively. With this outcome, we can

finally obtain an expression for the evolution operator in the position representation

$$\langle q_1|\,\hat{\mathbf{U}}\,|q_2\rangle = e^{\left(-2\pi iNV\left(\frac{Q_2+\alpha}{N}\right)\right)}\,\langle q_1|\,e^{\left(\frac{-2\pi iN\hat{p}^2}{2}\right)}\,|q_2\rangle \tag{3.136}$$

$$= e^{\left(-2\pi iNV\left(\frac{Q_2+\alpha}{N}\right)\right)}\sum_{m,m'=0}^{N-1}\langle q_1|p_m\rangle\,\langle p_m|\,e^{\left(\frac{-2\pi iN\hat{p}^2}{2}\right)}\,|p_{m'}\rangle\,\langle p_{m'}|q_2\rangle \tag{3.137}$$

where $\langle q|p_m\rangle$ is given by the discrete Fourier transform

$$\langle q_{1,2}|p_m\rangle = \frac{1}{\sqrt{N}}\exp\left(\frac{2\pi i}{N}(Q_{1,2}+\alpha)(m+\beta)\right). \tag{3.138}$$

So, the evolution operator for kicked systems becomes

$$\langle q_1|\,\hat{\mathbf{U}}\,|q_2\rangle = \frac{1}{N}e^{\left(-2\pi iNV\left(\frac{Q_2+\alpha}{N}\right)\right)}\sum_{m,m'=0}^{N-1}e^{\left(\frac{2\pi i}{N}(Q_1+\alpha)(m+\beta)\right)}e^{-\pi iN\left(\frac{m'+\beta}{N}\right)^2} \tag{3.139}$$

$$\times e^{\left(-\frac{2\pi i}{N}(Q_2+\alpha)(m'+\beta)\right)}\delta_{m,m'}$$

$$= \frac{1}{N}e^{\left(-2\pi iNV\left(\frac{Q_2+\alpha}{N}\right)\right)}\sum_{m=0}^{N-1}e^{\left(\frac{2\pi i}{N}(Q_1-Q_2)(m+\beta)\right)}e^{-\pi iN\left(\frac{m+\beta}{N}\right)^2} \tag{3.140}$$

When α and β are null, another expression can be obtained in order to determine the quantum maps

$$\langle q_1|\,\hat{\mathbf{U}}\,|q_2\rangle = \frac{1}{\sqrt{N}}\left|\frac{\partial^2 S(q_1,q_2)}{\partial q_1\partial q_2}\right|^{1/2}\exp\left[2\pi NS(q_1,q_2)\right]. \tag{3.141}$$

$S(q_1,q_2)$ are the corresponding generating function of classical maps - given by 2.97, 2.103, and 2.105. This formula resembles our expression for the wavefunction in general semiclassical systems 3.74.

As a result, we can now use the classical map equations to obtain their quantum versions. The standard map has the Hamiltonian 2.91, which leads to the following evolution operator

$$U^{(std)}_{Q_1,Q_2} = \frac{1}{N}\exp\left[\frac{iNK}{2\pi}\cos\left(2\pi\frac{Q_1+\alpha}{N}\right)\right]\sum_{Q'=0}^{N-1}\exp\left[\frac{2\pi i}{N}(Q'+\beta)(Q_2-Q_1)\right]$$

$$\times\exp\left[i\pi\frac{(Q'+\beta)^2}{N}\right]. \tag{3.142}$$

For the Harper map, the procedure is the same but with 2.99, and the quantum map becomes

$$U^{(hrp)}_{Q_1,Q_2} = \frac{1}{N}\exp\left[\frac{-iNA}{2\pi}\cos\left(2\pi\frac{Q_1+\alpha}{N}\right)\right]\sum_{Q'=0}^{N-1}\exp\left[\frac{2\pi i}{N}(Q'+\beta)(Q_2-Q_1)\right] \times \exp\left[\frac{-iNL}{2\pi}\cos\left(2\pi\frac{Q'+\beta}{N}\right)\right]. \tag{3.143}$$

However, the perturbed cat map is an Anosov map, and we only have the action available. Thus, the quantum map is obtained from 3.141 and gives

$$U^{(cat)}_{Q_1,Q_2} = \frac{1}{\sqrt{iN}}\exp\left[\frac{2\pi i}{N}(Q_1^2 - Q_1Q_2 + Q_2^2) + \frac{iN}{2\pi}\kappa\sin\left(2\pi Q_1/N\right)\right]. \tag{3.144}$$

As aforementioned, all the quantum information is encompassed in the evolution operator. Since our dissertation revolves around the eigenfunctions of U_{Q_1,Q_2}, all we have seen about semiclassical wavefunction in sections 3.2 and 3.3 must be detectable in $\psi_k(q)$ for great values of N. To illustrate this, we have plotted a phase space representation for the quantum map intensities known as the Husimi representation. Here, we have to project the eigenfunctions onto a coherent state $|q,p\rangle$ centered at the point $(q,p)\in\mathbb{T}^2$. In figure 3.4, we have the Husimis of three eigenstates and their amplitudes in the inset for three different values of the stochastic parameter $K = 0.3$, 2.05, and 10.

We start with a small K within the near-integrable regime; our classical standard map is mostly covered with KAM tori, with only a few islands formed from the perturbation - 2.21a. Therefore, in the quantum version of the phase space, we can see many eigenstates collapsing in KAM tori as stated in the section 3.2.1 - for instance, the Husimi in the upper figure 3.4a. In addition, we have already seen with the Gutzwiller trace formula that stable periodic orbits also leave their mark on the wavefunction. Consequently, some states portray this phenomenon as the Husimi in the lower figure 3.4a.

By enhancing the perturbation to $K = 2.05$, the classical map becomes a mixture of stable islands and a chaotic sea, called the mixed regime and described in figure 2.21b. Once more, the stable periodic orbits are present, as the central island in the lower panel in figure 3.4b. Nevertheless, in the upper panel of figure 3.4b, the quantum

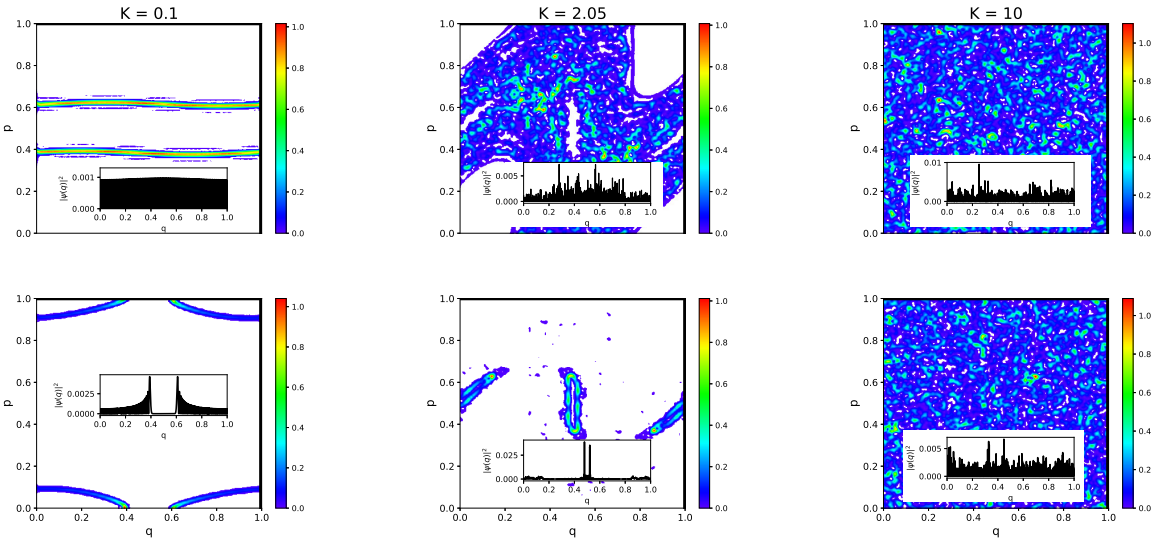

(A) (B) (C)

FIGURE 3.4. Husimi function $|\langle q,p|\psi\rangle|^2$ of typical states projected onto the coherent states $|q,p\rangle$, with $N = 2098$, $\beta = 0$, and $\alpha = 1/4$. The inset shows the respective intensity plots. (A) In the near-integrable regime with $K = 0.1$, the eigenstates are trapped by the KAM tori (upper panel), and some already formed stable islands (lower panel). (B) The $K = 2.05$ results are divided by chaotic and island states, although a mixed state seldom occurs. (C) The fully chaotic parameter $K = 10$ has states distributed over all quantum phase space. The comparison with the classical map in figure 2.21c is enticing.

states' Husimi also captures the unstable trajectories where the particle floats around the phase space.

Finally, $K = 10$ is when the classical system is predominantly chaotic (figure 2.21c), and the eigenstates reflect its stochasticity (upper and lower Husimi of figure 3.4c). In addition, those eigenfunctions are dubbed chaotic states since they are conjectured to behave as random complex vectors. Being known as the quantum-ergodic limit [47], this conjecture is evidenced by our Husimi results and the amplitudes' spread in the position representation.

The same structure can be seen with the other quantum maps: kicked Harper and perturbed cat map. For the near-integrable regime in the classical Harper map, we have obtained the figure 2.22a with $A = 0{,}1$. In figure 3.5a, its quantum counterpart again has states featuring the KAM tori and stable islands, as expected from the semiclassical theory. The $A = 3.56$ sets the mixed regime (classical figure 2.22b), and the quantum map states collapse into stable islands (Husimi of the upper figure 3.5b)

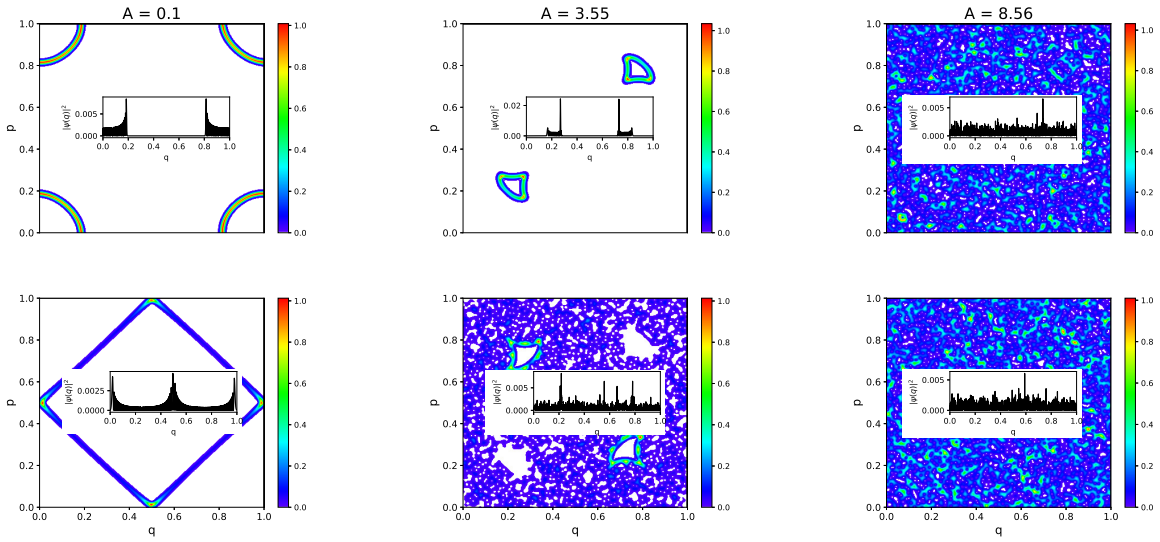

(A) (B) (C)

FIGURE 3.5. Husimi function $|\langle q,p|\psi\rangle|^2$ of typical states projected onto the coherent states $|q,p\rangle$, with $N = 2000$, $\beta = 1/4$, and $\alpha = 1/4$. The inset shows the respective intensity plots. (A) With the near-integrable parameter $A = 0.1$, the states are marked by the KAM tori (lower panel) and some stable islands (upper panel). (B) The eigenstates with $A = 2.05$ are divided by chaotic and island states, as in the standard map case. (C) The Fully chaotic parameter $A = 10$ gives states distributed over all quantum phase space.

and chaotic sea (Husimi of the lower figure 3.5b). At last, the quantum and classical maps, presented respectively by figure 3.5c and 2.22c, match another time for the chaotic regime $A = 8.56$.

In the perturbed cat map, we do not have the presence of a near-integrable regime. However, if we select a $\kappa = 6.67$, the system gives rise to stable structures, as in figure 2.23b. Consequently, from the semiclassical reasoning, islands stamp the eigenstates (upper panel in figure 3.6b), and others print the presence of a chaotic sea (lower panel in figure 3.6b). Lastly, the $\kappa = 0.2$ sets a fully chaotic Anosov map, and the quantum states reflect its stochastic configuration. In addition, the presence of unstable periodic orbits, regardless of the turmoil of the chaotic sea, is evidenced in the semiclassical eigenstates. Despite Husimi not exposing this character in figure 3.6a, one can readily note in the intensities with position - those marks are the well-known scars [11].

In the next chapter, we shall enter the kernel of the dissertation. We are now able

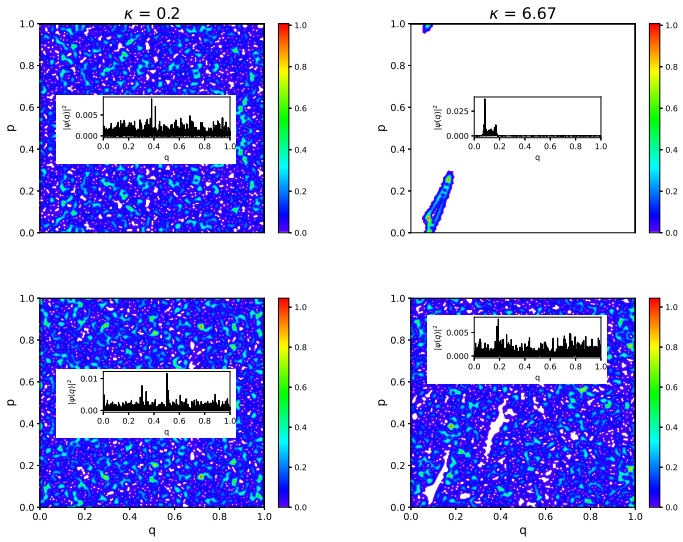

(A) (B)

FIGURE 3.6. Husimi function $|\langle q,p|\psi\rangle|^2$ of typical states projected onto the coherent states $|q,p\rangle$, with $N = 2113$. The inset shows the respective intensity plots. (A) The $\kappa = 0.2$ corresponds to a completely chaotic regime, which passes on for the quantum states. (B) For $\kappa = 6.67$, the map has a great chaotic sea leading to many eigenstates of the form of the lower panel and holds a pair of islands also captured by the quantum system (upper panel).

to understand the root of the eigenstates and their semiclassical implications, which includes classical knowledge about the system and quantum description through trace formula. The semiclassical intensities of the states can be examined, and we shall concentrate on their extreme events. In other words, in possession of the intensities distributions, we shall analyze their tail, also being a shortcut to localization.

Chapter 4

Extreme events in eigenstates of quantum maps

The connection between localization and Floquet systems has been present in quantum chaos debates for a long time [16, 48, 49, 50]. Carrying the system information, the wavefunction accentuates regions where its classical counterpart ends up expressing a low diffusion or a certain of confinement. A well-known instance is in the kicked rotator setting, where momentum eigenfunctions imitate the same classical feature of momentum low diffusion and display localization in its quantum representation.

Nevertheless extreme value theory is another branch that has recently been employed to explore those wavefunctions singularities and has motivated this work. The statistical theory of extremes focuses on examining and forecasting further extremes. As stated by Gumbel [2], the statistical studies of extreme events address two issues: first, from a known distribution, the individual observations that fall outside of what is expected. The second is whether there is typical behavior in the occurrence of those extreme values.

Therefore, taking the intensities of the eigenstates and evaluating their distributions, our observations that take place apart from previous regular values are characterized by extreme events. In that reasoning, we start by showing two motivating studies in that line: the Lakshminarayan et al. [9] with the extreme statistics of the chaotic states, and the Srivastava et al. [10] with the record statistic of kicked states in different classical regimes. Thereafter, the intensities distributions of the quantum

maps will be displayed, and we shall look at the outliers which will feature localized states. In addition, we shall present a guideline measure, the kurtosis, that is a direct observer of extreme data.

4.1 Extreme statistics

Since our aim is in the extreme events of eigenstates of the quantum maps and the semiclassical whys and wherefores of them, only superficial coverage of the extreme value theory will be addressed. However, there will be further references to complete detail of the topics.

We begin setting up an independent and identically distributed (i.i.d) variables

$$X_1, X_2, \ldots, X_{m-1} \tag{4.1}$$

and defining its maximum as $M_m = \max\{X_1, X_2, \ldots, X_{m-1}\}$. The cumulative distribution $F(x)$, i.e., the probability that X_i will take a value less than or equal to x, with normalizing sequences a_m and b_m can be written as [2]

$$F(x) = P\{a_m(M_m - b_m) \leq x\}. \tag{4.2}$$

Consequently, there are three possible limiting universal distributions for the extreme maximal events [51]:

type I: Gumbel distribution

$$F(x) = \exp(-e^{-x}), \quad \infty < x < \infty \tag{4.3}$$

type II: Fréchet distribution

$$F(x) = \begin{cases} 0, & x \leq 0 \\ \exp(-x^{\xi}), & \text{for some } \xi > 0, x > 0 \end{cases} \tag{4.4}$$

type III: Weibull distribution

$$F(x) = \begin{cases} \exp(-(-x)^{\xi}), & \text{for some } \xi > 0, x \leq 0 \\ 1, & x > 0. \end{cases} \tag{4.5}$$

Those tenets from (i.i.d) variables are elementary guidelines in order to contrast with deviations of correlated processes.

In the article of Lakshminarayan et al. [9], they were interested in describing the extreme events in the eigenstates of chaotic quantum systems. Particularly, their focus was solely on chaotic states since they emulate complex random vectors from the quantum-ergodic hypothesis. The only caution is the inert correlation of the intensities within the state: the normalization constraint

$$\sum_{Q=0}^{N-1} |\psi_n(q = Q/N)|^2 = 1, \quad n = 0, \dots N-1. \tag{4.6}$$

Nonetheless, this delta correlation is very weak similar to a "broken-stick" problem - breaking a stick with random lengths but into a fixed number of pieces [52]. For this reason, taking the intensities of the chaotic states as the variables

$$|\psi_0(0)|^2, |\psi_0(1/N)|^2, \dots, |\psi_0((N-1)/N)|^2, \dots, |\psi_{N-1}((N-1)/N)|^2, \tag{4.7}$$

their distribution of extreme maximal events does not fall far from the result of (i.i.d) variables 4.1. In fact, the group has shown that the complex random vectors subjected to a normalization constraint follow a Gumbel distribution for their extreme events. The non-normalized form of the Gumbel is

$$\exp\{-e^{-(x-\mu)/\beta}\} \tag{4.8}$$

where μ is the mode and β gives the standard deviation indirectly - $\sigma = \beta\pi/\sqrt{6}$. Thus, the chaotic states of N-dimensional Hilbert space were found to follow

$$f(|\psi(q)|^2, N) = \exp\{-e^{-N(|\psi(q)|^2 - \ln N/N)}\}. \tag{4.9}$$

The expression agrees with the result in figure 4.1 where appropriate normalization has been taken.

On top of that, as suggested in the article and implied from the quantum-ergodic limit, the same distribution must follow independently of the quantum map for a chaotic state. Consequently, in figure 4.2, we plot the results for the other covered systems in their respective chaotic regimes: kicked Harper map and the perturbed cat map, where they confirm the proposition.

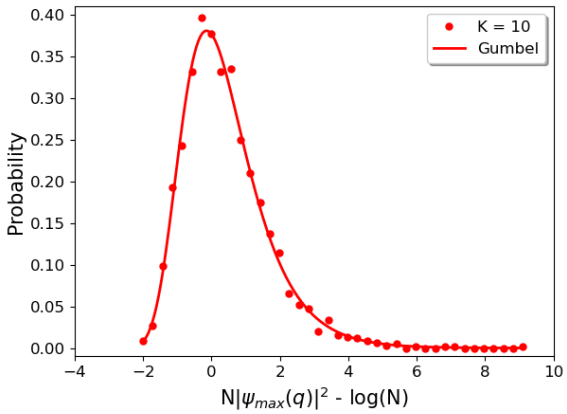

FIGURE 4.1. The probability densities of the scaled maximum intensity of chaotic eigenstates in the position basis for the quantum kicked rotor with K = 10, N = 2098. The continuous line is the fit of the Gumbel over the data.

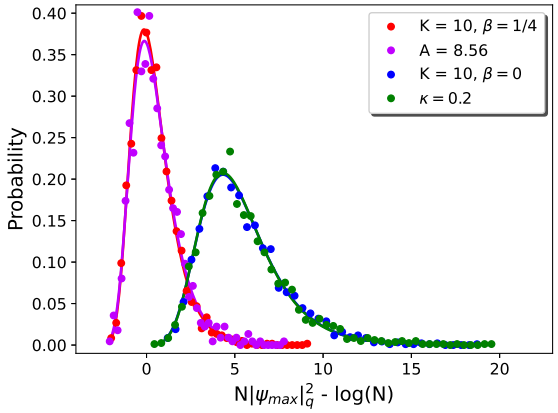

FIGURE 4.2. The probability densities of the scaled maximum intensity of chaotic eigenstates in the position basis for the quantum kicked rotor with $K = 10$, $N = 2098$, $\alpha = 1/4$, one with $\beta = 1/4$ (red dots) and other with $\beta = 0$ (blue dots); the quantum kicked Harper map with $A = 8.56$, $N = 2000$, $\alpha = 1/4$, and $\beta = 1/4$ (pink dots); and the quantum perturbed cat map with $\kappa = 0.2$ and $N = 2113$ (green dots). The continuous lines are the fits of the Gumbel over the data for each parameter value.

Another fundamental work is from Srivastava et al. [10] that instead of taking only the extreme events, they were interested in how the intensities values surmount each other as the Q index varies. This procedure is regarded through Record statistics. In order to grasp this concept, let us consider a finite time series $\{X_t, t = 1, \ldots, N\}$ of a variable X - as depicted for a random walk in figure 4.3. The corresponding record series $R(t)$ is initiated by the first term of the variable $R(1) = X_1$ and for subsequent

times $R(t)$ follows the rule

$$R(t) = \max\left(X_t, R(t-1)\right), \tag{4.10}$$

where $R(t)$ is called the upper record sequence. From the same definition, a lower record sequence can be defined just by changing the maximum to a minimum in 4.10.

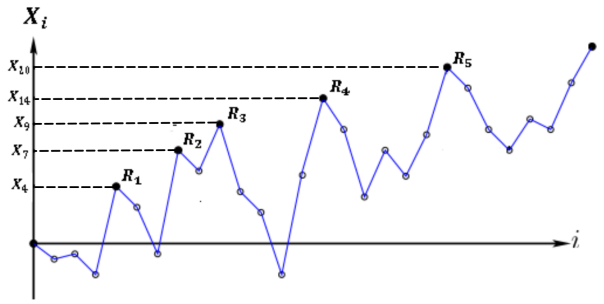

FIGURE 4.3. Illustration of a time series of random variables and how the record series is created from the sequence.[53]

Hence, record statistics is another tool that enables us to assess the tail regions of the variables' distributions. Namely, as occurs in the unitary ensembles, the eigenstates intensities of chaotic systems are uniformly distributed over a standard simplex [54]. They are already known to follow the exponential density, as can be seen in figure 4.4.

The tail region of 4.4 justifies the investigation of the records statistics since, even for strong chaotic states, there are departures from the exponential distribution. Srivastava et al. have taken the intensities and formulated them as time series of variables, where the "time" is substituted by the index $Q = 0, \ldots, N-1$. Therefore, given a eigenstate $\psi(q = Q/N)$, the record is established by

$$R(t) = \max\{|\psi(q = t/N)|^2, R(t-1)\}. \tag{4.11}$$

Likewise to Lakshminarayan's approach [17], Srivastava et al. have selected N-dimensional complex random vectors with the delta correlation and discovered their record distribution. The pleasing result was the appearance of another Gumbel with the form for $N \to \infty$

$$f(t, N) = \exp\left\{-e^{-N(t-\ln t/N)}\right\} \tag{4.12}$$

where the mean is $\mu = \ln t/N$ and $\beta = 1/N$. Similar to the extreme maximum values distribution, when chaotic states are taken from the quantum maps, their record

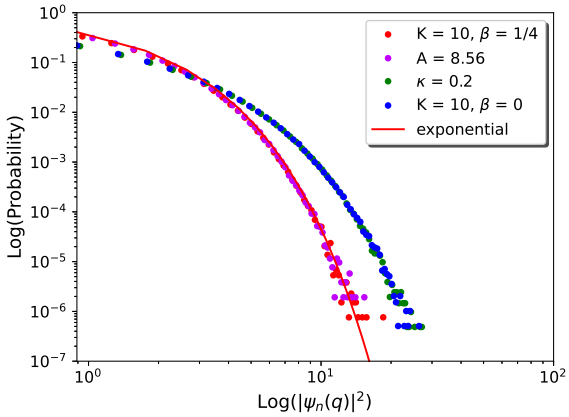

FIGURE 4.4. Intensity distribution of eigenstates in the position basis of the three quantum maps. The quantum standard map at $N = 2098$, $K = 10$, $\alpha = 1/4$, and $\beta = 1/4$ is the closest to the exponential distribution (red dots), but for $\beta = 0$ (blue dots), it follows the cat map result. The quantum kicked harper map at $N = 2000$, $\alpha = 0{,}25$, $\beta = 0{,}25$, and $A = L = 8.56$ (pink dots) also lies in the exponential. The quantum cat map at $N = 2113$ and $\kappa = 0.2$ (green dots) is shifted from the exponential - regarding the time-reversal symmetry

distribution agrees with the Gumbel prediction. In figure 4.5, we plot the case for all quantum maps, and one can readily see their concurrence.

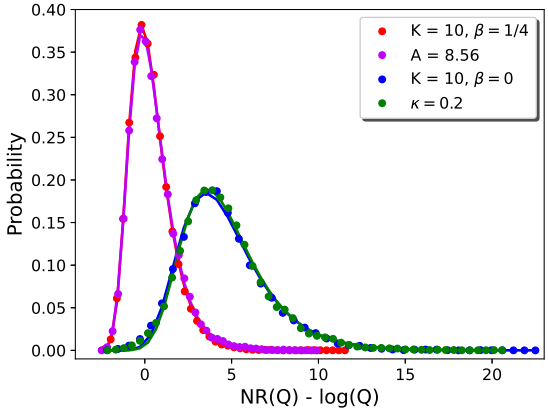

FIGURE 4.5. The distribution of the upper records for eigenfunctions of the quantum kicked rotor with $K = 10$, $N = 2098$, and $\alpha = 1/4$, one for $\beta = 1/4$ (red dots) and other for $\beta = 0$ (blue dots); the quantum kicked Harper map with $A = 8.56$, $N = 2000$, $\alpha = 1/4$, and $\beta = 1/4$ (pink dots); and the quantum perturbed cat map with $\kappa = 0.2$ and $N = 2113$ (green dots). The continuous lines are the fits of the Gumbel over the data for each parameter value.

One point that caught our attention is the discrepancy of the maximum intensity

(4.2) and record (4.5) distributions for the perturbed cat map and the standard map $\beta = 0$ when confronted with the outcomes of Lakshminarayan et al. and Srivastava et al. Consequently, it introduces and displays the effects of the quantum phases, i.e., the results pinpoint the role of symmetry in the intensities of quantum maps eigenstates.

In fact, the deviation from the broken time-reversal symmetry distributions of the chaotic states was notable in advance from the intensities distribution figure 4.4. The impact already has shown intricate since the distributions no longer fit into the exponential. At the end of chapter 5, a more qualitative discussion is made in this regard, which is another gateway to the exploitation of eigenfunction properties.

On top of that, despite Srivastava including a reliable discussion about the records of other sorts of states, such as near-integrable or mixed, we dive deep into those regions and push to deliver a semiclassical perspective for the results that will come up. To begin, in order to obtain a general outlook, we have plotted the distributions for each quantum map (see figure 4.6) and considered parameters that lead the system to near-integrable, mixed, and chaotic regimes in order of comparison.

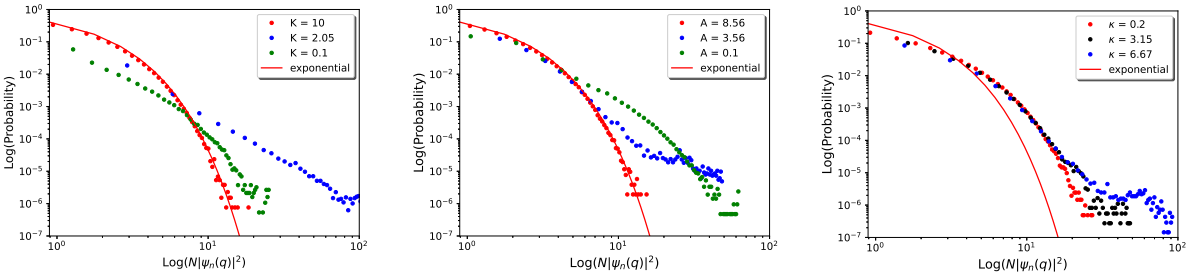

(A) (B) (C)

FIGURE 4.6. Intensity distribution of eigenstates in the position basis of the three quantum maps. (A) The quantum standard map at $N = 2098$, $\alpha = 1/4$, and $\beta = 1/4$. The parameters used are $K = 0.1$ (near-integrable) with a prominent tail, $K = 2.05$ (mixed) largest tail reached similar to a power-law, and $K = 10$ (fully chaotic) closest to the exponential distribution. (B) The quantum kicked harper map at $N = 2000$, $\alpha = 1/4$, and $\beta = 1/4$. The parameters used are $A = L = 0.1$ (near-integrable) that has a prominent tail again in spite of the KAM tori states, $A = L = 3.56$ (mixed) with the largest tail, and $A = L = 8.56$ (fully chaotic) has the smallest tail. (C) The quantum cat map at $N = 2113$. The stochastic parameters used are $\kappa = 0.2$ (fully chaotic) shifted from the exponential - regarding the time-reversal symmetry - and $\kappa = 6.67$ (mixed) with the heaviest tail.

We have set $N = 2098, 2000,$ and 2113 for the quantum standard map, kicked Harper map, and perturbed cat map, respectively. The chaotic parameters $K = 10$, $A = 8.56$, and $\kappa = 0.2$, as we have seen, lay in the exponential distribution - regardless of the shift observed in the perturbed cat map which has to do with the β-symmetry. However, it becomes interesting when we start to vary the parameters. For instance, we can select a range where the system is near-integrable; the map is covered predominantly with KAM tori, but some stable islands also take place. Thus, $K = A = 0.1$ has been set providing this regime. From figure 4.6a and 4.6b, an explicit departure from the exponential can be observed.

Nevertheless, at least in position representation, those regions would be expected to behave similarly to random vectors. This demeanor comes from the fact that the KAM tori end up localizing their momenta (see figure 3.4a and 3.5a and their insets) and distributing nearly uniformly the position. For the kicked Harper map, we can see a more close capture of the exponential, but the difference is more explicit in the standard map. One point that has also been addressed in [10] is that the intensity discrepancy possibly originates in the parity symmetry, in which the position $q = 1/2$ is peaked in many states of the quantum standard map distorting the statistics.

Finally, the richest regime is the mixed one, which boasts chaotic orbits and stable islands coexisting on the map. We have picked three representative parameters $K = 2.05$, $A = 3.56$, and $\kappa = 6.67$ where skimming their distributions swiftly, a significant deviation to the exponential is perceived. In figure 4.6, they end up with an L-shape tail, and this characteristic has already been visualized in other quantum chaotic systems. For example, in linear optical microresonators where light undergoes a chaotic scattering, the amplitude of light distributions also produces L-tails [55]. Therefore, the L-shape tail positively indicates the appearance of extreme events, which has recently been attributed to the generation of rouge waves or freak waves. This concept has its origin in oceanography since of the giant waves with a low but not zero probability of coming up.

4.2 Kurtosis

The subject matter of extreme values and record statistics is correlated with small probabilities; both are concerned with the tail region of the distribution. Specifically, these theories assess the high intensities in particular positions, which means localized states. The immediate example is the little deviation in the tail of the exponential distribution for chaotic states in figure 4.4, which can be directly related to the concept of scars - unstable periodic orbits being highlighted by the eigenstates 3.4.

Wondering about a more statistical approach with extreme values theory and record statistics and a more quantum chaos procedure with semiclassical theory and localization, we have proposed to bring a simple, well-known way to measure extreme events from the probability theory and statistics. The kurtosis of the distribution provides a way to quantify the number of extreme intensities and their increase in probability.

Based solely on the statistical moments, the kurtosis furnishes a feasible computation and wide applicability, i.e., it does not limit to intensities of wavefunctions. In addition, to fulfill the quantum-chaology side, we shall show that the kurtosis is equivalent to the usual way to measure localization, the inverse partition ratio - section 4.3. Thus, in order to begin with this prospect, let us define it properly and see what it can tell us about extreme intensities.

The kurtosis simplicity begins in its definition; it is the fourth standardized moment

$$Kurt = \tilde{\mu}_4 = \mu_4/\mu_2^2, \tag{4.13}$$

e.i., the fourth moment is divided by the standard deviation squared. The pivotal factor is that the number and size of outliers or extreme values actually determine the kurtosis. Thus, it is unequivocal its broad usage in the financial realm; for instance, in risk management for insurance and banking fields [56, 57]. To put it simply, by reckoning and evaluating the outliers, the kurtosis measures the "tailedness" of a probability distribution, which means that a high kurtosis corresponds to a heavy tail, whereas a low kurtosis indicates a rather light tail.

Nevertheless, this transparency brought by the kurtosis provokes some limitations. In truth, the value of the fourth standardized moment is insufficient to obtain complete information about how heavy the tail is. This lies in the fact that it evaluates the whole distribution and not solely the tail, as happens for maximum intensities and records. However, as we shall see, for our purposes, the kurtosis resumes categorically the information that we need about extreme and localization.

Having aptly outlined the kurtosis, we have in our hands a value representing the whole tail of eigenstate intensities distribution. Moreover, taking the benefit of working with quantum maps, we have a single stochastic parameter controlling their classical regimes. So we are able to obtain an extensive framework of extreme events by considering kurtosis as a function of the perturbation parameters.

Therefore, we reach one of the prominent results of this dissertation in figure 4.7. We have calculated the kurtosis intensity $|\psi_n(q)|^2$ distributions and varied the stochastic parameters $K, A,$ and κ for each quantum map. In addition, the dimension of the Hilbert space have not been altered, so $N = 2098, 2000,$ and 2113 for the quantum standard map, the kicked Harper map, and the perturbed cat map, respectively.

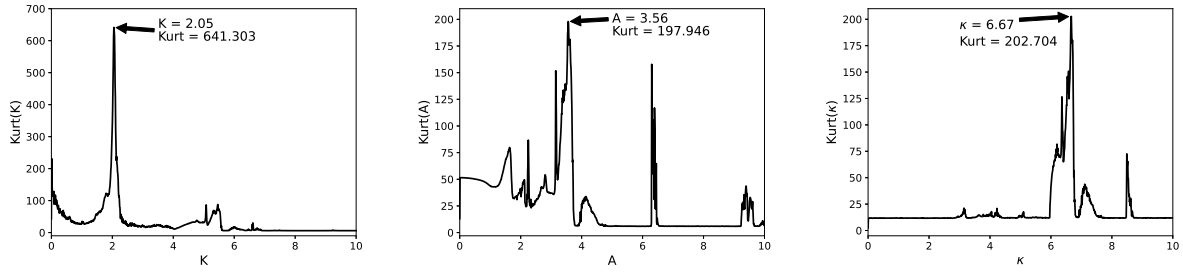

(A) (B) (C)

FIGURE 4.7. Kurtosis of the eigenstates intensity distribution of the three quantum maps as a function of each stochastic parameter. (A) For the quantum standard map, a sharp peak in the kurtosis is achieved for $K = 2.05$ where we have set $N = 2098$, $\alpha = 1/4$, $\beta = 1/4$, and $dK = 0.01$. (B) For the quantum kicked Harper map, there are two sharp peaks where the largest is for $A = 3.56$. We have set $N = 2000$, $\alpha = 1/4$, $\beta = 1/4$, and $dA = 0.01$. (C) For the quantum perturbed cat map, the $\kappa = 6.67$ is the sharp peak parameter where we have set $N = 2113$ and $d\kappa = 0.01$.

First of all, let us examine the standard map outcome. From section 2.3.1, low values of K, especially lower than $K = 0.9716354$ where the last KAM torus is de-

stroyed, the system is predominantly filled with KAM tori. Also, because of the Poincaré-Birkhoff theorem, some stable islands are present. Having set that, we have seen that the wavefunction captures both structures in the semiclassical limit. Therefore, a small value of the kurtosis is expected since the KAM tori end up distributing the eigenstate in the position, but it is not observed in figure 4.7a.

The explanation may lay in two circumstances; the first is the undeniable presence of stable islands (see the lower figure 3.4a), which enhance the intensities. The second is the aforementioned parity issue. The distribution is distorted from the exponential - significantly in the beginning - and from the fact that kurtosis entails all the distribution, it becomes protruded.

On the other side of the spectrum, we have the high values of K, which leads to an almost fully chaotic phase space. The chaotic states are conjectured to behave as random complex vectors, in addition to some being scared by the unstable period orbits. Consequently, in figure 3.4a, the expectation and the results agree on a low and steady kurtosis value, which just enhances moderately in the presence of scars.

Lastly, the central part is in the K values where the system is mixed: stable islands amidst the chaotic sea. As we shall discuss in the next chapter 5, this region provides ample information and different influences on the eigenstates amplitudes. To point out a few, we have bifurcations of orbits, cantori barriers, scars, and stable islands. In that sense, we can observe a wide range of values in kurtosis, but for a specific value $K = 2.05 \pm 0.01$, the kurtosis reaches its highest value. Moreover, the $Kurt \simeq 641,303$ is obtained in a sharp peak, indicating some drastic effect in the system.

Now, we pass to the other quantum maps and compare the concordances and peculiarities with the standard map. First, in figure 4.7b, we have the kicked Harper map's result, and it is promptly visible that for low values of A (its near-integrable regime), the kurtosis is similar to the standard map's case. The kicked Harper map has stables islands that accentuate the extremes, but the parity fact seems not to play the same role of bringing states to a particular position. In addition, this contrast can also be seen in the intensity distribution 4.6, where Harper's map actually lies in the exponential initially.

The chaotic regime with high A completely agrees with the standard map's result. Although some great kurtosis values are reached midway, those circumstances are linked with stable islands' appearance, turning them into a mixed regime. Lastly, again for middle A where the system is mixed, the kurtosis has its predominance, and its highest value is located in a sharp peak for $A = 3.56 \pm 0.01$.

The last map is the perturbed cat map with only two classical domains: chaotic and mixed. In figure 4.7c, the chaotic values of κ exhibit the foreseen low kurtosis. However, once more, the mixed regime provides the kurtosis outbreak and a sharp peak for its highest value, in this case for $\kappa = 6.67 \pm 0.01$.

Having exposed the kurtosis issue, in the next chapter, we shall address what semiclassical theory can provide as an explanation of kurtosis scenery and even if there is a semiclassical approximation for it. On top of that, the main point in question is the sudden summit in the mixed regime parameters. Thus, it deserves further discussion, including an investigation of whether it has semiclassical, pure quantum, or alternative reasons.

4.3 Inverse Participation Ratio

In order to provide further evidence of the localization in the position basis of the eigenstates intensities, we bring the inverse participation ratio (IPR). IPR is a conducive measure for localization and studying deviations from quantum ergodicity. We define it for the eigenstates of the quantum maps as [58, 59]

$$\text{IPR} = \frac{1}{3}\sum_{n=0}^{N-1}\sum_{Q=0}^{N-1}|\psi_n(q = Q/N)|^4. \tag{4.14}$$

The $1/3$ factor is a normalization from the random matrix theory for orthogonal ensemble, i.e., a IPR $= 1$ represents states randomly spread all over the accessible positions. Conversely, for states where IPR > 1, the localization is established. In fact, the equation 4.14 is called average IPR since, in general, each state has its respective value of it, which ends up with IPR$_n$. Nevertheless, for the connection with kurtosis, the sum over the states $\sum_n$ must be included.

That said, likewise the kurtosis results, we have plotted the average IPR value against the stochastic parameters for each quantum map. The result is in figure 4.8 for the quantum standard map with $N = 2098$, the kicked Harper map with $N = 2000$, and the perturbed cat map with $N = 2113$. First, we can rapidly see that the overall structures that we find in the kurtosis are still present. Chiefly, the presence of the sharp peak in the same mixed regions of the parameters that we have seen in the kurtosis outcomes, especially for the standard map 4.8a and the cat map 4.8c.

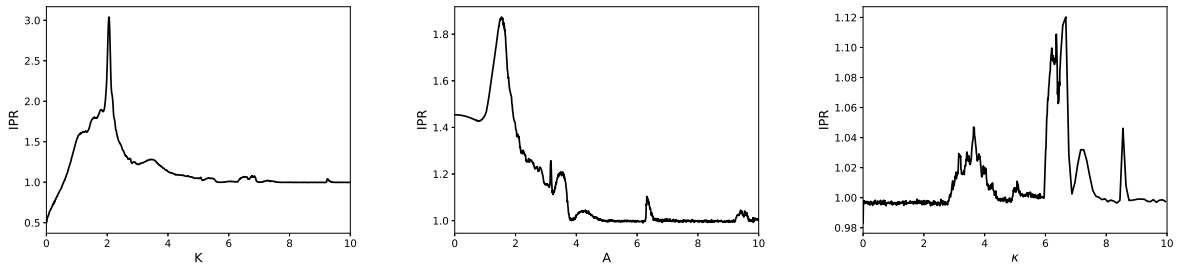

(A) (B) (C)

FIGURE 4.8. Inverse Participation Ratio of the eigenstates intensity distribution of the three quantum maps as a function of each stochastic parameter. (A) For the quantum standard map, once more, a sharp peak in the kurtosis is observed for $K = 2.05$ where we have set $N = 2098$, $\alpha = 1/4$ $\beta = 0$, and $dK = 0.01$. (B) For the quantum kicked Harper map, the near-integrable zone is more accentuated, bringing further deliberation. We have set $N = 2000$, $\alpha = 1/4$ $\beta = 1/4$, and $dA = 0.01$. (C) For the quantum perturbed cat map, the same parameter $\kappa = 6.67$ has a sharp peak in IPR where we have set $N = 2113$ and $d\kappa = 0.01$.

The kicked Harper map has shown up as an invariable obstacle, and the hurdle is even more explicit in the next chapter 5 when we shall seek for N-dependence of the intensities distribution moments. Harper's near-integrable regime is not clearly separate from the mixed regime as the standard map's case, leading to significant values in kurtosis 4.7b, and consequently, in the average IPR 4.8b. Therefore, the map aptly displays the intrinsic and non-universal idiosyncracies that mixed regimes affect on semiclassical systems [60].

Lastly, for our chaotic parameters, we are able to verify the ergodic hypothesis of the chaotic states since the IPR reckoning lies in the unitary value. Hence, despite all the limitations involved in dealing with the kurtosis to provide localization information, the well-established IPR measure corroborates our kurtosis examination.

Chapter 5

Semiclassical kurtosis and localization subject

All the discussion brought up in the last chapter leads us to grasp and interpret the kurtosis results in figure 4.7. The fourth standardized moment has been chosen in order to furnish us with a value representing the tail of the eigenstates intensities of semiclassical systems: the quantum maps. The tail region is concerned with extreme events - large values with small probabilities. Concomitantly, huge intensity $|\psi(q)|^2$ means an extremely high probability of finding the system at the position q, in other words, localized states.

The existence of this linking thread from the kurtosis and localization is extremely advantageous since the branch of localization in semiclassical systems has already been vastly studied - to mention a few [48, 16, 50, 15]. Therefore, chapter 3 has provided the essential background to us in order to elucidate the prominent influences that classical structures have in the wavefunctions of semiclassical systems, especially regarding localization. By these means, we begin finding a general semiclassical expression for the kurtosis with the assistance of the Gutzwiller trace formula. Thereafter, a particular formula can be stated for quantum maps and for each covered map. We also present what sort of information and limitations are involved with the semiclassical expression.

Finally, as an addendum, we make a more qualitative analysis of the play role of the quantum phases in the appearance of extreme events. The motivation comes from both phases α and β since the former is linked to the intensities prevalence of a

particular position - as $q = 1/2$ in the standard map - and the latter shifts the whole distribution positively - as in the standard and perturbed cat map in figure 4.5. This examination is intriguing since it is a purely quantum effect and reverberates throughout the semiclassical systems.

5.1 Bogomolny's scar formula

First of all, what becomes evident with the thorough discussion in section 3.3 is the fundamental relation in semiclassical systems, the Gutzwiller trace formula 3.111. Consequently, obtaining an expression for kurtosis is a rational guideline, mainly because it provides the density of states.

The first procedure, in fact, is some steps earlier than the trace formula: the Green function relation 3.68, when $\mathbf{q} = \mathbf{q}'$ can be written as

$$\sum_n |\psi_n(\mathbf{q})|^2 \delta(E - E_n) = -\frac{1}{\pi} \mathrm{Im} G(\mathbf{q}, \mathbf{q}, E) \tag{5.1}$$

where we have to keep in mind that energy is a positive complex number $E \to E + i\epsilon$ in order to ensure convergence. As aforementioned at the end of the section 3.3, it is impossible to see perfectly the contribution of a specific orbit, be it unstable or stable. That means we must have to forgo individual knowledge of energy levels. However, we can assemble energy levels via the Trace Formula and obtain approximate responses.

Therefore, the procedure is to smooth the delta in equation 5.1 using the complex feature of the energy. In particular, there are two main smoothings to advance in the spectrum knowledge: the exponential smoothing, where a Lorentzian is considered

$$\delta(E - E_n) \simeq \delta_\epsilon(E - E_n) = \frac{\epsilon/\pi}{(E - E_n)^2 + \epsilon^2} \tag{5.2}$$

which height is $1/\pi\epsilon$ and width ϵ. The second is the Gaussian smoothing

$$\delta(E - E_n) \simeq \delta_\epsilon(E - E_n) = \frac{1}{2\sqrt{\pi}\epsilon} e^{-(E-E_n)^2/2\epsilon^2} \tag{5.3}$$

which width is ϵ. Because the delta smoothing groups some levels, the operation is similar to an average, but with the Lorentzian or the Gaussian giving the proper weight. On top of that, both are broadly used and have their advantages and disadvantages.

For the sake of this work, we shall manage with both; however, in different circumstances. We select the Lorentzian case to perform an average in the energy, that is, gather intervals of levels. Nevertheless, afterward, another average will be required in position - basically, convolutions - and then a Gaussian smoothing is adopted.

Having set the smoothness condition, let us see how we can obtain information from the eigenstates intensities $|\psi_n(\mathbf{q})|^2$ from the expression 5.1. First, considering the semiclassical limit $\hbar \to 0$, the levels will be so dense that the left-hand side of the equation can be approximated to the average of the intensity with respect to the weighted states multiplied by the mean level density $\bar{\rho}$ 3.110

$$\sum_{n=0}^{\infty} |\psi_n(\mathbf{q})|^2 \delta_\epsilon(E - E_n) \approx \langle |\psi_n(\mathbf{q})|^2 \rangle \bar{\rho}(E). \tag{5.4}$$

Now, as the semiclassical limit has been stated, the right-handed side of 5.1 will render the semiclassical Green function 3.96; however, when $\mathbf{q}' = \mathbf{q}'' = \mathbf{q}$

$$G(\mathbf{q}, E) = \frac{2\pi}{(2\pi i\hbar)^{(f+1)/2}} \sum_j \frac{1}{|\dot{\mathbf{q}}|} \left| \det - \frac{\partial^2 S_j}{\partial \mathbf{y}' \partial \mathbf{y}''} \right|^{1/2} \exp\left[\frac{i}{\hbar} S_j(\mathbf{q}, E) - i\mu_j \frac{\pi}{2} \right] \tag{5.5}$$

where f is the degree of freedom, the sum over j represents the trajectories, and μ_j is their Maslov index. One detail that must have attention is that the Gutzwiller trace formula cannot be applied here since the lack of integration over position $\mathbf{q}$ simplifies the expression with the usage of the stationary-phase method. In addition, integration is not even desirable by the fact we want to explore the possibilities of enhancements in the intensities for particular positions.

Namely, the wavefunctions information we are looking for is their kurtosis; in other words, we are interested in the moments of the wavefunctions. Following Berry's idea for the spectral staircase [61], the moments are directly available when the Green function is divided by a summation between a mean value and a fluctuation, as in 3.111. Consequently, an ingenious procedure made in Keating and Prado [14], which was mainly inspired by the iconic work of Bogomolny [62], consists of not integrating over all positions $\mathbf{q}$ but from performing a local average $\langle \dots \rangle_{\mathbf{q}}$ with respect to $\mathbf{q}$.

In order to maintain smoothness, the local average is chosen to be a convolution with a normalized Gaussian, where its width reserves further discussion. First, apply-

ing the local average into the equation 5.1, after the evaluation of the energy average with 5.4 and 5.5, we become with

$$\langle\langle|\psi_n(\mathbf{q})|^2\rangle\rangle_{\mathbf{q}}\bar{\rho}(E) \approx -\frac{1}{\pi}\langle \mathrm{Im}G(\mathbf{q},E)\rangle_{\mathbf{q}}. \tag{5.6}$$

Here we can see our wavefunction intensities being average both in energy $\langle\dots\rangle$ and in position $\langle\dots\rangle_{\mathbf{q}}$. In addition, the convolution of the Green function will enable us to perform the stationary phase method and obtain helpful information from it.

Semiclassically, emulating the trace formula, the convolution of the Green function will select the periodic orbits and those trajectories which are very proximate to it, i.e., trajectories where $\mathbf{p}'$ and $\mathbf{p}''$ are very close but not equal. However, linearizing the equation about the periodic orbits leaves only the action to the quadratic term

$$\begin{aligned} -\frac{1}{\pi}\langle \mathrm{Im}G(\mathbf{q},E+i\epsilon)\rangle_{\mathbf{q}} \;\simeq\; & \frac{\Omega(\mathbf{q},E)}{(2\pi\hbar)^f} - \mathrm{Im}\frac{2}{(2\pi i\hbar)^{(f+1)/2}}\sum_p \frac{1}{|\dot{\mathbf{q}}|}\left|\det -\frac{\partial^2 S_p}{\partial\mathbf{y}'\partial\mathbf{y}''}\right|^{1/2} \\ & \times\exp\left[\left(\frac{i}{\hbar}S_p+\frac{1}{2}|\det(W)|\mathbf{y}^2\right)-i\sigma_p\frac{\pi}{2}\right]e^{\left(-\epsilon\frac{T_p}{\hbar}\right)} \end{aligned} \tag{5.7}$$

where the sum is over the period orbits p, σ_p is the Maslov index of the periodic orbits, $\mathbf{y}$ are the Gutzwiller tangential coordinates, and $\Omega(\mathbf{q},E)$ is the contribution from the zero-length trajectories 3.110 but without the integration over the position

$$\Omega(\mathbf{q},E) = \int d\mathbf{p}\delta(E-H(\mathbf{q},\mathbf{p})). \tag{5.8}$$

Moreover, we have separated the energy's real and imaginary parts, generating an exponential decay from 3.63 to ensure convergence. This dissociation makes explicit the contribution of solely periodic orbits of period $T_p \leq \hbar/\epsilon$.

As we have seen in section 2.1.4 about periodic orbits, we can write the action derivatives in terms of the monodromy matrix, which gives us information about the neighborhood of the periodic orbits. Therefore, from 2.71

$$\left|\det -\frac{\partial^2 S_p}{\partial\mathbf{y}'\partial\mathbf{y}''}\right|^{1/2} = |\mathcal{B}|^{1/2} = \frac{1}{\sqrt{[\mathbf{M}]_{12}}} \tag{5.9}$$

and 3.104

$$|\det(W)| = \frac{\det(\mathbf{M}-\mathbf{I})}{[\mathbf{M}]_{12}}, \tag{5.10}$$

we can rewrite 5.7 as

$$-\frac{1}{\pi}\langle \mathrm{Im}G(\mathbf{q},E+i\epsilon)\rangle_{\mathbf{q}} \simeq \frac{\Omega(\mathbf{q},E)}{(2\pi\hbar)^f} - \mathrm{Im}\frac{2}{(2\pi i\hbar)^{(f+1)/2}}\sum_p \frac{1}{|\dot{\mathbf{q}}|\sqrt{[\mathbf{M}]_{12}}} \times \exp\left[\frac{i}{\hbar}\left(S_p+\frac{1}{2}\frac{\det(\mathbf{M}-\mathbf{I})}{[\mathbf{M}]_{12}}\mathbf{y}^2\right)-i\mu_p\frac{\pi}{2}\right]e^{\left(-\epsilon\frac{T_p}{\hbar}\right)}. \quad (5.11)$$

Now, we finally can assemble 5.6 to get an expression for the intensities, also known as Bogomolny's scar formula

$$\langle\langle|\psi_n(\mathbf{q})|^2\rangle\rangle_{\mathbf{q}} \approx \frac{\Omega(\mathbf{q},E)}{(2\pi\hbar)^f\bar{\rho}(E)} - \mathrm{Im}\frac{2}{(2\pi i\hbar)^{(f+1)/2}\bar{\rho}(E)}\sum_p \frac{1}{|\dot{\mathbf{q}}|\sqrt{[\mathbf{M}]_{12}}} \times \exp\left[\frac{i}{\hbar}\left(S_p+\frac{1}{2}\frac{\det(\mathbf{M}-\mathbf{I})}{[\mathbf{M}]_{12}}\mathbf{y}^2\right)-i\sigma_p\frac{\pi}{2}\right]e^{\left(-\epsilon\frac{T_p}{\hbar}\right)}. \quad (5.12)$$

Namely, we aptly break the wavefunction amplitudes into a mean plus a fluctuation, as was sought.

On top of that, the expression 5.12 already offers us information about the semiclassical wavefunction. First, let us see the mean value of the averaged semiclassical wavefunction

$$\frac{\Omega(\mathbf{q},E)}{(2\pi\hbar)^f\bar{\rho}(E)} = \frac{\int d\mathbf{p}\delta(E-H(\mathbf{q},\mathbf{p}))}{\int d\mathbf{q}d\mathbf{p}\delta(E-H(\mathbf{q},\mathbf{p}))} \equiv \mu(\mathbf{q},E). \quad (5.13)$$

In classically ergodic systems, it represents the quantum-ergodic limit [47, 63, 64], which comes from the Berry and Voros assumption of the Shnirelman theorem [62] that the average square of the eigenfunctions in the semiclassical limit coincides with the projection of the classical microcanonical distribution to coordinate space.

Secondly, the fluctuation reveals the intricate contribution of the periodic orbits. From 5.12, their weight is proportional to $\sqrt{\hbar^{f-1}/[\mathbf{M}]_{12}|\dot{\mathbf{q}}|^2}$ and can be seen around it in the narrow band of width $\sqrt{\hbar[\mathbf{M}]_{12}/\det(\mathbf{M}-\mathbf{I})}$ which is known as complex Gaussian fringes [14]. Along with the width of the fringe, we are able to discuss the local position average since we want to have the finest resolution to perceive the wavefunction structures. Consequently, the convolution must have a width that is small compared to the length-scale of the fringes, i.e., it must scale as $\hbar^\delta$ with $\delta > 1/2$. In addition, the convolution width must have been large to the de Broglie wavelength $\sim \hbar$, then $\delta < 1$.

Having set the convolution, we can notice that the double average of the intensities conveniently separates it into the mean and the fluctuation parts. Thus, their

moments are given simply by

$$\mu_{2m} = \frac{1}{\Delta q}\int \left(\langle\langle|\psi_n(\mathbf{q'})|^2\rangle\rangle_{\mathbf{q}'} - \mu(\mathbf{q}', E)\right)^{2m} d\mathbf{q'}, \tag{5.14}$$

where Δq is the volume of integration independent of $\hbar$. As a result, recalling the definition of the kurtosis in 4.13, we have just to substitute 5.12 in 5.14 for $m = 2$ and $m = 1$ to obtain the semiclassical formula for the kurtosis

$$Kurt = \frac{(\Delta q)^{-1}\int \left(\sum_p \mathrm{Im}A_p(\mathbf{q}', E)e^{\left(i\mathfrak{S}_p(\mathbf{q}',E)/\hbar - i\sigma_p\pi/2\right)}e^{(-\epsilon T_p/\hbar)}\right)^4 d\mathbf{q'}}{\left[(\Delta q)^{-1}\int \left(\sum_p \mathrm{Im}A_p(\mathbf{q}', E)e^{\left(i\mathfrak{S}_p(\mathbf{q}',E)/\hbar - i\sigma p\pi/2\right)}e^{(-\epsilon T_p/\hbar)}\right)^2 d\mathbf{q'}\right]^2} \tag{5.15}$$

where $A_p(\mathbf{q}, E)$ is the amplitude

$$A_p(\mathbf{q}, E) = \frac{2}{(2\pi i\hbar)^{(f+1)/2}\bar{\rho}(E)}\frac{1}{|\dot{\mathbf{q}}|\sqrt{[\mathbf{M}]_{12}}} \tag{5.16}$$

and the expanded action $\mathfrak{S}_p$ is

$$\mathfrak{S}_p = S_p + \frac{1}{2}\frac{\det(\mathbf{M}-\mathbf{I})}{[\mathbf{M}]_{12}}\mathbf{y}^2. \tag{5.17}$$

Despite being thorough and general, the resulting expression 5.15 still seems tangled to elucidate about the kurtosis, as in figure 4.8. Nevertheless, in order to acquire information about a semiclassical quantity, the problem will revolve around the $\hbar$ dependence. For instance, for a two degree of freedom system ($f = 2$) with solely unstable periodic orbits[1], the amplitude A_p furnishes $\hbar^{1/2}$ since $\bar{\rho}(E) \sim \hbar^{-2}$. Owing to the proportionality $\mu_{2m} \propto A_p^{2m}$, the contribution is $\hbar^{2m/2}$.

On top of that, we must consider the $\hbar$ dependence from the coordinates $\mathbf{y}$ in the complex exponential, which comes up from the differential $d\mathbf{q}'$. Their contribution is carried out by rescaling $\mathbf{y}$ to remove the $\hbar$ factor from the exponent. Because $\mathbf{y}$ is squared in 5.17, there will be another $\hbar$ dependence equals to $\hbar^{1/2}$. Therefore, in this case, the moments μ_{2m} of 2-dimensional systems fully with unstable periodic orbits scales as $\hbar^{(2m+1)/2}$; and their kurtosis scales as

$$Kurt = \mu_4/\mu_2^2 \sim \frac{\hbar^{5/2}}{(\hbar^{3/2})^2} \sim \hbar^{-1/2}. \tag{5.18}$$

[1] where the expansion of $\mathfrak{S}_p$ in 5.17 is sufficient

Nevertheless, for general systems, unstable periodic orbits abound but concurrently with stable orbits, bifurcations, and cantori. Those other classical structures may affect the $\hbar$-dependence, mainly the bifurcations demonstrated in Keating & Prado issue [14]. The orbits bifurcate when $\det(\mathbf{M}-\mathbf{I})=0$, which makes the expanded action $\mathfrak{S}_p$ $\mathbf{y}$-independent as if the fringes would be infinitely wide. Keating & Prado have shown that only taking higher terms from the action does not cover all sorts of bifurcations. To summarize, they work around the Almeida-Hannay method [65], which transforms the Green function into a mixed position-momentum space, and an action called normal form gives the configuration of the bifurcation's neighborhood. The resultant is an additional $\hbar$-dependence $\sim\hbar^{\gamma}$ for different sorts of bifurcations.

That being said, along with the expression 5.15, we may find the semiclassical kurtosis for the three selected quantum maps. Moreover, we shall address how it responds when the semiclassical limit $N\to\infty$ is considered in order to elucidate the sharp peaks in the mixed regime.

Before going any further, an equivalent relation of 5.1 can be obtained for the propagator operator of the quantum maps. It just requires careful manipulation with a very well-known function called the Wigner function $W(\mathbf{q},\mathbf{p})$.

The demand for a quantum phase space pushed physicists to wonder how to overcome the Heisenberg principle. Nevertheless, Wigner in 1932 [66] introduced a function dependent on position and momentum, taking into account the uncertainty principle. For a general system with f degrees of freedom, it is defined as

$$W(\mathbf{q},\mathbf{p})=\frac{1}{(2\pi\hbar)^f}\int d\mathbf{Q}\Psi(\mathbf{q}+\mathbf{Q})\Psi^*(\mathbf{q}-\mathbf{Q})e^{-i\mathbf{Q}\cdot\mathbf{p}/\hbar}. \tag{5.19}$$

Likewise, in the case of the quantum maps that the Hilbert space is finite with a dimension N, the Wigner function associated with the nth eigenstate $\psi_n(q=Q/N)$ is

$$w_n(q,p)=\frac{1}{2N}\sum_{X=0}^{2N-1}\psi_n((Q+X/2)/N)\psi_n^*((Q-X/2)/N)e^{-2\pi iXp/N}, \tag{5.20}$$

where if $Q\pm X/2$ is not a integer then $\psi_n(Q\pm X/2)$ is null. In addition, $q=Q/N$ and $p=m/N$ can only assume integers and half-integers between 0 and $N-1$ because $Q,m=0,\ldots,N-1$.

If we take the kth power of the propagator $\hat{\mathbf{U}}$ and act it into the eigenstates $|\psi_n\rangle$ given by 3.132, we have the following equation

$$\hat{\mathbf{U}}^k |\psi_n\rangle = e^{ikE_n} |\psi_n\rangle . \tag{5.21}$$

Therefore, the matrix expression of the kth power of the propagator in position basis can be written as

$$\begin{aligned} U^k_{Q_1,Q_2} &= \langle q_1| \hat{\mathbf{U}}^k |q_2\rangle = \sum_{n=0}^{N-1} \langle q_1| \hat{\mathbf{U}}^k |\psi_n\rangle \langle \psi_n|q_2\rangle \\ &= \sum_{n=0}^{N-1} e^{ikE_n} \langle q_1|\psi_n\rangle \langle \psi_n|q_2\rangle = \sum_{n=0}^{N-1} e^{ikE_n} \psi^*_n(q_1)\psi_n(q_2). \end{aligned} \tag{5.22}$$

We may now insert $\sum_{k=0}^{N-1} e^{-ikE_j}$ in both sides of the equation 5.22

$$\sum_{k=0}^{N-1} e^{-ikE_j} U^k_{Q_1,Q_2} = \sum_{k=0}^{N-1}\sum_{n=0}^{N-1} e^{ik(E_n-E_j)} \psi^*_n(q_1)\psi_n(q_2) \tag{5.23}$$

$$= N \sum_{n=0}^{N-1} \delta_{E_n,E_j} \psi^*_n(q_1)\psi_n(q_2). \tag{5.24}$$

That said, we go back to the definition of the Wigner function 5.20 and insert the delta as follows

$$\begin{aligned} \sum_{n=0}^{N-1} w_n(q,p)\delta_{E_n,E_j} &= \frac{1}{2N} \sum_{X=0}^{2N-1}\sum_{n=0}^{N-1} \psi_n((Q+X/2)/N)\psi^*_n((Q-X/2)/N) \\ &\quad \times \delta_{E_n,E_j} e^{2\pi i X p/N}, \end{aligned} \tag{5.25}$$

and from 5.24, we have a relation between the Wigner function and the propagator

$$\begin{aligned} \sum_{n=0}^{N-1} w_n(q,p)\delta_{E_n,E_j} &= \frac{1}{2N^2} \sum_{k=0}^{N-1}\sum_{X=0}^{2N-1} \langle (Q_1+X/2)/N| \hat{\mathbf{U}}^k |(Q_2-X/2)/N\rangle \\ &\quad \times e^{-2\pi i X p/N} e^{-iE_j k}. \end{aligned} \tag{5.26}$$

Finally, rewriting 5.26, we end up with

$$\sum_{n=0}^{N-1} w_n(q,p)\delta_{E_n,E_j} = \frac{1}{2N^2} \sum_{k=0}^{N-1} e^{-E_j k} W_k(q,p), \tag{5.27}$$

where $W_k(q,p)$ is called the Weyl transform

$$W_k(q,p) = \sum_{X=0}^{2N-1} U^k_{Q_1+X/2,Q_2-X/2} e^{-2\pi i X p/N}. \tag{5.28}$$

Along similar lines, as we have done for the delta function in 5.1, we shall extend the contribution from other eigenstates around the nth state - an energy average. To this, we take the equation 5.22 but insert the summation $\sum_k \exp(-k(iE_m+\epsilon))$ on each side

$$\begin{aligned}\sum_k e^{(-ikE_m-\epsilon k)}U^k_{Q_1,Q_2} &= \sum_k e^{(-ikE_m-\epsilon k)}\sum_{n=0}^{N-1} e^{ikE_n}\psi_n^*(q_1)\psi_n(q_2)\\ &= \sum_{n=0}^{N-1}\psi_n^*(q_1)\psi_n(q_2)\sum_k e^{(-ik(E_m-E_k)-\epsilon k)}. \end{aligned} \tag{5.29}$$

In fact, the second summation is the inverse Fourier transform of the Lorenztian $\delta_\epsilon(E_m-E_n)$ as 5.2, so

$$\sum_k e^{(-iE_m-\epsilon k)}U^k_{Q_1,Q_2} = \sum_{n=0}^{N-1}\delta_\epsilon(E_m-E_n)\psi_n^*(q_1)\psi_n(q_2). \tag{5.30}$$

If we make $q_1 = (Q+X/2)/N$, $q_2 = (Q-X/2)/N$, include the sum $\sum_{n=0}^{2N-1}$ and $\exp(-2\pi ipX/N)/2N$, the resulting equation will be

$$\sum_{n=0}^{N-1}\delta_\epsilon(E_m-E_n)w_n(q,p) = \mathrm{Re}\frac{1}{2N}\sum_{k=0}^{\infty} e^{(-ikE_m-\epsilon k)}W_n(q,p) \tag{5.31}$$

where the real part was taken into account since the left-hand side must be real.

One of the many advantages aspects of the Wigner function is attributed to its ability to directly inform the wavefunction both in momentum and position representation just with an integral. Then, from 5.19,

$$\int d\mathbf{p}W(\mathbf{q},\mathbf{q}) = |\psi(\mathbf{q})|^2 \quad \int d\mathbf{q}W(\mathbf{q},\mathbf{q}) = |\psi(\mathbf{p})|^2. \tag{5.32}$$

For a finite Hilbert space, we have

$$\frac{1}{N}\sum_p w_n(q,p) = |\psi_n(q)|^2 \quad \frac{1}{N}\sum_q w_n(q,p) = |\psi_n(p)|^2. \tag{5.33}$$

Therefore, because we are interested in the eigenstates intensities in the position space of the quantum maps, we insert the sum in p in 5.31

$$\sum_{n=0}^{N-1}\delta_\epsilon(E_m-E_n)\frac{1}{N}\sum_p w_n(q,p) = \mathrm{Re}\frac{1}{2N}\sum_{k=0}^{\infty} e^{(-ikE_m-\epsilon k)}\sum_{X=0}^{2N-1} U^k_{Q+X/2,Q-X/2}\frac{1}{N}\sum_p e^{-2\pi iXp/N}$$

$$\sum_{n=0}^{N-1}\delta_\epsilon(E_m-E_n)|\psi_n(Q/N)|^2 = \mathrm{Re}\frac{1}{2N}\sum_{k=0}^{\infty}e^{(-ikE_m-\epsilon k)}\sum_{X=0}^{2N-1}U^k_{Q+X/2,Q-X/2}\delta_{X,0}$$
$$= \mathrm{Re}\sum_{k=0}^{\infty}e^{(-ikE_m-\epsilon k)}U^k_{Q,Q} \quad (5.34)$$

where the expression is the quantum maps analog to 5.1. It becomes even more familiar when we open in mean-plus-fluctuation form

$$\sum_{n=0}^{N-1}\delta_\epsilon(E_m-E_n)|\psi_n(Q/N)|^2 = 1+\mathrm{Re}\sum_{k=1}^{\infty}e^{(-ikE_m-\epsilon k)}U^k_{Q,Q}. \quad (5.35)$$

Moreover, instead of the normal form of the Lorentzian 5.2, we adhere to a smooth and periodic Lorentzian function

$$\delta_\epsilon(x)=\frac{1-e^{-\epsilon\cos(x)}}{1+e^{-2\epsilon}-2e^{-\epsilon}\cos(x)}. \quad (5.36)$$

If ϵ is large number then $\delta_\epsilon(x)\approx 1$ or $\delta_\epsilon(x)\to 2\pi\delta(x)$ as $\epsilon\to 0$. In the semiclassical limit $N\to\infty$, the left-hand side of 5.35 is similar to 5.4, which is the energy average multiplied by the mean density $\bar{\rho}$. In the case of quantum maps, the mean density is just N^2. Applying the average in the position, we finally obtain Bogomolny's scar formula for the quantum maps

$$\langle\langle|\psi_n(Q/N)|^2\rangle\rangle_q \approx \frac{1}{N}+\frac{1}{N}\mathrm{Re}\sum_{k=1}^{\infty}e^{(-ikE_m-\epsilon k)}\langle\langle U^k_{Q,Q}\rangle\rangle_q. \quad (5.37)$$

Once more, we distinctly notice the mean reflecting the quantum-ergodic limit, where there is an equal probability of the wavefunction being in any position. The position average of the propagator's trace gives the contribution from the periodic orbits to the fluctuations. In addition, the width of the convolution in the q-average must be over a range smaller than N and larger than the de Broglie wavelength ($\Delta q = 1/N$).

In 5.37, the trace of the propagator plays the role of the Green function for quantum maps. Consequently, the q-average selects the closed orbits nearby the periodic orbits - the fixed points q_f of the classical maps. On top of that, the work of finding classical orbits is already difficult; the kth power of $U_{Q,Q}$ makes the resolution even

[2]The mean density of states counts the average number of energy levels in an energy interval of length one. Since all N energies are in the unitary interval, then $\bar{\rho}=N$ [67]

more intricate. To deal with this issue, we adjust ϵ such that only simple powers become relevant. For instance, if ϵ is large enough, the real exponential $\exp(-\epsilon k)$only leaves $k = 1$ as the main contribution of the fluctuation in 5.37. This configuration is convenient because we have the quantum maps formulae in 3.142, 3.143, and 3.144.

In this case, we shall not focus on the quantum phases α and β, then we set them null and utilize the equation 3.141 for the propagators. In order to reach the q-averaged quantum map, we will need to linearize the action over the fixed points, which are essentially defined as

$$\frac{\partial S}{\partial q}\Big|_{q=q_f} = 0 \tag{5.38}$$

and then we expand the action in the exponential until the second order as in 5.7 for each map.

To begin, the action of the standard map is given by 2.97, and then its fixed points satisfy

$$\frac{K}{2\pi}\sin\left(2\pi q_f\right) = -m \tag{5.39}$$

where m is the integer that deals with the unity modulus in the momentum, and so the q-average evolution operator with $\alpha = \beta = 0$ for a convenient expression

$$\langle U^{(std)}_{Q,Q}\rangle_q \approx \frac{1}{\sqrt{iN}}\exp\left[2\pi i N S_{(std)}\left(q_f, q_f\right)\right]\exp\left[-i\pi N K\cos\left(2\pi q_f\right)\Big(\frac{Q}{N} - q_f\Big)^2\right]. \tag{5.40}$$

Furthermore, with the action of the kicked Harper map in 2.103, the expression for the fixed points is

$$\frac{A}{2\pi}\sin\left(2\pi q_f\right) = m \tag{5.41}$$

then the expanded quantum map becomes

$$\langle U^{(hrp)}_{Q,Q}\rangle_q \approx \frac{1}{\sqrt{N|L|}}\exp\left[2\pi i N S_{(hrp)}\left(q_f, q_f\right)\right]\exp\left[\pi i N A\cos\left(2\pi q_f\right)\Big(\frac{Q}{N} - q_f\Big)^2\right]. \tag{5.42}$$

Finally, from the action 2.105, the relation that identifies the fixed points of the perturbed cat map is

$$q_f = \frac{1}{2}\Big(m - l - \frac{\kappa}{2\pi}\cos\left(2\pi q_f\right)\Big), \tag{5.43}$$

where l is also an integer, but it handles the unity modulus in the position. Thus, the q-average evolution operator is given by

$$\langle U^{(cat)}_{Q,Q}\rangle_q \approx \frac{1}{\sqrt{iN}} \exp\left[2\pi i N S_{(cat)}\left(q_f, q_f\right)\right] \exp\left[i\pi N(2-\kappa\sin\left(2\pi q_f\right))\Big(\frac{Q}{N}-q_f\Big)^2\right]. \quad (5.44)$$

Therefore, emulating the same reasoning to reach out 5.15, we are able to get the kurtosis semiclassical formula for quantum maps, but first, we need the moments' equations. From 5.14, the moments are

$$\mu_{2m} = N^{2m}\sum_{Q=1}^{N}\left(\langle\langle|\psi_n(Q/N)|^2\rangle\rangle_q - \frac{1}{N}\right)^{2m} \quad (5.45)$$

and substituting 5.37 we get

$$\mu_{2m} = \sum_{Q=1}^{N}\left(\mathrm{Re}\sum_{n=1}^{\infty} e^{(-ikE_m-\epsilon k)}\langle\langle U^k_{Q,Q}\rangle\rangle_q\right)^{2m}. \quad (5.46)$$

By definition of the kurtosis, we have its semiclassical form for quantum maps

$$Kurt = \frac{\sum_{Q=1}^{N}\left(\mathrm{Re}\sum_{k=1}^{\infty} e^{(-ikE_m-\epsilon k)}\langle\langle U^k_{Q,Q}\rangle\rangle_q\right)^4}{\left[\sum_{Q=1}^{N}\left(\mathrm{Re}\sum_{k=1}^{\infty} e^{(-ikE_m-\epsilon k)}\langle\langle U^k_{Q,Q}\rangle\rangle_q\right)^2\right]^2} \quad (5.47)$$

The first thing to consider is that when the maps are completely chaotic, i.e., only unstable orbits, the second-order expansion of the actions is sufficient. Consequently, we will have moments scaling as $N^{(1-2m)1/2}$ since there is N^{-m} from the amplitude and $N^{1/2}$ from the exponent. The semiclassical kurtosis is predicted to scale as

$$Kurt = \frac{\mu_4}{(\mu_2)^2} \sim \frac{N^{-3/2}}{(N^{-1/2})^2} \sim N^{-1/2}. \quad (5.48)$$

5.2 Results of the intensities kurtosis

For our calculations of the N-dependence of the kurtosis, we have settled to plot the moments μ_4 and μ_2 separately. The reason lies in the fact that any variation in the second moment μ_2 will be amplified from the kurtosis definition 4.13. On top of that, the oscillation could be reduced if we increase as much as possible the N values.

However, we are hampered by computational effort; for instance, only the reckoning of the eigenvectors scales like N^3.

In figures 5.1a and 5.2a, we have plotted the $\log \mu_4$ and $\log \mu_2$ versus $\log N$ for the chaotic parameters $K = 10$, $A = 8.56$, and $\kappa = 0.2$. Despite the fluctuations, we can see the concordance with the semiclassical prediction of $N^{(1-2m)/2}$: $-1/2$ to μ_2 and $-3/2$ to μ_4, resulting in the kurtosis scaling as $N^{-1/2}$ for the chaotic regime of the quantum maps. However, a point must be stated about the considerable difference in the size of the fluctuations. For the standard map and kicked Harper map, although we have selected chaotic parameters, the classical maps are known to be not completely hyperbolic; there are undetectable stable structures spread around the map, which end up disturbing the results. Conversely, the classical perturbed cat map belongs to an Asonov system and is proven to be fully hyperbolic without any sort of stable entity, leading to less variation in this regard.

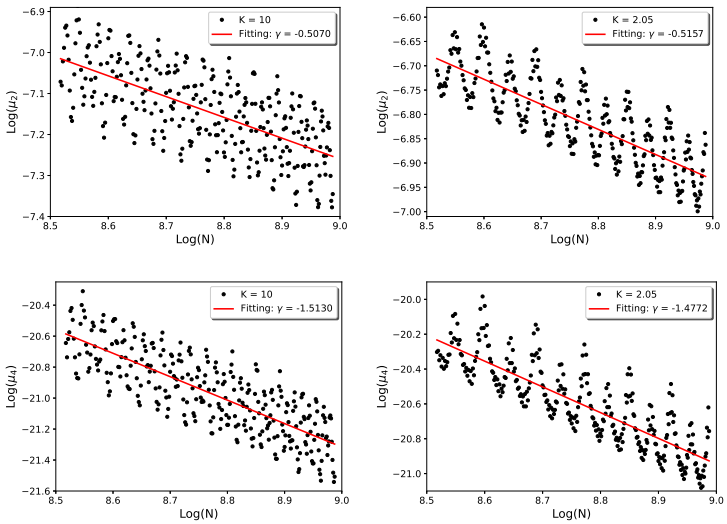

(A) (B)

FIGURE 5.1. The logarithm of moments μ_2 (upper panel) and μ_4 (lower panel) plots against $\log N$ for the quantum standard map, where we have set $\beta = 0$, $\alpha = 0$, $\epsilon = 2.2$, $E_m = \pi/4$, and the q-average of size $0.02N^{1/2}$ (Gaussian convolution width). (A) The moments for $K = 10$ are consistent with the predicted power-law dependence $N^{-m+1/2}$, despite some fluctuation around it. (B) Furthermore, the moments of the mixed parameter $K = 2.05$ have intriguing oscillations, but if we reckon their decaying exponent, they do not explain the sharp peaks observed in 4.7a. The best-fitting straight line is in red for all plots, along with their gradient γ.

Now, for the mixed regimes values, we have the calculation of the N-dependence for each quantum map and have settled the particular values of parameters where the sharp peaks have taken place in the kurtosis. To begin with, the standard map provides us the figure 5.1b for $K = 2.05$. It is interesting in both moments the characteristic oscillation, which probability comes from the complex exponential action in the trace of the quantum propagators. The expected departure from $N^{(1-2m)/2}$ scaling is achieved as advanced by Keating & Prado [14], and the oscillations are found on decaying as N^{γ}, with $\gamma \approx 0.52$ for μ_2 and $\gamma \approx 1.48$ for μ_4.

Nevertheless, for the perturbed cat map, oscillations for the mixed regime parameter $\kappa = 6.67$ were not present (see figure 5.2b). The power-law dependence of N is then skewed from the chaos as expected, which may be attributed to the emergence of many bifurcations. Finally, the kicked Harper map has shown an innate convolution that the propagator 3.141 has not converged, and the other option 3.140 takes a massive computational effort. Therefore, Harper's results will be addressed in future work.

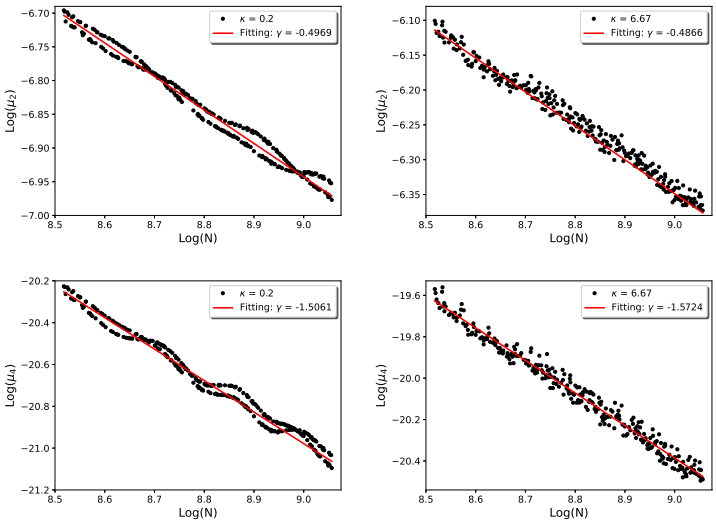

(A) (B)

FIGURE 5.2. The logarithm of moments μ_2 (upper panel) and μ_4 (lower panel) plots against $\log N$ for the quantum perturbed cat map, where we have set $\epsilon = 2.2$, $E_m = \pi/4$, and the q-average of size $0.02N^{1/2}$ (Gaussian convolution width). (A) The moments for $\kappa = 0.2$ are consistent with the predicted power-law dependence $N^{-m+1/2}$, despite some fluctuation around it. (B) However, the moments of the mixed parameter $\kappa = 6.67$ do not have definite-period oscillation, just the variations as observed in the fully chaotic case. Also, the best-fitting straight line is in red for all plots, along with their gradients γ.

If we gather the scaling results of the three maps in the specific parameters where we have found the sharp peaks and compare them to the chaotic parameters. In that case, we see that the Berry twinkling exponents [61] may not explain the drastic difference between those singular parameters and the other mixed values, in addition to living in blank the localization culprit. Nevertheless, we acknowledge that this affirmation deserves more data reading larger N, especially for the results 5.1b and 5.2b. Higher Ns lead to fewer fluctuations and more secure analyses about the N dependence of the kurtosis - our results are solely primary.

In addition, to enhance the complexity of the kurtosis problem, when the logarithmic of it is taken from the pure (without any average) eigenstates intensities, we can see a clear power-law growth in figure 5.3a for the standard map. This observation means as we go to the semiclassical limit $N \to \infty$, the kurtosis reaches and includes even more localized states in the system. Figure 5.3a can be compared to the same procedure for the pure chaotic states 5.3b where it does not have a clear power-law dependence.

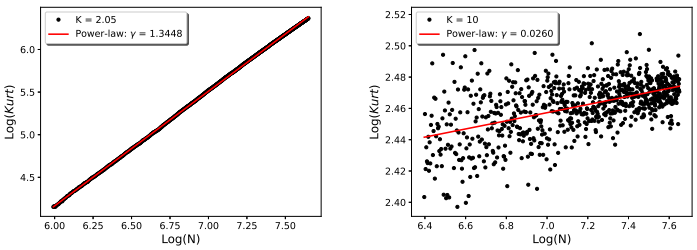

(A) (B)

FIGURE 5.3. The logarithm of the pure kurtosis plots against $\log N$ for the quantum standard map. Pure kurtosis means that any sort of average for the eigenstate's intensities has been performed. (A) The kurtosis for $K = 2.05$ grows as a power-law with N, with a considerable exponent $\gamma \simeq 1.34$. (B) The kurtosis for the chaotic parameter $K = 10$ does not present a conclusive dependence of N only seems to be a small increase. Those results showcase the richness of the eigenstates that our average may be overlooking.

There is another prospect of the kurtosis boost that deserves further investigation, the stable periodic orbits. Recently, we have taken the standard map with $K = 2.05$ and separated the states that scar the corner islands, the central island, and the chaotic sea (see figure 3.4b to picture the panorama). Since we cannot assess pre-

cisely the trace of the kth power of the propagator to catch each contribution, we calculate the scaling exponents for each structure; the result is in figure 5.4. Separately, the states manage to depict the moment growth that we see of pure kurtosis. However, owing to the proximity of the moments μ_4 and μ_2, the kurtosis ended up being a decay which agrees with the theory from 5.47 but not with the outcome 5.3a.

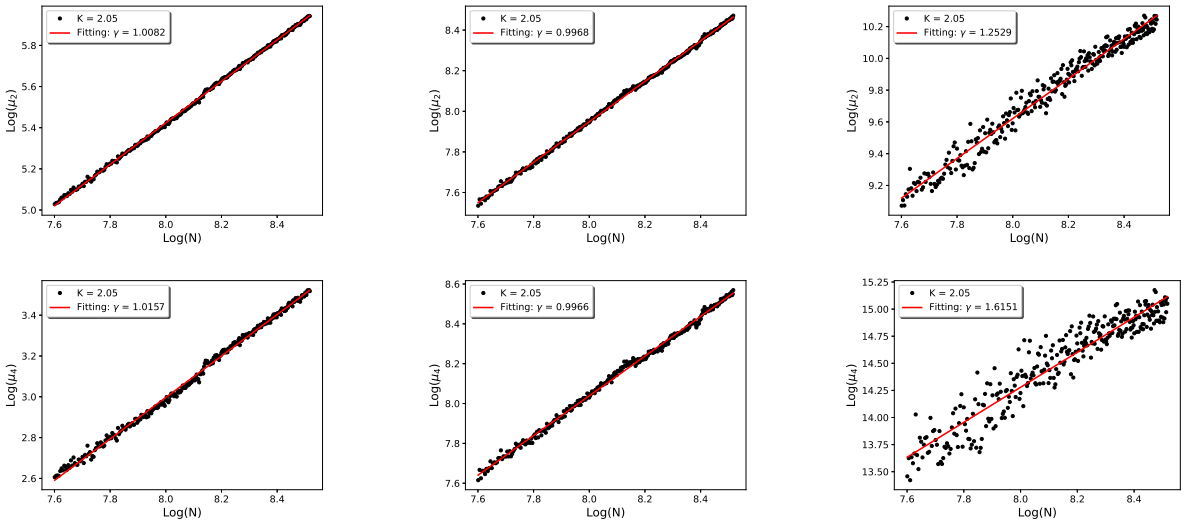

(A) (B) (C)

FIGURE 5.4. Results of the q-averaged moments in order to grasp the kurtosis boosters. We have separated the eigenstates into three groups: central islands, corner islands, and chaotic sea states. Afterward, we have plotted for each group the logarithm of moments μ_2 (upper panel) and μ_4 (lower panel) plots against $\log N$ for the quantum standard map, where we set $\beta = 0$, $\alpha = 1/4$, $\epsilon = 2.2$, $E_m = \pi/4$, and the q-average of size $0.02N^{1/2}$ (Gaussian convolution width). (A) The moments for the chaotic states and for the corner islands (B) picture the growth in moments as the pure kurtosis portraits. However, their resulting kurtosis still gives us a semiclassical decay. Furthermore, the moments of the central islands (C) have the highest growth - drawing attention to be a prospective source - but once more, its resulting kurtosis is decaying.

Moreover, since we are dealing with kurtosis, we are able to bring a statistical perspective to the localization problem swiftly. First, if we take a look only at the intensities distributions in figure 4.6 and their respective outcomes in the kurtosis 4.7, an aspect that promptly draws attention is the transition from the chaotic to the mixed system. The classical hyperbolic map conveys to the quantum intensities a random feature that makes them fall under an exponential distribution.

Nevertheless, when the stochastic parameters are tuned to the mixed regime,

the richness of classical structures comes up and transfers to the states in an aggregate way. Their intensities distributions start to behave as a power law - figure 4.6a is the most explicit instance. This suggests a pseudo-phase-transition character in the intensities distributions, especially when we plot the standard variation of the distributions against the parameters (see figure 5.5). For those same values where the sharp peaks arise, there is a sudden increase in the standard variation μ_2 that ratifies this sort of phase transition. Ultimately, this other prospect deserves further investigation on its own, including more statistical evidence.

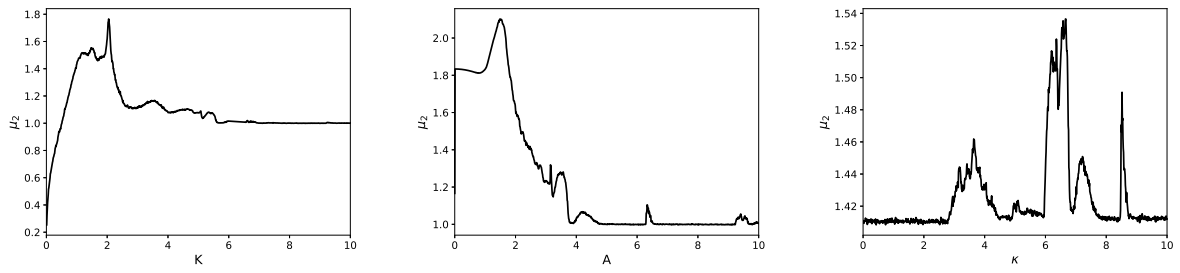

(A) (B) (C)

FIGURE 5.5. Standard variation of the eigenstate-intensity distribution of the three quantum maps as a function of each stochastic parameter. For all three maps, there is a sudden increase in the second moment of the intensities distribution for the same values of the kurtosis sharp peak, alluding to a pseudo-phase-transition. (A) We have set $N = 2098$, $\alpha = 1/4, \beta = 0$, and $dK = 0.01$ for the quantum standard map. (B) For the quantum kicked Harper map, we have set $N = 2000$, $\alpha = 1/4, \beta = 0$, and $dA = 0.01$, which is the only one that diverges from the sharp-peak point, but its near-integrable adversity has already been exposed. (C) Finally, for the quantum perturbed cat map, we have set $N = 2113$ and $d\kappa = 0.01$.

Finally, as aforementioned, especially in section 4.3, the kurtosis of the intensities distributions and the localization of the eigenstates are intrinsically integrated. Consequently, it is worth briefly mentioning what is known about the localization problem in quantum maps and semiclassical systems in general since it is a vast, well-studied branch and will further enlarge the kurtosis panorama.

When it comes down to mixed phase space, where chaos divides its dominance with stable islands, the semiclassical issue is far from a thorough description but with known resolutions. First, we refer to KAM tori, in particular, the cantori [3] effect in the

[3]They are broken KAM tori that are designed as invariant Cantor sets.

wavefunction. Geisel et al. [48] have shown that those structures, which trap classical trajectories into regions of phase space, do equivalently with the quantum wavefunction. Both KAM tori and cantori make the wavefunction confined, and an exponential decay is seen outside them [4].

Another unexpected contribution published by Kús et al. [68] was the so-called periodic ghost orbits. It is just an additional term in the semiclassical approximation but not corresponding to real classical periodic orbits. The ghost solutions are basically complex periodic orbits with complex actions $S \to S' + iS''$ where their contributions will naturally disappear when we take the semiclassical limit. In particular, those contributions become apparent before bifurcations, meaning that the quantum states are first feeling the bifurcation of the classical system. A prominent example is tangent bifurcation, where two periodic orbits bifurcate from no periodic orbit at all. Therefore, it is another evidence of the bifurcations positively influencing the localization and, in fact, may boost the kurtosis in our case.

Last but not least, Mehlig et al. [15] in the same description as KAM tori and cantori, acknowledge that stable islands also confine the trajectories in phase space, and this feature would be transported to the wavefunction in the quantum realm. They could separate the states from chaotic and stable islands - likewise, our last attempts - and manage to show that the classical traps from the islands give rise to wavefunction localization.

5.3 Quantum phase contribution

To conclude, rather than just being stuck on classical influences in the semiclassical system, we also investigate, albeit more qualitatively, a purely quantum effect in the extreme events of the intensities: the quantum phases' contribution to the kurtosis. The β phase controls time-reversal symmetry, and its influence is well-known where the chaotic quantum matrices follow a CUE (Circular unitary ensembles) or COE (Circular orthogonal ensembles) depending on the configuration of β - zero for COE and CUE otherwise. Conversely, the α controls the parity symmetry, but any noteworthy

[4] The procedure is similar to the wavefunction at the edges of the finite well.

influence has been observed in semiclassical physics [17].

We have only focused on the standard map for the following quantum phase's analyses since there is no indication of different scenarios for other quantum maps. First, we have settled $\beta = 0$ - then the system becomes invariant under a time-reversal transformation - and compared the intensity distributions of figure 4.6a with the plot for the time-reversal invariance condition in figure 5.6 for the same parameters K. From the result 5.6, it is immediately visible a shift from the $\beta = 1/4$ for the chaotic parameter $K = 10$, which was previously noted for the quantum perturbed cat map distributions. On top of that, this feature is not exclusive to chaotic states and is carried over to the other parameter values. For instance, the $K = 0.1$ is positively affected in the tail of the distributions - favoring its extreme events. On the contrary, for the $K = 2.05$, the tail apparently loses its weight, which will reflect in the kurtosis value.

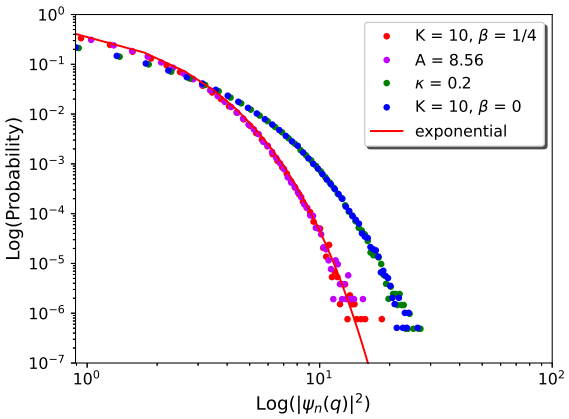

FIGURE 5.6. Intensity distribution of eigenstates in the position basis of the quantum standard map at $N = 2098$, $\alpha = 1/4$, and $\beta = 0$ (time-reversal symmetry is not broken). Comparing with $\beta = 1/4$ in the figure 4.6a, we observe the same departure from the exponential for the chaotic parameter $K = 10$, similar to the perturbed cat map. Also, for the $K = 0{,}1$ in the near-integrable regime, a positive influence in the tail can be noted. On the other hand, the mixed parameter $K = 2.05$ is negatively affected by the symmetry.

In order to closely examine the quantum phases' effect, we have selected three specific parameters $K = 10$, $K = 0.1$, and $K = 2.05$, to plot their kurtosis as a function of β (see figure 5.7) and α (see figure 5.8). In a general aspect, β acts in distinct ways in each case. For $K = 10$ and $K = 0.1$, the kurtosis reaches its maximum when the system has time-reversal symmetry ($\beta = 0$), and on the contrary, $K = 2.05$ has its minimum

for this condition. The anti-periodic condition $\beta = 1/2$ positively affects the mixed state and negatively affects the near-integrable and chaotic states. Notably, the broken conditions seem to have only a transitioning character between the periodic $\beta = 0$ and anti-periodic $\beta = 1/2$ symmetry.

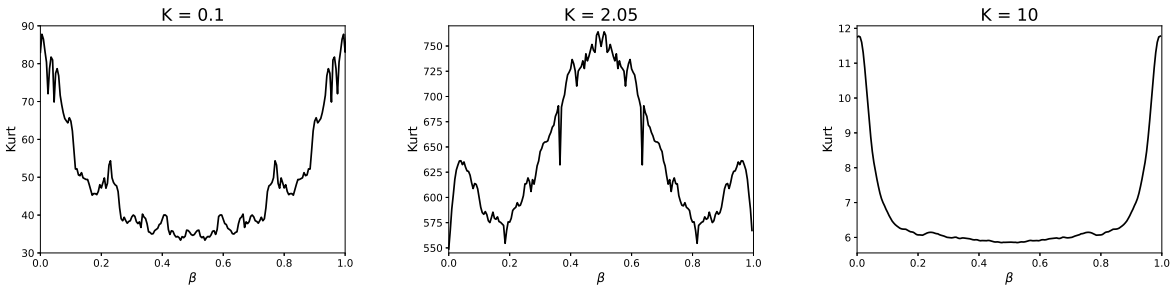

(A) (B) (C)

FIGURE 5.7. Kurtosis of the intensity distribution of the quantum standard map as a function of the quantum phase β for different parameters, where we have set $N = 2098$, $\alpha = 1/4$, and $d\beta = 0.01$. (A) For $K = 0.1$, the complex dependence is crystal-clear; besides that, the maximum kurtosis is achieved for $\beta = 0$ and reaches a minimum for $\beta = 1/2$. (B) In the mixed regime $K = 2.05$, another dependency is obtained where maximum kurtosis for $\beta = 1/2$ and minimum for $\beta = 0$. (C) The chaotic parameter $K = 10$ resembles the near-integrable one, although it is relatively smoother than $K = 0.1$.

The parity symmetry has already been mentioned about its influence on the intensities, mainly in Srivastava et al. [10]. However, when we bring them to the same panorama as executed for the β influence, the results are more erratic. Figure 5.8 showcases the outcomes of the α-dependence on the kurtosis for the quantum standard map. It is promptly visible that the near-integrable and chaotic parameters - figure 5.8a and 5.8c respectively - have an unclear and irregular influence on the extreme events of the eigenstates intensities. In fact, what draws attention is the figure 5.8b that only the mixed regime seems to be regularly impacted by the parity symmetry, with kurtosis being favored for totally broken symmetry and hindered for conservation parameters as $\alpha = 0$ and $1/2$.

Therefore, throughout these qualitative examinations, we can perceive that the quantum phases' presence generates a rich off-shot that could be explored more deeply in the semiclassical systems.

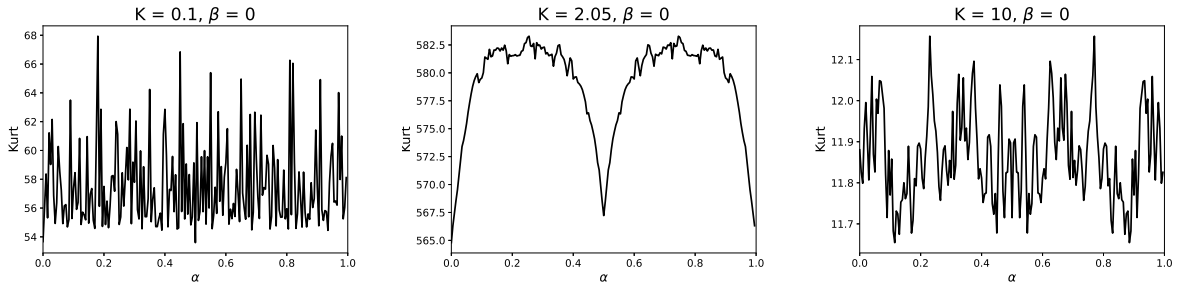

(A) (B) (C)

FIGURE 5.8. Kurtosis of the intensity distribution of the quantum standard map as a function of the quantum phase α for different parameters, where we have set $N = 2098$, $\beta = 1/4$, and $d\alpha = 0.01$. (A) For $K = 0.1$ and (C) $K = 10$, the fluctuating influence of the parity symmetry is evident where there is no evidence of regular behavior. Nevertheless, in the mixed regime (B) $K = 2.05$, the intensities seem to depend more orderly on α, reaching maximums near the broken parameter $\alpha = 1/4$ and minimums near the symmetry conservation $\alpha = 0$ and $1/2$.

Chapter 6

Conclusion

Nowadays, the rogue waves have turned into an active topic that almost any distinct physical generator is being published [55]. Aside from the countless contributions that quantum maps have been providing, in this dissertation, we have shown that their eigenstates intensities in the position basis produce extreme events (rogue waves in this case) only through a one-parameter variation. In order to illustrate its broad coverage, we have dealt with three semiclassical systems: the standard map, kicked Harper map, and the perturbed cat map.

Despite freak waves generation being interesting per se, we have mainly been interested in a close investigation of those extreme events, especially their formation. For this reason, we have explored all the basic tenets that concern the semiclassical theory, which includes classical mechanics, especially deterministic chaos in chapter 2, and quantum mechanics with the relinquishment of the Schrodinger equation and the implementation of classical knowledge to prescribe the quantum wavefunctions in chapter 3.

Our investigation covered recent studies with extreme and record statistics of the eigenstate intensities, which provided a motivation to explore different classical regions of the quantum maps, i.e., the near-integrable and mixed regimes. Since the work revolves around extreme events or the tail region of the intensities distributions, we have proposed measuring the distributions' kurtosis in order to obtain immediate information. Hence, we have had a value that surmised the extensive framework of the distribution tails and plotted them as a function of the stochastic parameters for each quantum map. The results corroborated the observations with the amplitude of

the chaotic cases; moreover, they highlighted specific parameters in the mixed regime with significant values of kurtosis - sharp peaks - displaying a singularity for these conditions present in all three maps.

Having been triggered by semiclassical physics, we developed Bolgomony's scar formula to obtain a semiclassical expression for the moments of the eigenstates and, consequently, the kurtosis. The approach was to compare the power-law scaling predicted for hyperbolic states, and any deviation was a signature of bifurcations or otherwise stable islands. From the results of the moments, the first terms of the fluctuation may not explain the sudden increase that occurs in the mixed regime of the quantum maps. However, because of the programming limit of our machinery, they must not be discarded yet since they deserve more data for even bigger N values.

On the other hand, by separating the contributions of chaotic and stable stables, we have found the stable states show an increase in the moments as we approach the semiclassical limit in a similar way as the pure intensities behave. Thus, it suggested a next way to be explored in order to dive deep into the kurtosis of the mixed quantum states.

Moreover, instead of looking at classical structures and their effect on the quantum wavefunctions, we have taken advantage of the quantum maps formulation and perceived a purely quantum influence on the extreme intensities. We could see the complex relationship between the parity symmetry α and the time-reversal symmetry β. Therefore, the results culminate in periodic (anti-periodic) boundary conditions of β negatively (positively) influencing the kurtosis of near-integrable and chaotic states; and the diametrically opposed happens for the mixed regime. Nevertheless, the same picture could not be drawn for the parity symmetry since α is mostly erratic for near-integral and chaotic states, but a regular behavior has been observed for the mixed regime states. In a general manner, the quantum phases originally from the symmetry of the quantum system also played a role in the extremes, acting differently on the tails depending on the corresponding classical regime.

Ultimately, the study has shown its broadness and richness in many segments of science. The next steps are firmly the approach with separate states and stable islands contributions, in addition to absorbing knowledge from statistical mechanics to

observe the phenomenon as a sort of phase transition between exponential and power-law distribution.

Appendix A

The Maslov phase

To begin, we set the unidimensional Hamiltonian $H = p^2/2m + V(q)$ and apply the WKB approximation similar to section 3.2. The action is distinctly doubled-valued since it can be divided into two layers

$$W_{\pm}(q) = \pm \int p(q)dq = \pm \int_{q_0}^{q} \sqrt{2m[E - V(q)]}, \tag{A.1}$$

where the trajectory goes from q_0 to q.

In order to determine the semiclassical wavefunction 3.30, we have to deal with the amplitude. In particular, owing to the system being integrable, the action I is simply given by equation 2.65

$$I = \frac{1}{2\pi} \oint_{\gamma} pdq = \frac{1}{\pi} \int_{q_1}^{q_2} dq \sqrt{2m[E - V(q)]}, \tag{A.2}$$

where the irreducible circuit γ runs along the turning points q_1 and q_2.

The previous equation A.2 conveys that dE/dI is a constant in both layers; then, the determinant of the WKB approximation can be rewritten as

$$\begin{aligned}
\det\left(\frac{\partial^2 W}{\partial \mathbf{q} \partial \mathbf{I}}\right) &= \det\left(\frac{\partial^2 W}{\partial \mathbf{I} \partial \mathbf{q}}\right) = \det\left(\frac{\partial}{\partial \mathbf{I}} \frac{\partial W}{\partial \mathbf{q}}\right), & \text{(A.3)} \\
&= \det\left(\frac{\partial}{\partial \mathbf{I}} \sqrt{2m[E - V(q)]}\right) = \det\left(\frac{dE}{dI} \frac{\partial}{\partial E} \sqrt{2m[E - V(q)]}\right), & \text{(A.4)} \\
&= \det\left(\frac{dE}{dI} \frac{1}{2\sqrt{2m[E - V(q)]}}\right) = \frac{1}{2p} \frac{dE}{dI}, & \text{(A.5)}
\end{aligned}$$

and the time-independent semiclassical wavefunction $\psi_I(q)$ for $q_1 \leq q \leq q_2$ is

$$\psi_I(q) = c \left| \frac{1}{2p} \frac{dE}{dI} \right|^{1/2} \left[e^{iW_+/\hbar} + e^{iW_-/\hbar} \right]. \tag{A.6}$$

In addition, we can write a similar expression when $q < q_1$ or $q > q_2$, which arises a decreasing exponential as the exponent turns into a real and negative value. We combine the constants to exhibit a more ordinary format

$$\psi(q) = \begin{cases} \psi_-(q) = \frac{C_1}{\sqrt{p}} e^{iW_+/\hbar} + \frac{C_2}{\sqrt{p}} e^{iW_-/\hbar}, & E > V(q) \\ \psi_+(q) = \frac{D}{\sqrt{p}} e^{-\left|\int p dq\right|/\hbar}, & E < V(q). \end{cases} \tag{A.7}$$

Now, as depicted in figure A.1, let us consider the region around the returning points $q = q_1$ and $q = q_2$ where the momentum is null, and the determinant diverges. The first step is to expand the potential's Taylor series

$$V(q) = V(q_j) + (q - q_j)dV/dq + \mathcal{O}(q^2), \quad j = 1, 2$$

and take only the first-order terms. So, we have

$$E - V(q) \cong -(q - q_j)dV/dq = F(q - q_j)$$

as F being the force in the returning points q_j, and the momentum becomes

$$p = \sqrt{2m[E - V]} \simeq \sqrt{2m[F(q - q_j)]}. \tag{A.8}$$

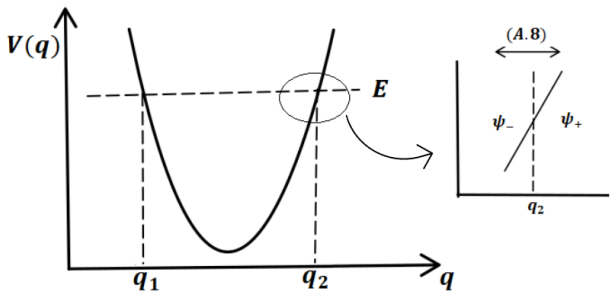

FIGURE A.1. Exemplification of a potential V with the returning points q_1 and q_2 given by $E = V(q_j)$. On top of that, it displays the validity of the approximation A.8 and the border of each wavefunction expression of A.7 around q_j.

Nevertheless, considering the potential being smooth at the returning points, we must connect both solutions of A.7 when $q \approx q_j$. Landau [69] have proposed that, although the semiclassical approximation lost its validity for $q = q_j$, we may assume that there is a smooth path within the complex plane that the wavefunction can cross the region $q = q_j$.

In order to pass over the complex plane, the action integral must be converted to a complex expression. This is simply performed by defining $(q - q_2) = \rho e^{i\phi}$ [1], and the action becomes a path integral with constant $\rho = |q - q_2|$

$$\int \sqrt{q - q_2} dq = \frac{2}{3}(q - q_2)^{3/2} \tag{A.9}$$

$$= \frac{2}{3}\rho^{3/2} e^{3i\phi/2} = i \int \rho^{3/2} e^{i3\phi/2} d\phi \tag{A.10}$$

$$\int \sqrt{q - q_2} dq = i \int \rho^{3/2} e^{i3\phi/2} d\phi = \frac{2}{3}\rho^{3/2} \left(\cos \frac{3i\phi}{2} + i \sin \frac{3i\phi}{2} \right) \tag{A.11}$$

In fact, the integral transport from $q < q_2$ to $q > q_2$ as in figure A.2. The limits are $\phi = 0$ for the right direction and $\phi = \pi$ for the left direction, summed up as

$$\int \sqrt{q - q_2} dq = \begin{cases} \frac{2}{3}\rho^{3/2} =, \frac{2}{3}(q - q_2)^{3/2} & \text{for } \phi = 0 \\ \frac{-2i}{3}\rho^{3/2} =, \frac{-2i}{3}(q - q_2)^{3/2} & \text{for } \phi = \pi. \end{cases} \tag{A.12}$$

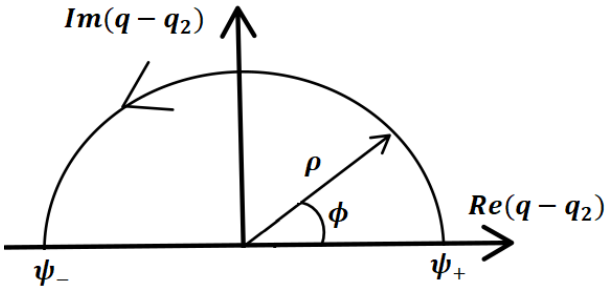

FIGURE A.2. Complex path given by the wavefunction from ψ_+ to ψ_- in order to deal with the singularity in the returning point q_2.

Therefore, the connection must obey the following rule: the right ψ_+ integral

$$-\frac{1}{\hbar}\int p dq = -\frac{\sqrt{2mF}}{\hbar}\int \sqrt{q - q_2} dq = -\frac{2}{3}\frac{\sqrt{2mF}}{\hbar}(q - q_2)^{3/2} \tag{A.13}$$

is transported to the left ψ_- integral

$$-\frac{2i}{3}\frac{\sqrt{2mF}}{\hbar}(q - q_2)^{3/2} = -i\frac{\sqrt{2mF}}{\hbar}\int \sqrt{q - q_2} dq = -\frac{i}{\hbar}\int p dq. \tag{A.14}$$

[1] we shall consider only the passage from one returning point q_2 but the explanation similarly fits for q_1.

The solutions of A.7 only will coincide whether the amplitudes uphold

$$\begin{aligned} \frac{D}{\sqrt{p}} &\rightarrow \frac{C_2}{\sqrt{p}} \\ \frac{D}{(2F(q-q_2))^{1/4}} &\rightarrow \frac{C_2}{(2F(q-q_2))^{1/4}} \\ D\rho^{-1/4}e^{i\phi/4}|_{\phi=0} &\rightarrow C_2\rho^{-1/4}e^{i\phi/4}|_{\phi=\pi} \\ C_2 &= De^{-i\pi/4} \end{aligned} \tag{A.15}$$

We can see that this integral path transported the wavefunction from $E < V(q)$ to the second term of $E > V(q)$ in A.7. If we consider the circuit in figure A.2 from $\phi = 0$ to $\phi = -\pi$, it will lead us to the first term of $E > V(q)$ and the relation

$$C_1 = De^{i\pi/4}. \tag{A.16}$$

As a result, the final the wavefunction for $q < q_2$ is the amalgamation of both outcomes

$$\psi(q) = \frac{D}{\sqrt{p}}\left(e^{\frac{i}{\hbar}\int_{q_2}^{q} pdq}e^{i\pi/4} + e^{-\frac{i}{\hbar}\int_{q_2}^{q} pdq}e^{-i\pi/4}\right) \tag{A.17}$$

$$= 2\frac{D}{\sqrt{p}}\cos\left(\frac{1}{\hbar}\int_{q_2}^{q} pdq + \frac{\pi}{4}\right). \tag{A.18}$$

We notice from equation A.18 that the divergence - attributed from the returning points - in the amplitude of the semiclassical wavefunction is solved by a phase addition of $e^{i\pi/4}$. By extension, the same procedure can be performed around the returning point q_1 getting

$$\psi(q) = 2\frac{D'}{\sqrt{p}}\cos\left(\frac{1}{\hbar}\int_{q_1}^{q} pdq - \frac{\pi}{4}\right) \tag{A.19}$$

$$= 2\frac{D'}{\sqrt{p}}\cos\left(\frac{1}{\hbar}\int_{q_1}^{q_2} pdq - \frac{\pi}{2} + \frac{1}{\hbar}\int_{q_2}^{q} pdq + \frac{\pi}{4}\right). \tag{A.20}$$

For $q_1 < q < q_2$, the equations A.18 and A.20 must coincide, consequently, $D = D'(-1)^n$ and the first two terms in A.20 gives us the quantization rule

$$\frac{1}{\hbar}\int_{q_1}^{q_2} pdq = \left(n + \frac{\pi}{2}\right), \tag{A.21}$$

with n as an integer. This condition is the renowned Bohr-Sommerfeld quantization rule, which exhibits the quantum energy levels available since the left-hand side of

A.21 is the action variables I_n as in 2.65. Therefore, the equation showcases the accessible values of I_n leading to a discrete energy spectrum for integrable systems.

The identical reasoning can be expanded to more degrees of freedom. Whereas only returning points cause divergence at the amplitude for unidimensional cases, there are more general entities called caustics (in which returning points are also included) that produce $\partial\mathbf{p}/\partial\mathbf{q} \to \infty$ for L degrees of freedom. Therefore, whenever the system crosses a point where they are present, the wavefunction ends up earning a phase $e^{i\pi/4}$ to compensate for the divergence.

To put it simply, let us go back to the previous example and delineate its phase space - figure A.3). The returning points q_1 and q_2 are respectively located at the points A and B, where between them, the semiclassical wave A.7 is valid. To avoid the divergence at the A and B, we transport to momentum space $\psi(p)$ through a Legendre transformation since the momenta are well-defined in A and B with no divergence. This technique is known as Maslov formulation [70] and has been pleasingly presented by Percival [71].

Nevertheless, $\psi(p)$ has an amplitude dependent on $\partial\mathbf{q}/\partial\mathbf{p}$ from the Legendre transformation. Consequently, the points C and D cause the divergence of the determinant and are considered momentum returning points, which means another phase is earned to compensate for it. The wavefunction comes back to position space $\psi(q)$ through an inverse Legendre transformation until it reaches again its returning points.

To sum up, every time a returning point in both representations is crossed, we must include a phase. Thus, defining the Maslov index μ is convenient, which counts the number of times a phase was included in the circuit divided by two (because of the doubled representation). For a general degree of freedom, the conclusion is the Maslov index counts for every sort of caustics in the irreducible circuit γ_i and leads to what is known as the EBK rule base upon the tori quantization as in A,21

$$\oint_{\gamma_i} \mathbf{p}(\mathbf{q}, \mathbf{I}) d\mathbf{q} = 2\pi\hbar \left(n_i + \frac{\mu_i}{4}\right) = 2\pi I_i. \tag{A.22}$$

Because energy is specified by $E = H(\mathbf{I})$, the energy levels are

$$E_{\mathbf{n}} = H\left[\mathbf{I} = \hbar\left(\mathbf{n} + \frac{\boldsymbol{\mu}}{4}\right)\right]. \tag{A.23}$$

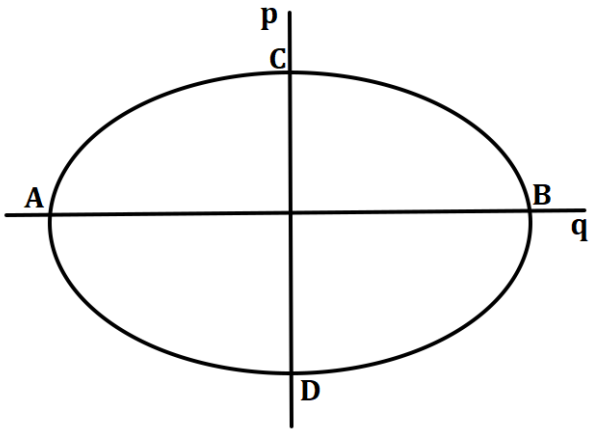

FIGURE A.3. Illustration of the energy surface in phase space of a unidimensional Hamiltonian, where A and B are returning points in position representation, and C and D are returning points in momentum representation. For each of them, we must include an additional phase in the wavefunction for respective representation.

In addition, the semiclassical wave is written as

$$\psi_{\mathbf{I}}(\mathbf{q},t) = c\sum_j \left|\det\left(\frac{\partial^2 W_j}{\partial \mathbf{q}\partial \mathbf{I}}\right)\right|^{1/2} e^{iW(\mathbf{q},\mathbf{I})/\hbar - i\alpha_j\pi/4}. \tag{A.24}$$

where α_i reckons the caustics in position representation and the sum in j accounts for the multivalued character of the function W.

Bibliography

[1] S. Albeverio, V. Jentsch, and H. Kantz, *Extreme Events in Naure and Society*. Springer, 2006.

[2] E. J. Gumbel, *Statistics of Extremes*. Dover Publications Inc., 2004.

[3] C. Bonatto, S. D. Prado, F. L. Metz, J. R. Schoffen, R. R. B. Correia, and J. M. Hickmann, "Super rogue wave generation in the linear regime," *Phys. Rev. E*, vol. 102, p. 052219, 2020.

[4] R. da Silva and S. D. Prado, "A simple study of the correlation effects in the superposition of waves of electric fields: The emergence of extreme events," *Physics Letters A*, vol. 384, no. 11, pp. 126–231, 2020.

[5] D. Carpentier and P. Le Doussal, "Disordered XY models and coulomb gases: Renormalization via traveling waves," *Phys. Rev. Lett.*, vol. 81, pp. 2558–2561, 1998.

[6] S. N. Majumdar and P. Krapivsky, "Extreme value statistics and traveling fronts: various applications," *Physica A: Statistical Mechanics and its Applications*, vol. 318, no. 1, pp. 161–170, 2003.

[7] C. A. Tracy and H. Widom, "Level-spacing distributions and the Airy kernel," *Communications in Mathematical Physics*, vol. 159, no. 1, pp. 151 – 174, 1994.

[8] C. A. Tracy and H. Widom, "On orthogonal and symplectic matrix ensembles," *Communications in Mathematical Physics*, vol. 177, no. 3, pp. 727 – 754, 1996.

[9] A. Lakshminarayan, S. Tomsovic, O. Bohigas, and S. N. Majumdar, "Extreme statistics of complex random and quantum chaotic states," *Phys. Rev. Lett.*, vol. 100, p. 044103, 2008.

[10] S. C. Srivastava and A. Lakshminarayan, "Records in the classical and quantum standard map," *Chaos, Solitons & Fractals*, vol. 74, pp. 67–78, 2015.

[11] E. J. Heller, "Bound-state eigenfunctions of classically chaotic hamiltonian systems: Scars of periodic orbits," *Phys. Rev. Lett.*, vol. 53, no. 16, pp. 1515–1518, 1984.

[12] R. Mackay, J. Meiss, and I. Percival, "Transport in hamiltonian systems," *Physica D: Nonlinear Phenomena*, vol. 13, no. 1, pp. 55–81, 1984.

[13] M. V. Berry, J. P. Keating, and S. D. Prado, "Orbit bifurcations and spectral statistics," *Journal of Physics A*, vol. 31, 1998.

[14] J. Keating and S. Prado, "Orbit bifurcations and the scarring of wave functions," *Proceedings of The Royal Society A: Mathematical, Physical and Engineering Sciences*, vol. 457, pp. 1855–1872, 2001.

[15] B. Mehlig, K. Müller, and B. Eckhardt, "Phase space localization and matrix element distributions in systems with mixed classical phase space," *Phys. Rev. E*, vol. 59, pp. 5272–5277, May 1999.

[16] S. Fishman, D. R. Grempel, and R. E. Prange, "Chaos, quantum recurrences, and anderson localization," *Physical Review Letters*, vol. 49, pp. 509–512, 1982.

[17] A. Lakshminarayan, "Classical and quantum chaos plus rmt and some applications," in *SERC School-2009, Delhi University: Lecture Notes*, (Bangalore, India), 2009.

[18] H. Goldstein, *Mechanics*. Pearson, 3 ed., 2001.

[19] M. Gutzwiller, *Chaos in Classical and Quantum Mechanics*. Springer-Verlag, 1990.

[20] S. D. Prado, "Quebra de simetrias em sistemas hamiltonianos: efeitos clássicos e quânticos," *UNICAMP Master's dissertation*, 1992.

[21] V. I. Arnold, *Mathematical Methods of Classical Mechanics*. Springer, 2 ed., 1997.

[22] L. D. Landau and E. M. Lifshitz, *Classical Mechanics*, vol. 1. Butterworth-Heinemann, 3 ed., 1976.

[23] M. A. M. de Aguiar, "Tópicos de mecânica clássica," *notes from UNICAMP*, 2009.

[24] A. M. Ozorio de Almeida, *Hamiltonian Systems: Chaos and Quantization*. Cambridge Monographs on Mathematical Physics, Cambridge University Press, 1989.

[25] M. A. M. de Aguiar, "O limited semiclássico da mecânica quântica," *notes from UNICAMP*, 1998.

[26] M. V. Berry, "Regular and irregular motion," *AIP Conference Proceedings*, vol. 46, no. 1, pp. 16–120, 1978.

[27] J. M. Greene, "A method for determining a stochastic transition," *Journal of Mathematical Physics*, vol. 20, no. 6, pp. 1183–1201, 1979.

[28] V. I. Arnold and A. Avez, *Ergodic Problems of Classical Mechanics*. Benjamin, 1968.

[29] K. R. Meyer, "Generic bifurcation of periodic points," *Transactions of the American Mathematical Society*, vol. 149, no. 1, pp. 95–107, 1970.

[30] E. Ott, *Chaos in Dynamical Systems*. Cambridge University Press, 2 ed., 2002.

[31] B. V. Chirikov, *Research concerning the theory of non-linear resonance and stochasticity*. CERN, 1971.

[32] P. Leboeuf, J. Kurchan, M. Feingold, and D. P. Arovas, "Phase-space localization: Topological aspects of quantum chaos," *Phys. Rev. Lett.*, vol. 65, pp. 3076–3079, 1990.

[33] P. G. Harper, "Single Band Motion of Conduction Electrons in a Uniform Magnetic Field," *Proceedings of the Physical Society A*, vol. 68, no. 10, pp. 874–878, 1955.

[34] P. A. Boasman and J. P. Keating, "Semiclassical asymptotics of perturbed cat maps," *Proceedings: Mathematical and Physical Sciences*, vol. 449, no. 1937, pp. 629–653, 1995.

[35] M. Basilio de Matos and A. M. Ozorio de Almeida, "Quantization of anosov maps," *Annals of Physics (New York)*, vol. 237, no. 1, 1995.

[36] A. Einstein, "On the quantum theorem of sommerfeld and epstein," *Deutsche Physikalische Gesellschaft Verhandlungen*, vol. 19, no. 6, pp. 82–92, 1917.

[37] Brillouin, L., "Notes on undulatory mechanics," *J. Phys. Radium*, vol. 7, no. 12, pp. 353–368, 1926.

[38] J. B. Keller, "Corrected bohr-sommerfeld quantum conditions for nonseparable systems," *Annals of Physics*, vol. 4, no. 2, pp. 180–188, 1958.

[39] G. Casati and J. Ford, *Stochastic Behavior in Classical and Quantum Hamiltonian Systems: Volta Memorial Conference, Como 1977*. Lecture Notes in Physics, Springer-Verlag, 1977.

[40] M. C. Gutzwiller, "Phase-integral approximation in momentum space and the bound states of an atom," *Journal of Mathematical Physics*, vol. 8, no. 10, pp. 1979–2000, 1967.

[41] M. C. Gutzwiller, "Phase-Integral Approximation in Momentum Space and the Bound States of an Atom. II," *Journal of Mathematical Physics*, vol. 10, no. 6, pp. 1004–1020, 1969.

[42] M. C. Gutzwiller, "Energy Spectrum According to Classical Mechanics," *Journal of Mathematical Physics*, vol. 11, no. 6, pp. 1791–1806, 1970.

[43] M. C. Gutzwiller, "Periodic Orbits and Classical Quantization Conditions," *Journal of Mathematical Physics*, vol. 12, no. 3, pp. 343–358, 1971.

[44] J. H. V. Vleck, "The correspondence principle in the statistical interpretation of quantum mechanics," *Proceedings of the National Academy of Sciences*, vol. 14, no. 2, pp. 178–188, 1928.

[45] J. McClure and R. Wong, "Multidimensional stationary phase approximation: boundary stationary point," *Journal of Computational and Applied Mathematics*, vol. 30, no. 2, pp. 213–225, 1990.

[46] M. V. Berry and M. Tabor, "Level clustering in the regular spectrum," *Proc. R. Soc. Lond. A*, vol. 356, no. 1686, pp. 375–394, 1977.

[47] A. I. Shnirelman, "Ergodic properties of eigenfunctions," *Uspekhi Mat. Nauk*, vol. 29, pp. 181–182, 1974.

[48] T. Geisel, G. Radons, and J. Rubner, "Kolmogorov-arnol'd-moser barriers in the quantum dynamics of chaotic systems," *Phys. Rev. Lett.*, vol. 57, pp. 2883–2886, 1986.

[49] M. K. Henry, J. Emerson, R. Martinez, and D. G. Cory, "Localization in the quantum sawtooth map emulated on a quantum-information processor," *Phys. Rev. A*, vol. 74, pp. 062–317, 2006.

[50] A. Lakshminarayan and N. L. Balazs, "Quantum relaxation is studied in coupled quantum baker's maps," *Journal of Statistical Physics*, vol. 77, pp. 311–344, 1994.

[51] F. Davide, V. Lucarini, T. G., and V. S., "Generalized extreme value distribution parameters as dynamical indicators of stability," *International Journal of Bifurcation and Chaos*, vol. 22, no. 11, 2012.

[52] T. Huillet, "Sampling problems for randomly broken sticks," *Journal of Physics A: Mathematical and General*, vol. 36, no. 14, p. 3947, 2003.

[53] S. N. Majumdar and R. M. Ziff, "Universal record statistics of random walks and lévy flights," *Phys. Rev. Lett.*, vol. 101, p. 050601, 2008.

[54] I. Bengtsson and K. Zyczkowski, *Geometry of Quantum States: An Introduction to Quantum Entanglement*. Cambridge University Press, 2006.

[55] C. Liu, A. Di Falco, T. F. Krauss, and A. Fratalocchi, "Rogue waves generated through quantum chaos," in *2013 Conference on Lasers & Electro-Optics Europe & International Quantum Electronics Conference CLEO EUROPE/IQEC*, pp. 1–1, 2013.

[56] A. Gabrielsen, A. Kirchner, Z. Liu, and P. Zagaglia, "Forecasting value-at-risk with time-varying variance, skewness and kurtosis in an exponential weighted moving average framework," *Annals of Financial Economics*, vol. 10, no. 01, p. 1550005, 2015.

[57] J. V. Healy, M. Dixon, B. J. Read, and F. F. Cai, "Non-parametric extraction of implied asset price distributions," *Physica A: Statistical Mechanics and its Applications*, vol. 382, no. 1, pp. 121–128, 2007. Applications of Physics in Financial Analysis.

[58] I. Varga, P. Pollner, and B. Eckhardt, "Quantum localization near bifurcations in classically chaotic systems," 1999.

[59] W. F. de Oliveira and G. Q. Pellegrino, "Chaos-based potentials in the one-dimensional tight-binding model probed by the inverse participation ratio," *Computational and Applied Mathematics*, vol. 37, pp. 3995–4006, 2018.

[60] B. Eckhardt, S. Fishman, J. Keating, O. Agam, J. Main, and K. Müller, "Approach to ergodicity in quantum wave functions," *Phys. Rev. E*, vol. 52, pp. 5893–5903, 1995.

[61] M. V. Berry, J. P. Keating, and H. P. Schomerus, "Semiclassical asymptotics of perturbed cat maps," *Universal twinkling exponents for spectral fluctuations associated with mixed chaology*, vol. 456, no. 1937, p. 1659–1668, 2000.

[62] E. B. Bogomolny, "Smoothed wave functions of chaotic quantum systems," *Physica D: Nonlinear Phenomena*, vol. 31, no. 2, pp. 169–189, 1988.

[63] Y. Colin de Verdière, "Ergodicité et fonctions propres du laplacien," *Séminaire Équations aux dérivées partielles (Polytechnique) dit aussi "Séminaire Goulaouic-Schwartz"*, 1984-1985. talk:13.

[64] S. Zelditch, "Uniform distribution of eigenfunctions on compact hyperbolic surfaces," *Duke Mathematical Journal*, vol. 55, no. 4, pp. 919–941, 1987.

[65] A. M. O. de Almeida and J. H. Hannay, "Resonant periodic orbits and the semiclassical energy spectrum," *Journal of Physics A: Mathematical and General*, vol. 20, no. 17, pp. 58–73, 1987.

[66] E. Wigner, "On the quantum correction for thermodynamic equilibrium," *Phys. Rev.*, vol. 40, pp. 749–759, 1932.

[67] D. Ullmo and S. Tomsovic, "Introduction to quantum chaos," *UNESCO Encyclopedia of Life Support Sciences*, 2014.

[68] M. Kuś, F. Haake, and D. Delande, "Prebifurcation periodic ghost orbits in semiclassical quantization," *Phys. Rev. Lett.*, vol. 71, pp. 2167–2171, 1993.

[69] L. D. Landau and E. M. Lifshitz, *Quantum Mechanincs*, vol. 3. Pergamon Press, 2 ed., 1965.

[70] V. Maslov and M. Fedoriuk, *Semi-classical Approximations in Quantum Mechanics*. Springer, 1981.

[71] I. C. Percival, *Semiclassical theory of Bound States*. John Wiley & Sons, Ltd, 1977.